Research report

Heat transfer characteristic of advanced loop thermosyphon with check value (ALT/CV) containing nanofluids

By
Assist. Prof. Dr. Thanya Parametthanuwat

Grant by

The Thailand Research Fund
and
King Mongkut's University of Technology North Bangkok

Acknowledgments

Financial support was provided for T. Parametthanuwat from the Thailand Research Fund and the Faculty of Industrial Technology and Management at King Mongkut's University of Technology North Bangkok via Grant No. TRG-5780179. S. Rittidech, Head of the Heat Pipe and Thermal Tool Design Research Unit (HTDR), Faculty of Engineering, Mahasarakham University, Thailand, and Y. Ding Birmingham, Centre for Thermal Energy Storage School of Chemical Engineering, University of Birmingham, UK provided support to T Parametthamuwat. N. Bhuwakietkunjohn also provided technical support.

Abstract

This report is focus on heat transfer characteristic advanced loop thermosyphon with check value (ALT/CV) containing nanofluids. It will highlight theories for investigating heat transfer characteristic. Points of importance will be emphasize, with significance given to the heat transfer characteristics of ALT/CV and their use in this experiment. The chapter I present work aims to study the effects of operating temperature, loop and check valve on thermal performance of nanofluids in an ALT/CV. The chapter II present theoretical consideration to study the thermosyphon, heat transfer characteristics, dimensionless, nanofluids and surfactant. The chapter III describes the results and discussions of silver nanofluids properties when preparing for filled as working fluids in ALT/CV. It is divided into a number of sections to determine the thermal properties of silver nanofluids containing surfactant. The chapter IV describes the heat transfer rate behaviour of an advanced loop thermosyphon with check valve(ALT/CV) which is filled with silver nanofluids and containing oleic surfactant (OA) and potassium oleate surfactant (OAK+). Also included are the explanation of dimensionless and the behaviour characteristics in the ALT/CV. The filling ratios are 30, 50 and 80% with respect to evaporator volume. The heat was supplied of 20%, 40%, 60%, 80% and 100% of heater (2,000 Watt). Five working fluids are: deionized water, deionized water based silver nanoparticles concentration of 0.5 wt% (NP), NP containing 0.5, 1 and 1.5 wt% of OA and OAK+ respectively. The dimensionless parameters on ALT/CV are such as $\frac{Lo_{size}}{D_i}$, Pr, Bo, Ja, Co, Cd, Ga_m, Pe_m, Ar, Gr and Z. Then, all of dimensionless was to create a correlation equation with Kutaeladze number for predicting heat transfer of ALT/CV, shows as below;

$$q = 3.24\left[\frac{Lo_{size}}{D_i}^{6}\cdot\frac{\Pr^{6.2}\cdot Bo^{6.4}\cdot Ja^{6.2}\cdot Co^{5.2}\cdot Cd^{3.8}\cdot Ga_m^{1.5}}{Pe_m^{2.7}\cdot Ar^{0.4}\cdot Z^{0.2}\cdot Gr^{0.6}}\right]^{1.57}\times\left[\rho_v h_{fg}\left(\frac{\rho_v-\rho_l}{\rho_v^{2}}\right)\right]^{0.25}$$

The correlation equation is used to calculate and construct a design for the oven installed with ALT/CV (OALT/CV) shows in Chapter V.

CONTENTS

FIGURE CONTENTS

TABLE CONTENT

CHAPTER I INTRODUCTION

1. Background and explanation of the problem

A traditional two-phase closed thermosyphon (TPCT) is essentially a gravity-assisted wickless heat pipe, which utilizes the heat of evaporation and condensation as a working fluid. Contrary to the conventional heat pipe that uses the capillary force to return the liquid to evaporator, the TPCT uses gravity to return liquid to condensate. Since the evaporator of a TPCT is located in the lowest position, the gravitational force will support the capillary force’s duty [1] shown in Figure 1. The TPCT has a number of advantages these include it’s simple structure, has very small thermal resistance, high efficiency and low manufacturing costs. It has, therefore, been widely used in various applications. These include industrial heat recovery, electronic component cooling, turbine blade cooling and solar heating systems.

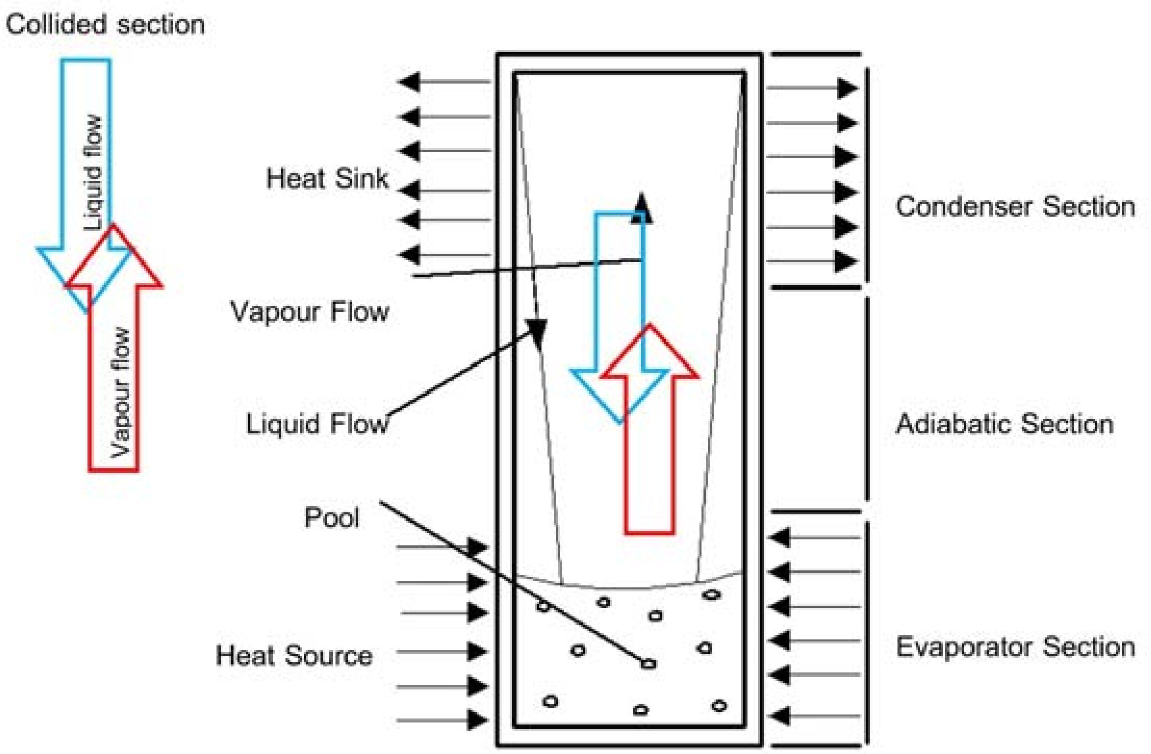

Figure 1 Schematic of the TPCT [2]

However, the traditional TPCT had disadvantage that is collision of liquid and vapour movement of inside them. Moreover, the point of importance, traditional TPCT had disadvantage behaviour caused to decrease heat transfer/heat flux [3, 4]. Figure 2A showed the condensate on the wall surface of the cooled section flow down on the form of liquid film to the heated section through the adiabatic section. Then break down into rivulet at a comparatively small heat flux. The film breakdown occurs; the heat transfer in the breakdown area is decreases and then the wall temperature rise. The wall temperature, however, does not rise continuously but reaches an equilibrium. This is because the breakdown heat flux is relatively small and because heat conduction through the tube wall appears gradually to prevail. This region is called“dry out” [5, 6]. The flow patterns of this region are presumed to correspond to Figure 2(B) and (C), and then the heated wall temperature, which had had a uniform temperature distribution, rose sharply at a lower half position of the heated section when the critical condition was reached. Since the rate of temperature rise of this region was faster than that of the dry-out region, this region is called the “burn-out” [5, 7, 8].

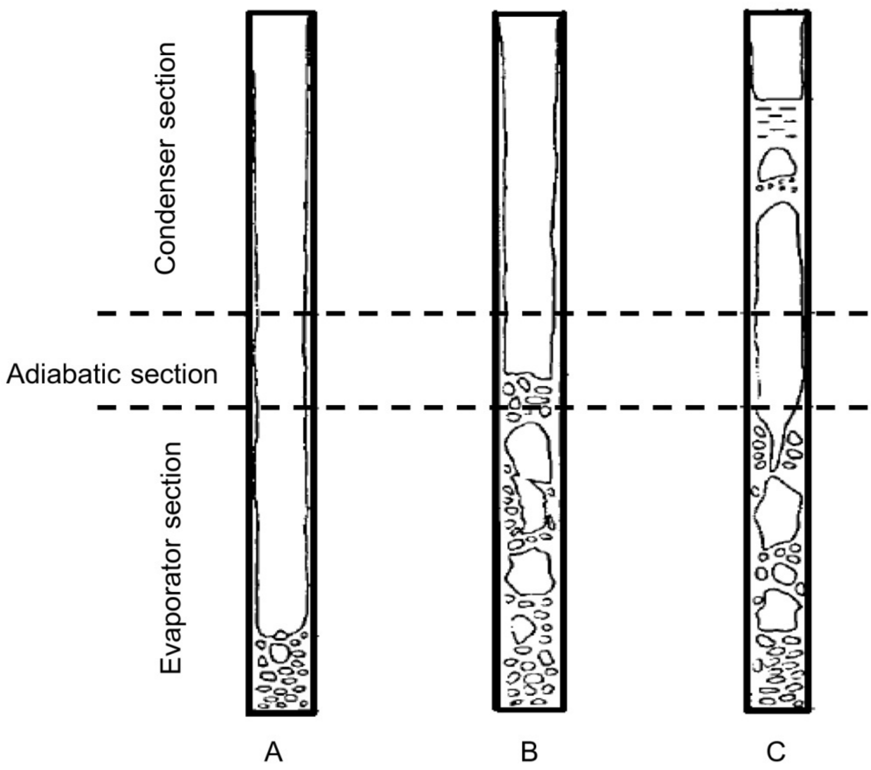

Figure 2 Flow pattern in traditional TPCT [5]

The check valve (CV) in Figure 3 is a buoyancy valve that consists of a stainless steel ball and copper tube, in which a ball stopper and conical valve seat are provided at the ends of the check-valves case: a conical valve seat is provided at the bottom of the case and a ball stopper is provided at the top of the case, respectively. The ball can move freely between the ball stopper and the conical valve-seat. The conical valve seat contacts the stainless-steel ball in order to prevent a reversal of the flow of the working fluid. The ball stopper allows the working fluid to travel to the condenser section for transferring heat. Thus, the CV was controlled vapour and fluid flow.

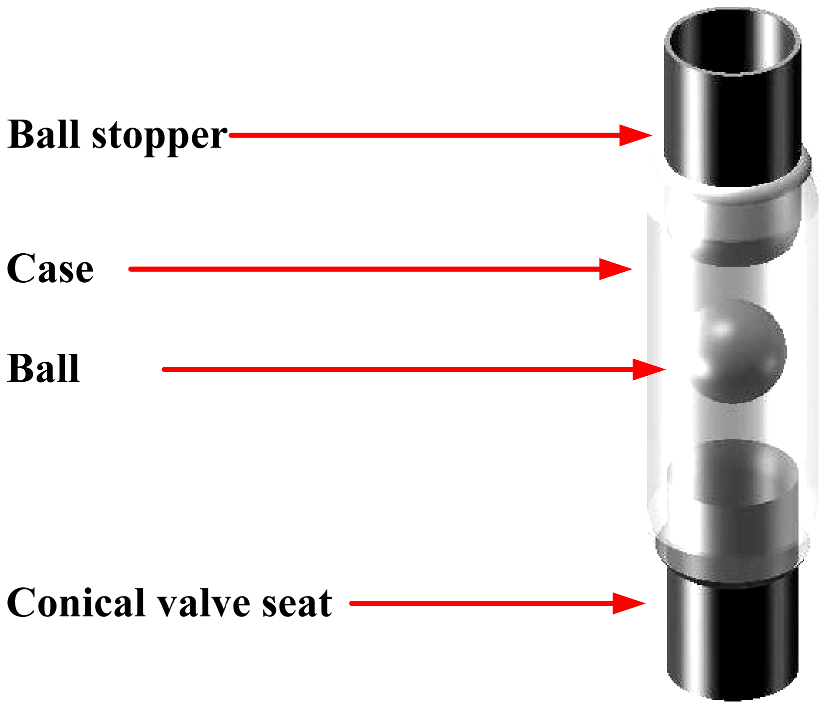

Figure 3 The check valve

For these reasons, advanced loop thermosyphon with check valve (ALT/CV) designed to solve the weak points in the limitation of heat being received in the evaporator area and the limitation of the condensing area. The TPCT made adjustments to for the problems which used an advanced loop thermosyphon with check valve (ALT/CV). The new type of thermosyphon (ALT/CV), shown in Figure 4 utilizes evaporation and the condensation of a working fluid inside to transport heat with a loop and control flow with check valve. Expectedly, the heat transfer rate of ALT/CV was superior in heat transfer rate over of all experimental conditions studied.

Finally, cooling is one of the most important challenges facing numerous industrial sectors. Despite the considerable amount of research and development focusing on industrial heat transfer requirements, major improvements in cooling capabilities are still insufficient. This is due to the fact that conventional heat transfer fluids possess poor heat transfer properties. One common method used to overcome this problem is to increase the surface area available for heat exchange. This leads to impractical enhancement in the size of the heat management system. Thus, there is a current need to improve the heat transfer capabilities of conventional heat transfer fluids. However, traditional fluids have poor heat transfer properties compared to most solids [9-11]. A new class of heat transfer fluid called "Nanofluids" which are engineered by suspending ultra fine metallic or non-metallic particles of nanometer dimensions in traditional fluids cooling [11, 12]. The applications would benefit from a decrease in the thermal resistance of the heat transfer fluid. Using nanofluids leads to smaller electric potential to reduce thermal resistance and improved heat transfer fluid. Nanofluids can used in the transportation, electronics, medical, food and manufacturing sectors. In addition, nanofluids consist of such particles suspended in liquid, typically convectional heat transfer liquids to enhance the thermal conductivity and convective heat transfer performance of the base liquids [10, 12].

More exploratory research is indeed required to benchmark the scope and applicability of these fluids in engineering systems. This present work aims to study the effects of operating temperature, loop and check valve on thermal performance of nanofluids in an advanced loop thermosyphon with check valve(ALT/CV). Thus, the ALT/CV used in this study was a special type that uses nanofluids in the ALT/CV to transfer heat from the evaporator to condenser, without any external energy requirement. The primary task is to create the correlation of the Kutateladza number. The ALT/CV was designed and tested in order to increase the heat transferred in oven application, which intensifies the ALT/CV's effectiveness.

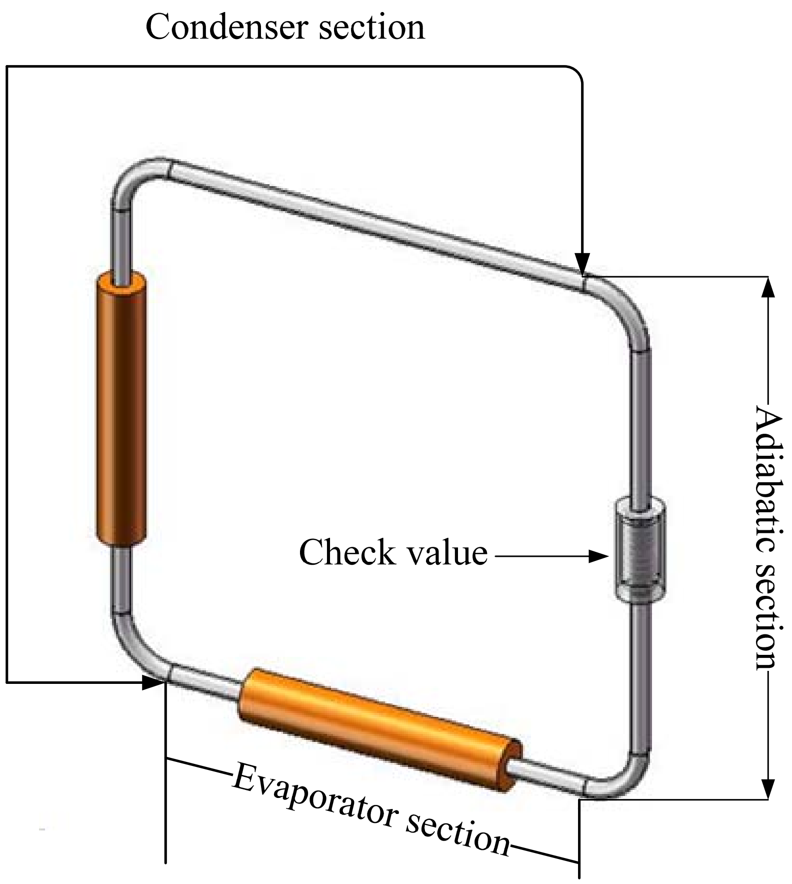

Figure 4 Schematic of the ALT/CV

2. Objectives of this study

To study the thermal properties of silver nanofluids

To study the effect of loop check valve, evaporator area, condenser area, operating temperature and working fluids of heat transfer rate of an advanced loop thermosyphon with check valve containing nanofluids contained oleic acid and potassium oleate surfactant.

To study the effect of dimensionless parameters on the heat transfer rate of an advanced loop thermosyphon with check valve containing nanofluids contained oleic acid and potassium oleate surfactant.

To create a correlation equation for predicting the heat transfer rate of an advanced loop thermosyphon with check valve containing nanofluids contained oleic acid and potassium oleate surfactant.

The equation in 3 was used to calculate and construct a design for the prototye of oven an advanced loop thermosyphon with check valve (OALT/CV) containing nanofluids contained oleic acid and potassium oleate surfactant.

3. Scope of study

Table 1 Controlled and variable parameters about Silver nanofluids properties[13]

The controlled parameters	• Deionized water mixed Silver nanofluids concentration of 0.5 wt% (NF) • Operating temperature of 20 °C to 80 °C • Shear rate ranges were 100 s^{-1} to 103 s^{-1}

Independent Variable	• Working fluid was:
	  o Deionized water (DI-water)
	  o DI-water containing surfactant
	  o NF
	  o NF containing surfactant

	Surfactant were: • Concentration of Oleic acid (OA) was 0.5, 1, and 1.5 wt% • Concentration of Potassium oleate (OAK^+) was 0.5, 1, and 1.5 wt%
Dependent Variable	The dependent variable was: • Thermal conductivity, specific heat, density, viscosity, contact angle and application of thermal enhancement • Rheological behaviour

Table 2 Controlled and variable parameters about Silver nanofluids thermal properties[13]

The controlled parameters	• Cylinder diameter and height of 1,500 mm and 3,000 mm. • The volumetric flow rate of 0.2–1.5 l/min
Independent Variable	• Heater (2,000 Watt) with diameter and height of 500 mm and 2,000 mm. • The heat was supplied of 20%, 40%, 60%, 80% and 100% of heater. • Working fluid was: o Deionized water (DI-water) o DI-water containing surfactant o NF o NF containing surfactant
	Surfactant were: • Concentration of OA was 0.5, 1, and 1.5 wt% • Concentration of OAK^{+} was 0.5, 1, and 1.5 wt%
Dependent Variable	Heat transfer enhancement

Table 3 Controlled and variable parameters about ALT/CV thermal performance and behaviour

The controlled parameters	• ALT/CV was made from copper tubewith inside diameter of 12.70 mm. • The temperature of cooling fresh air is at 25°C. • The ambient temperature is at 25°C. • The velocity of air inlet of condenser section is at 0.6 m/s.
Independent Variable	• The heat supplied 20%, 40%, 60%, 80% and 100% from heater 2,000 Watts. • The filling ratio was 30%, 50% and 80% respect to the evaporator section volume. • The ALT/CV had three sections, evaporator, adiabatic, and condenser, of loop equal size of 30 cm, 40 cm, and 50 cm, withinstallation fin of 8 FPI at condenser section. • Working fluid was: o Deionized water (DI-water) o DI-water containing surfactant o NF o NF containing surfactant
	Surfactant were: • Concentration of OA was 0.5, 1, and 1.5 wt% • Concentration of OAK^{+} was 0.5, 1, and 1.5 wt%
Dependent Variable	The dependent variable was: • Heat transfer rate (W) • Heat flux (W/m^2) • Thermal resistance (W/°C)

Table 4 Controlled and variable parameters about OALT/CV

The controlled parameters	• The heat supplied was LPG burner. • The filling ratio was 80% respect to the evaporator section volume. • ALT/CV was made from copper tubewith inside diameter of 12.70 mm. • The ALT/CV had three sections, evaporator, adiabatic, and condenser, of loop equal size of 30 cm, 40 cm, and 50 cm, withinstallation fin of 8 FPI at condenser section.
The variable parameters	Working fluid was: • Deionized water (DI-water) • DI-water containing surfactant • NF • NF containing surfactant
	Surfactant were: • Concentration of OA was 0.5, 1, and 1.5 wt% • Concentration of OAK^+ was 0.5, 1, and 1.5 wt%
Dependent Variable	The dependent variable was: • Total colour • Texture • Effectiveness • Sensory score

4. Expected Benefits

The thermal properties of silver nanofluids, will be clarified;

The effect of loop, filling ratios and check valve of heat transfer rate of an advanced loop thermosyphon with check valve containing nanofluids contained oleic acid and potassium oleate surfactant, will be clarified.

The effect of dimensionless parameters of heat transfer rate of an advanced loop thermosyphon with check valve containing nanofluids contained oleic acid and potassium oleate surfactant, will be clarified.

The correlation equation to predict the heat transfer rate of an advanced loop thermosyphon with check valve containing nanofluids contained oleic oleic acid and potassium oleate surfactant, will be achieved.

The prototype of an advanced loop thermosyphon with check valve oven containing nanofluids contained oleic acid and potassium oleate surfactant (OALT/CV), will be achieved.

In the future. an advanced loop thermosyphon with check valve in the study can be using practically in the many industries.

CHAPTER II THEORETICAL CONSIDERATION

1. Thermosyphon

Recently, investigators have been paid great attention to heat pipes and thermosyphons. Their mode of operation has also been investigated. The operation of a heat pipe is easily understood by using a cylindrical geometry, as shown in Figure 5. The components of a heat pipe are a sealed container (pipe wall and end caps), a wick structure, and a small amount of working fluid in liquid state, which is in equilibrium with its own vapour. The length of the heat pipe is divided into three parts: the evaporator section, adiabatic section and condenser section. In the selection of a suitable combination of three basic components, inevitably a number of conflicting factors may arise.

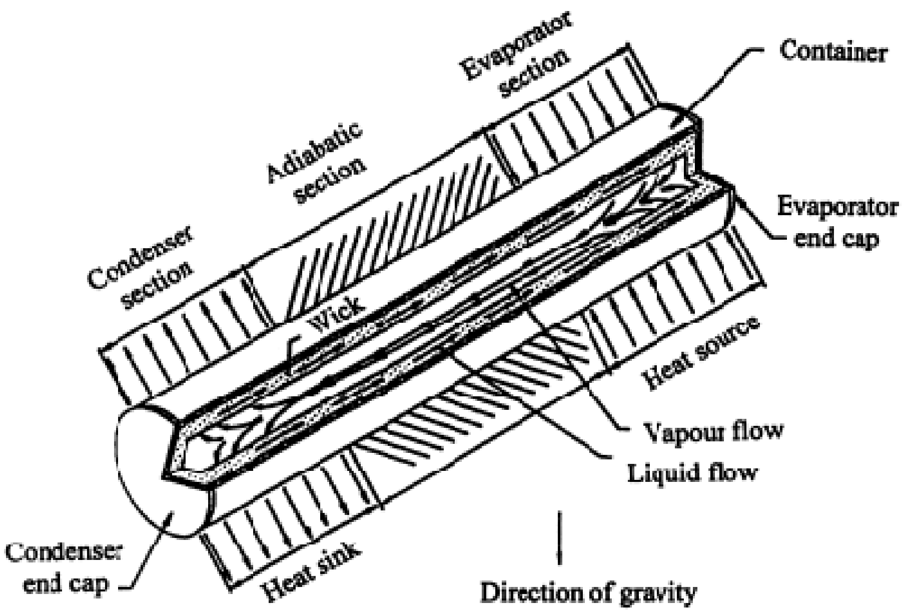

Figure 5 Schematic of a conventional heat pipe showing the principle of operation and circulation of the working fluid [14]

TPCT is actually a wickless, gravity-assisted heat pipe with a small amount of working fluid which is in equilibrium with its own vapor sealed inside container (pipe wall and end caps). The length of the TPCT (similar to heat pipe) is divided into three parts: evaporator section, adiabatic section and condenser section, as shown in Figure 6.

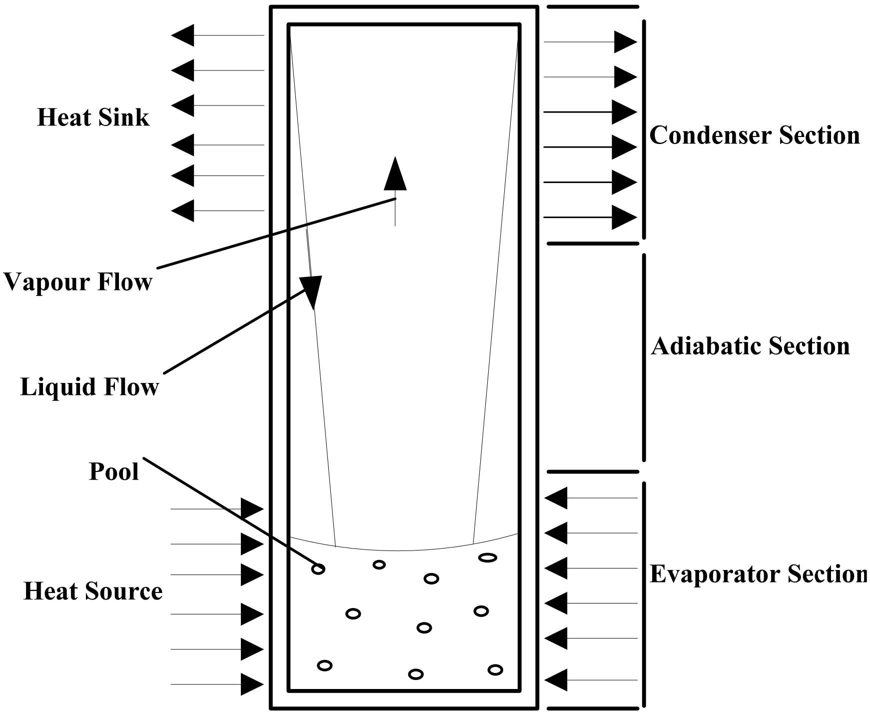

Figure 6 Schematic of the TPCT [2]

2. Heat transfer characteristics

The heat transfer performance ($Q_{\text{Theoretical}}$) of a TPCT can be calculated from the ratio of temperature difference between the evaporator and condenser (ΔT) and the total thermal resistance (Z_{Total}) as shown in equation (1) [14].

$$Q_{\text{Theoretical}} = \frac{\Delta T}{Z_{Total}} \tag{1}$$

Thus Δ T define by (2);

$$\Delta T_{\text{ln}} = \frac{(\text{T}_{\text{h,in}} - \text{T}_{\text{c,out}}) - (\text{T}_{h,\text{out}} - T_{c,in})}{\ln \dfrac{(\text{T}_{\text{h,in}} - \text{T}_{\text{c,out}})}{(\text{T}_{h,\text{out}} - T_{c,in})}} \tag{2}$$

The total thermal resistance can be explained based on the many factors which depend on the function or properties of the operation. This is shown as the total resistance of the thermal model by Engineering Sciences Data Unit Item No 80023, ESDU81038 [15].

2.1. Thermal resistance of thermosyphon

The TPCT is a simple heat transfer device allowing its performance to be clearly evaluated. The principle method to calculate performance is the total resistance calculation method ESDU81038 [15] and can be explained as follows;

The resistance of a TPCT device can be split into 10 valves and divided into 3 groups. The external resistance is the resistance from the outside wall of the TPCT at both the evaporator and condenser sections. The internal resistance is the resistance from the phase change, pool boiling or film boiling, when the vapour pressure drops along the pipe. The resistance from the material property is dependent on the type of material used. Resistance is explained as follows in Figure 7 [2].

2.2. External resistance (Z_1 *and* Z_9)

Z_1 and Z_9 represent the resistance from the external convection of the pipe:

$$Z_1 = \frac{1}{h_{eo} A_{eo}} \tag{3}$$

$$Z_9 = \frac{1}{h_{co} A_{co}} \tag{4}$$

2.3. Resistance from material property (Z_2 *and* Z_8)

Z_2 and Z_8 represent the resistance from the thermal conductivity if the material is:

$$Z_2 = \frac{\ln\left(D_o / D_i\right)}{2\pi L_e k_x} \tag{5}$$

$$Z_8 = \frac{\ln\left(D_o / D_i\right)}{2\pi L_c k_x} \qquad (6)$$

2.4. Internal resistance ($Z_2, Z_3, Z_4, Z_5, Z_6, Z_7$ **and** Z_{10})

Z_3 and Z_7 represent the internal resistance due to the working fluid of pool and film boiling and is devised into:

Z_{3p} is resistance from pool boiling; $\frac{1}{\Phi_3 g^{0.2} Q^{0.4} \left(\pi D_i L_e\right)^{0.6}}$ (7)

Z_{3f} is resistance from film boiling at the evaporator section; $\frac{CQ^{1/3}}{D_i^{4/3} g^{1/3} L_e \Phi_2^{4/3}}$ (8)

When $C = \left(\frac{1}{4}\right)\left(\frac{3}{\pi}\right)^{4/3} = 0.325$, Φ_2 is figure of merit (2); $\left(\frac{Lk_l \rho_l^2}{\mu_l}\right)^{0.25}$ and Φ_3 is figure of merit $0.325 \times \frac{\rho_l^{0.5} k_l^{0.3} C_{pl}^{0.7}}{\rho_v^{0.25} L^{0.4} \mu_l^{0.1}} \left[\frac{P_v}{P_a}\right]^{0.23}$. The condition using Z_{3p} and Z_{3f} is $Z_3 = Z3pF + Z3f\ (1-F)$ as equation (9). Fis filling ratio that is defined by; $\frac{\mathrm{V_l}}{\mathrm{AL_e}}$.

Z_7 is resistance from film boiling of the working fluid at the condenser section:

$$Z_7 = \frac{\mathrm{CQ}^{1/3}}{\mathrm{D_i^{4/3} g^{1/3} L_c} \Phi_2^{4/3}} \qquad (10)$$

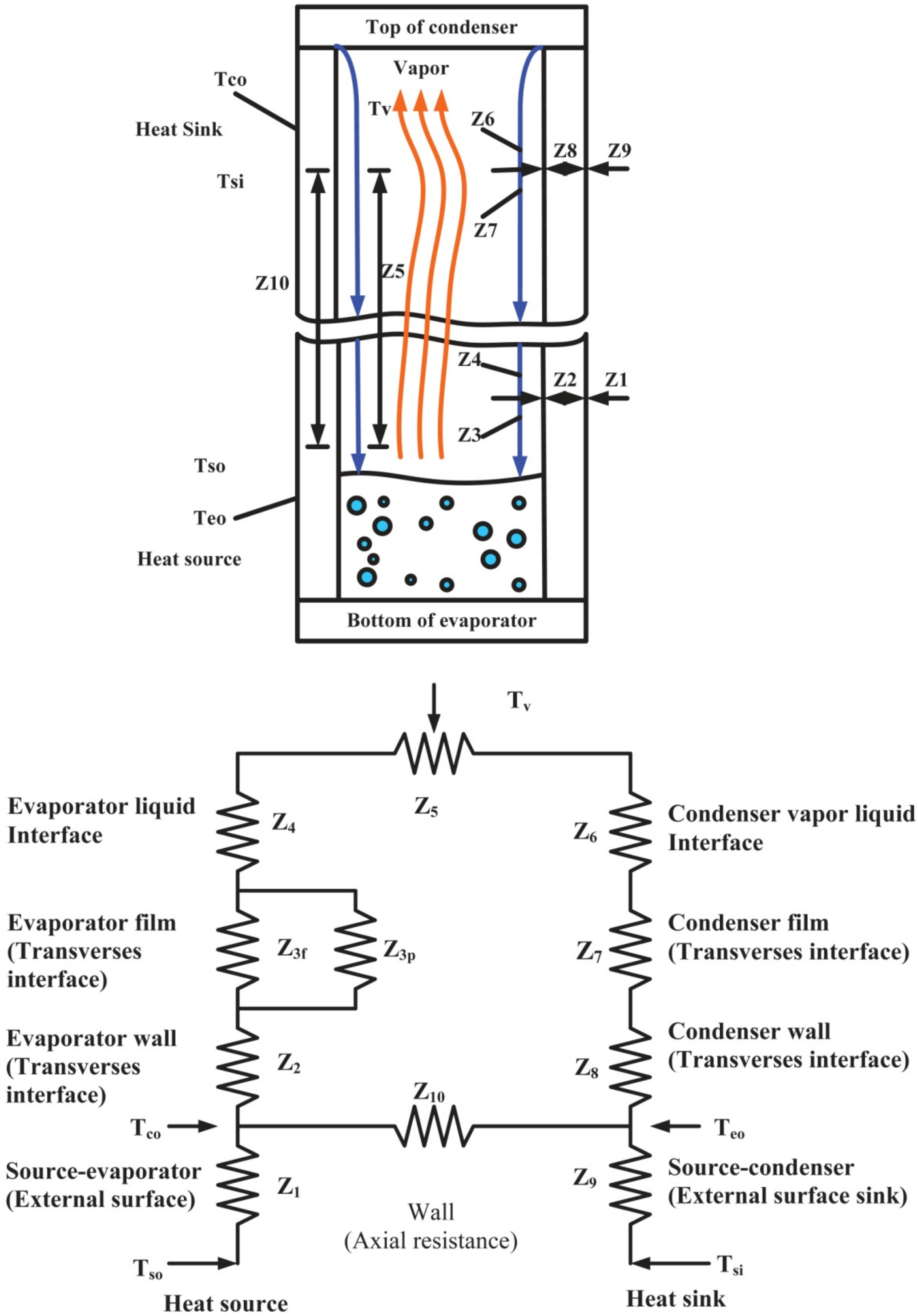

Figure 7 Model of total resistance of TPCT, ESDU 81038 [2]

Z_7 and Z_6 is resistance due to the phase change at the evaporator and condenser section respectively. Z_5 is resistance due to pressure drop along the pipe. Z_{10} is resistance due to heat conduction along the axial pipe. Normally, Z_4, Z_5, Z_7 and Z_{10} are of small valve and can be negligible.

Thus Z_{Total} can be defined as;

$$Z_{Total} = Z_1 + \left[(Z_2 + Z_3 + Z_4 + Z_5 + Z_6 + Z_7 + Z_8)^{-1} + (Z_{10})^{-1} \right]^{-1} + Z_9 \qquad (11)$$

2.5. Heat transfer coefficients

The heat transfer coefficient ($h_{coefficient}$) or film coefficient, in ALT/CV and in mechanics is the proportionality constant reciprocal the thermal resistance (Z_{Total}) and the thermodynamic driving force for the flow of heat [15-17]. The $h_{coefficient}$ can be evaluated using the following equation;

$$h_{coefficient} = \frac{1}{Z_{Total}} \qquad (12)$$

where, the data on temperature wall distributions, vapour temperature and thermal load were measured. The $h_{coefficient}$ has been referenced by many researchers [10-13]. Thus, this section focuses on pool boiling dynamics in evaporator section of ALT/CV. The $h_{coefficient}$ is an enhancement thermal performance in two phase transfer with nanofluids containing surfactant [18-20] under condition shown in Table 3.

2.6. Heat transfer rate analysis in prototye of oven an advanced loop thermosyphon (OALT/CV)

During the experiments, the variable parameter was controlled in order to calculate the heat transfer rate characteristics of OALT/CV using the calorific method. The following equations were used to calculate the actual heat transfer rate (Q_{act}) in equation (13), with maximum heat transfer rate $(Q_{\max})$ in equation (14), and then for error analysis recently compiled by Paramatthanuwat et al., [3] as follows:

$$Q_{act} = \dot{m}C_p\left(T_{in} - T_{out}\right) \tag{13}$$

and ;

$$Q_{\max} = \dot{m}C_p\left(T_e - T_c\right) \tag{14}$$

thus ;

$$Q = f\left(\dot{m}, T_e, T_c, T_{in}, T_{out}\right) \tag{15}$$

However, the ALT/CV and OALT/CV with a fin does not have a theoretical/mathematicical model to predict heat transfer rate at this point in time. Thus, the $Q_{\max}$ in equation (14) was compared with the theory about the heat rate of convection from the fin in equation (16) from Dewitt [21] as follows:

$$Q_{pre} = h\left[N\eta_f A_f + \left(A_t - NA_f\right)\right]\theta_b = hA_t\left[1 - \frac{NA_f}{A_t}\left(1-\eta_f\right)\right]\theta_b \tag{16}$$

Every temperature inside the oven is associated with the convection transfer of OALT/CV. In particular, there is a similarity between the diffusion of heat and the heat transfer coefficient. Defining a heat transfer coefficient depends on the heat flux, that is heat flow per unit area and the thermodynamic driving force for the flow of heat convection in equation (17). Also, represented in equation (16), it is consistent with Newton’s law of cooling and also following Incropera FP [22];

$$h = \frac{Q}{A}\left(T_{air} - T\right) \tag{17}$$

whereas the parameter convection coefficient in equation (16) was assumed to be equal to Equation (17) and the efficiency of a single fin shown in Figure 41 (Chapter V). Moreover, the prime of surface (A) in equation (16) was fixed to be equal to equation (17). Due to Equation (16) having a rectangular geometry it is similar to the loop thermosyphons which have convection heat transfer. The theorem equation (14) and equation (16) was similar. Due to the rectangular shape of the source resembling the ALT/CV from Equation (16), it was determined from this theory.

3. Dimensionless [2, 16, 23, 24]

A dimensionless quantity is a quantity without an associated physical dimension. It can be obtained from the relationship between a variable and a focused property for a particular phenomenon which occurs inside a ALT/CV. A dimensionless term in ALT/CV system, in practice, is defined by a fluids' behaviour, for example, flow of phase fluid, boiling point, condensation, exertion of buoyancy force or etc [23, 25]. A dimensionless quantities study can be explained as follows into 4 groups in Figure 8:

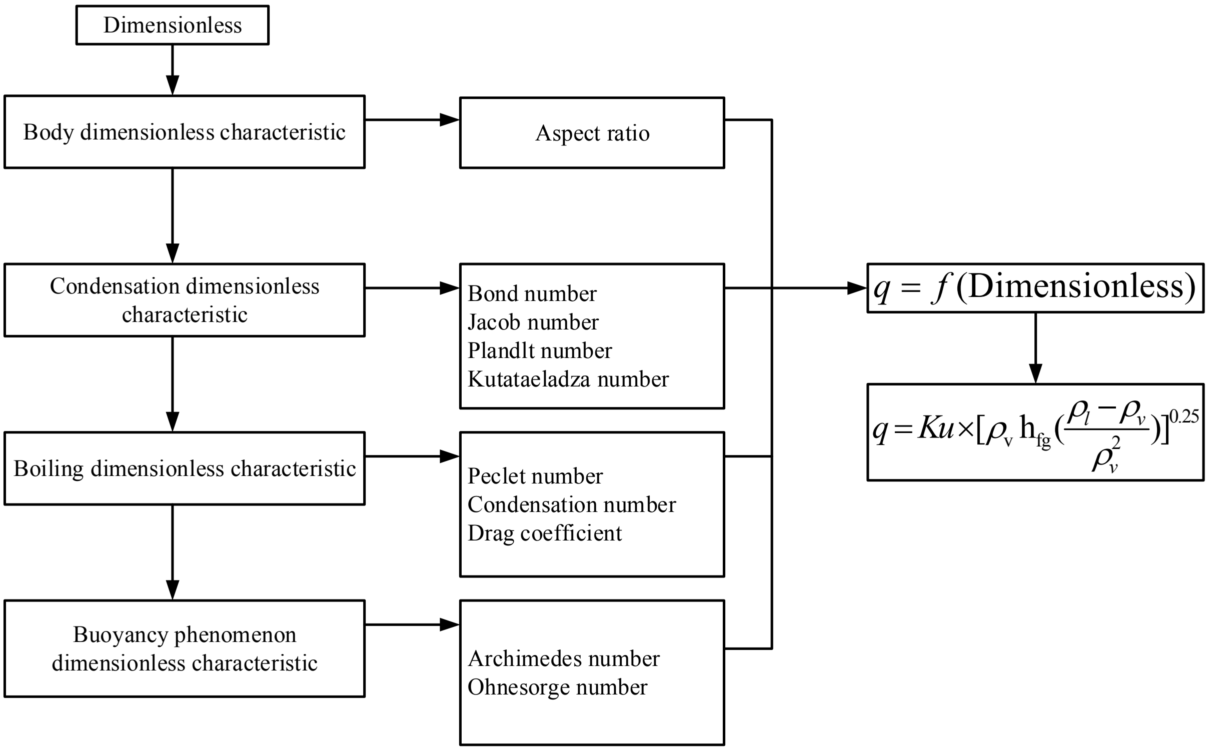

Figure 8 Dimensionless diagram

3.1. Body dimensionless characteristic

Aspect ratio represents the distance of physical motion for a working fluid (liquid and vapour). When the aspect ratio increased the heat transfer rate rose phenomenonlly. Therefore, the larger aspect ratio leads to pool boiling which occurs with the highest heat transfer rate. However, the phenomenon that approaches the inside of a confined channel has a lower heat transfer rate. The aspect ratio can be defined as the following equation (18):

$$Aspect\,ratio = \frac{L_e}{D_i} \tag{18}$$

3.2. Boiling dimensionless characteristic

Bond number (Bo) is the ratio of buoyancy force to the surface tension force. Bo can be used to explain boiling phenomenon inside an evaporator section and the state of the vapour bubbles nucleation. If the bond number reaches a threshold level for a particular liquid, then boiling occurs. Bo can be defined as the equation (19);

$$Bo = D_i [\mathrm{g} \frac{\rho_l - \rho_v}{\sigma}]^{0.5} \tag{19}$$

Jacob number (Ja)is the ratio of latent heat to sensible heat of the working fluid. It represents the ability of the phase change in the working fluid. When the working fluid's inner tube obtains heat, then heat has been transferred by a condensation dye to the latent high heat: Therefore, it can be transferred from one end of point to another end point with only a little change in temperature. The denominator is the heat of liquid film. Jais defined by the equation (20);

$$Ja = \frac{h_{fg}}{C_{pl} T_v} \tag{20}$$

Plandlt number (Pr) is the ratio of momentum diffusivity to the thermal diffusivity of liquid. It represents convection heat transfer in a tube that occurs when the vapour bubble moves from the evaporator section to the condenser section. As heat is collected, the vapour's heat transfer and density of heat flux will be enhanced with a high Pr. It can be defined by the equation (21):

$$\mathrm{Pr} = \frac{u_l C_{pl}}{k_l} \tag{21}$$

Note that if all the Bo, Ja and Pr have their valves lower than 1; there will be no occurrence of phase change.

Kutataeladza number (Ku) is the ratio of the heat flux to the critical heat flux of fluid. Kuis usually applied as the coefficient corresponding to the critical pool boiling and is defined as the ratio of the critical heat flux and the properties of the working fluid. The critical pool boiling starts when the boiling nucleation state is reached. This is when the vapour bubbles begin to spread over the heating surface. In flow boiling, the boiling nucleation state and the after states may be also discussed as the important heat transfer mechanisms; it may therefore be justified to apply Ku in an empirical correlation for the flow boiling within a ALT/CV. It can be defined as follows (22):

$$Ku = \left[\frac{q}{[\rho_v \, h_{fg} (\frac{\rho_l - \rho_v}{\rho_v^2})]^{0.25}} \right] \quad (22)$$

3.3. Condensation dimensionless characteristic

Peclet number (Pe) is the ratio of bulk heat transfer rate to conductive heat transfer rate. It is defined to be the ratio of the rate of advection of a physical quantity of the flow to the rate of diffusion of the same quantity driven by an appropriate gradient. In other words, it is the transport of heat to condensation. There is also the extreme limit for the motion according to small and large Pe with the absence gravity. It was shown that when the Peof the continuous fluid is small, that of the dispersed phase is high. The initial non equilibrium temperature distribution results in the thermal boundary layers that develop on the inner sides of the interfaces of the drops. A temperature variation of Pe along the interfaces is encountered. The induced thermo-motion is strongly unsteady and it leads to either the spontaneous coagulation of condensation in a cold fluid or to the evaporator section. Pe can be defined as follows (23):

$$\mathrm{P}e = \frac{LV\rho C_p}{k} \quad (23)$$

Condensation number (Co) is the liquid density ratio and hence the gravitational component and homogeneous theory for the momentum component (heat flux divided by the product of mass flux and latent heat of vaporization). The higher the valve of Co the easier for the condensate to return to the evaporator section. Co can be defined as follows (24):

$$Co = \frac{h}{k} \left[\frac{\mu^2}{g\rho^2} \right]^{\frac{1}{3}} \quad (24)$$

Drag coefficient (Cd) is proportional to gravitational and internal forces that predict momentum heat transfer rates dependent on the physical motion. Cd is a dimensionless quantity that is used to quantify the drag or resistance of an object in a fluid environment such as air or water. It is used in the drag equation, where a lower Cd indicates the object will have less aerodynamic or hydrodynamic drag. The drag coefficient is always associated with a particular surface area. Cd can be defined as follows (25):

$$Cd = \frac{g(\rho - \rho_{\mathrm{f}})\mathrm{L}}{\rho V^2} \quad (25)$$

3.4. Buoyancy phenomenon dimensionless characteristic

Archimedes number (Ar) determines the motion of fluid and solids due to density differences. Ar is dependent on dimension. It predicts the boiling phenomenon approach of internal boiling inside. Arcan be defined as follows (26):

$$Ar = \frac{g(\rho_{\mathrm{s}}\mathrm{L}^3)}{\mu^2}(\rho_{\mathrm{s}} - \rho_l) \quad (26)$$

Ohnesorge number (Z) is proportional to viscous force and to inertial force with surface tension. Zis generally used in momentum heat transfer rates and atomization. Z can be defined as follows (27):

$$Z = \frac{\mu}{(\mathrm{g}\,\rho\,\mathrm{L}\,\sigma)^{\frac{1}{3}}} \quad (27)$$

The above-stated dimensionless numbers were correlated with Ku in the form of function (28) to calculate the convection heat transfer capacity of one tube.

$$q = f(\text{Dimensionless}) \quad (28)$$

Thus:

q is heat flux, its equivalent Kutataeladza number (Ku) can be correlated in equation (29)

$$q = Ku \times [\rho_{\mathrm{v}}\, \mathrm{h}_{\mathrm{fg}} (\frac{\rho_l - \rho_v}{\rho_v^2})]^{0.25} \qquad (29)$$

From Equation (28) and (29) the heat flux and the ALT/CV at a vertical position can be evaluated. This will be shown in chapter 4.

4. Nanofluids[2]

A nanometer, 10^{-9} m, is about ten times the size of the smallest atom, such as hydrogen and carbon. However, a micron is barely larger than the wavelength of visible light, thus invisible to the human eye. A millimeter, the size of a pinhead, is roughly the smallest size available in present day machines. The range of scales from millimeters to nanometers is one million, which is also approximately the range of scales presently used in mechanical technology. From the largest skyscrapers to the smallest conventional mechanical machine parts.

Nanofluids are solid-liquid composite materials consisting of solid nanoparticles or nanofibers with typical sizes of 1-100 nm suspended in liquid. Nanofluids have attracted great interest recently due to reports of greatly enhanced thermal properties. For example, Table 5 to Table 7 show silver nanoparticle properties, a small amount (<1%volume fraction) of Ag nanoparticles or carbon nanotubes dispersed in ethylene glycol or oil, is reported to increase the inherently poor thermal conductivity of the liquid by 40% and 150%, respectively. Conventional particle-liquid suspensions require higher concentrations (>10%) of particles to achieve such enhancement. However, problems of theology and stability are amplified at high concentrations, precluding the widespread use of conventional slurries as heat transfer fluids. In some cases, the observed enhancement in thermal conductivity of a nanofluids in order of magnitude, were larger than predicted by well-established theories. Other perplexing results in this rapidly evolving field include a surprisingly strong temperature dependence of the thermal conductivity and a three-fold higher critical heat flux compared with the base fluids [26].

Table 5 Silver nanoparticle properties [2]

General properties	
Name, symbol, atomic number	silver, Ag, 47
Element category	transition metals
Standard atomic weight	107.8682 $g\cdot mol^{-1}$
Electron configuration	$4d^{10}\ 5s^{1}$
Electrons per shell	2, 8, 18, 18, 1
Physical properties	
Color	silver
Phase	solid
Density (near r.t.)	10.49 $g\cdot cm^{-3}$
Melting point	1234.93 K
Boiling point	2435K
Heat of fusion	11.28 $kJ\cdot mol^{-1}$
Heat of vaporization	250.58 $kJ\cdot mol^{-1}$
Specific heat capacity	25.350 $J\cdot mol^{-1}\cdot K^{-1}$(25°C)

Table 6 Vapour pressure of silver nanoparticles [2]

Vapour pressure						
P(Pa)	1	10	100	1 k	10 k	100 k
at T(K)	1283	1413	1575	1782	2055	2433

Table 7 Silver atomic properties [2]

Atomic properties	
Crystal structure	face-centered cubic
Crystal structure	1, 2, 3 (amphoteric oxide)
Electronegativity	1.93 (Pauling scale)
Ionization energies	1st: 731.0 kJ/mol 2nd: 2070 kJ/mol 3rd: 3361 kJ/mol
Atomic radius	144 pm
Covalent radius	145±5pm
Van der Waals radius	172 pm
Miscellaneous	
Magnetic ordering	diamagnetic
Electrical resistivity	15.87 nΩ·m(20°C)
Thermal conductivity	429 W·m−1·K−1(300K)
Thermal diffusivity	174 mm²/s(300 K)
Thermal expansion	18.9 µm·m−1·K−1(25°C)
Speed of sound (thin rod)	2680 m·s−1(r.t.)

4.1. Rheological properties of nanofluids [2, 27]

Rheological properties have a very important role in fluids flow. During application, nanofluids are likely to flow either by forced or natural convection and the flow properties such as viscosity are therefore, the essential to the study of suspensions containing particles the size of nanofluids. Rheology is defined as the study of the deformation of flow materials. When force is applied to a liquid, the liquid will flow to relieve the strain from this force. Different systems will resist this flow more than others, so this resistance is the measurement of the viscosity of the system [28, 29]. Newton first introduced a basic model to show the flow measurement of the liquid between two parallel platesas shown in Figure 9

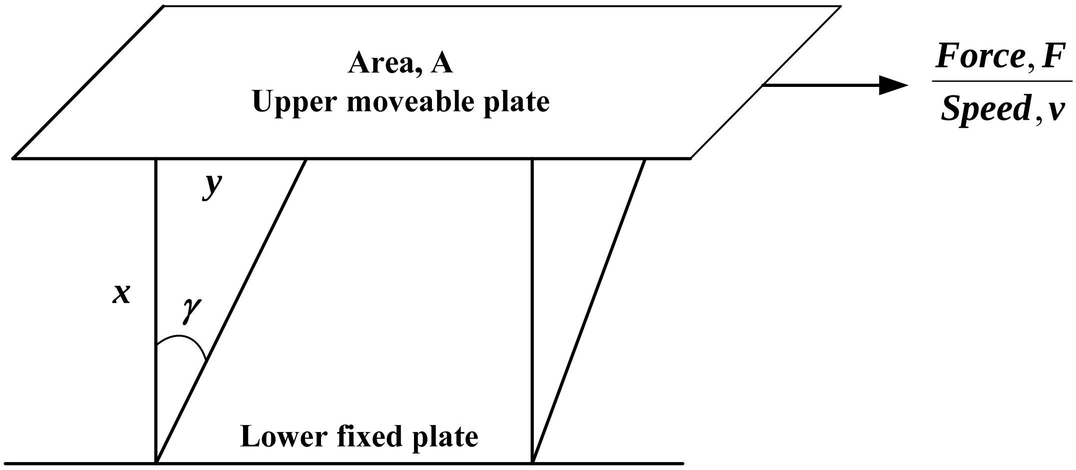

Figure 9 Rheology diagram analysis [29]

Using this model a number of common Rheology terms can be defined as follows:

Shear Stress (*SS*), the force experienced by the liquids is proportional to the area of the upper plate. SS is defined by the equation below;

$$\sigma = \frac{F}{A} \tag{30}$$

When: σ is shear stress, Nm^{-2}or Pa. F isforce, $m{\cdot}s^{-1}$. And A isarea upper moveable plate, m^2.

Shear Rate (*SR*), the velocity gradient or the rate of change of velocity at which one layer passes over an adjacent layer. SR is defined by equation below:

$$\gamma = \frac{dv}{dx} \tag{31}$$

When: γ is shear rate, s^{-1}. dv is the velocity of the moving plate, $m{\cdot}s^{-1}$. dx is the distance between the two parallel plates, *m*.

Shear Viscosity (*SV*) is expressed mathematically as,

$$\eta = \frac{SS}{SV} \tag{32}$$

The measurement was the resistance to the flow of liquid. Pascal.second (*Pa.s*) is the basic unit of *SV* but poise or centerpoise (*cp* is one hundredth of a Poise) is often used and one *cp* is equivalent to a millpascal second, *mPa.s*. When quoting *SV* the *SR* (measurement method/equipment used) should be stated together with the temperature at which the measurement was taken [28].

All materials that show flow behaviour are referred to as fluid. In all fluids, there is a frictional force between the molecules and, therefore display, curtain flow resistance which can be measured as a viscosity. The *SV* is a transporting property which refers to the resistance of material flow. When dealing with nanofluids, we are tempted to consider the dispersed medium under question, as ahomogeneous fluid characterized by the properties such as density and viscosity. This in turn, will only require a single set of mass and momentum conservation equation. However, such a simple picture will not provide a useful enough case where the fluid is unsteady and non-uniform [29].

4.2. Newtonian flow behaviour [2, 27]

Isaac Newton found that the shear force acting on a liquid is proportional to the resulting flow velocity. Hence, a fluid is said to be Newtonian if the viscosity remains constant with an increase in SR. Newtonian flow behaviour is observed in flow molecular liquids such as water, mineral oil (without polymer additives) and solvents. However, more complex flow behaviour is expected for fluid containing suspended particles [30]. Newtonian can be showed as in Figure 10.

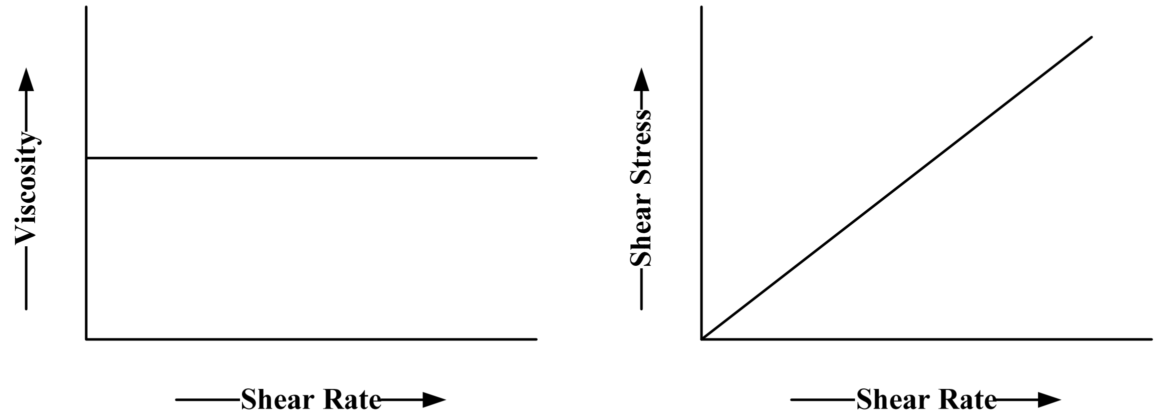

Figure 10 Newtonian fluid flow behaviour diagrams[28, 29]

4.3. Non-Newtonian flow behaviour [2, 27]

Fluids, whose SV changes with an increase in SR, are referred to as Non-Newtonian. These fluids could be further classified according to their flow behaviour. Shear-thinning and shear thickening flow behaviour is discussed in the following sections.

4.4. Shear-thinning flow behaviour [2, 27]

Shear-thinning or Pseudoplasticity, for samples that display shear-thinning behaviour, the SV is dependent on the degree of shear load (SL). Thus, the viscosity decreases with an increase in SS. In dispersions, shearing can cause the particles to change the flow direction and also the direction of the flow gradient. This can lead to disintegration of agglomerates or change in particle form. The interaction forces between particles may decrease during the process and cause a lowering in the flow resistance [30]. Shear thinning as shown in the Figure 11.

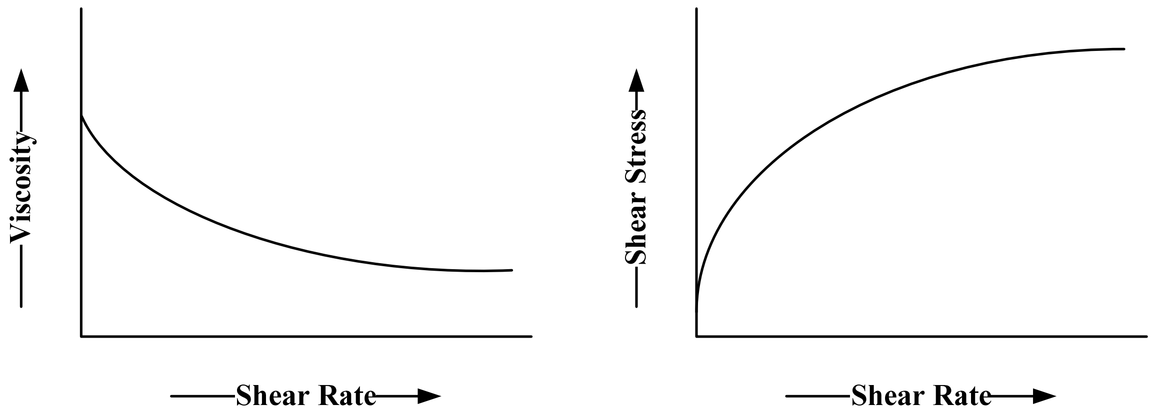

Figure 11 Shear-thinning flow behaviour diagrams[28, 29]

4.5. Shear-thickening flow behaviour [2, 27]

Shear-thickening is similar to shear-thinning fluids; the SV of sample displaying shear-thickening behaviour is also dependent on the degree of SL. Thus, the viscosity decreases but increases in SS. With highly concentrated suspension, the probability of particle interaction is much higher and may result in particles becoming wedged together thus increasing flow resistance. The particle shape plays an important role as, during the shearing process, the particle moves and rotates. For example, cube-shaped particles add more volume when rotating than spherical particles. Hence less free space is available for the liquid between the particles [28, 29]. Shear-thickening as shown in Figure 12.

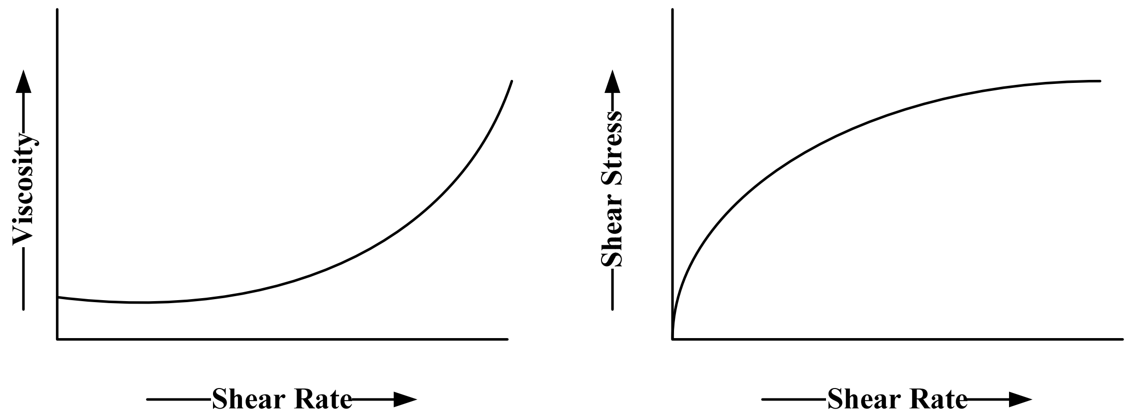

Figure 12 Shear-thickening diagram[28, 29]

4.6. Yield point [2, 27]

The yield point or yield stress refers to an external force required before a material will start to flow. A typical example is toothpaste; a certain amount of force must be applied before the toothpaste starts to flow [29]. The materials with yield point tend to flow in homogeneously.

4.7. The rheological properties analysis [2, 27]

This section describes the analysis model function; Newtonian and Non-Newtonian.

Newtonian behaviour flow behaviour is described formally using Newton's law and is defined as follows [29, 30];

$$\sigma = \gamma \cdot \eta \qquad (33)$$

When: σ is shear stress, Nm^{-2}or Pa. γ is shear rate, s^{-1}. η is viscosity, Pa.s.

Non-Newtonian behaviour for shear thinning and shear thickening flow behaviour, three model functions are required for flow without a yield point. The curved model function can be defined as follows [28, 30]:

$$\sigma = c \cdot \eta^{p} \qquad (34)$$

When: σ is shear stress, Nm^{-2} or Pa. c isthe flow coefficient (or power law index) Pa.s. p is the exponent, the following applies:

$p < 1$ for shear thinning.

$p > 1$ for shear thickening.

p = 1 for Newtonian behaviour.

4.8. The yield point flow curve analysis [2, 27]

The Bingham flow model can be defined as follows:

$$\sigma = \sigma_B + \eta_B \cdot \gamma \qquad (35)$$

When σ_B is the Bingham yield point. η_B is the Bingham flow coefficient as shown below in Figure 13

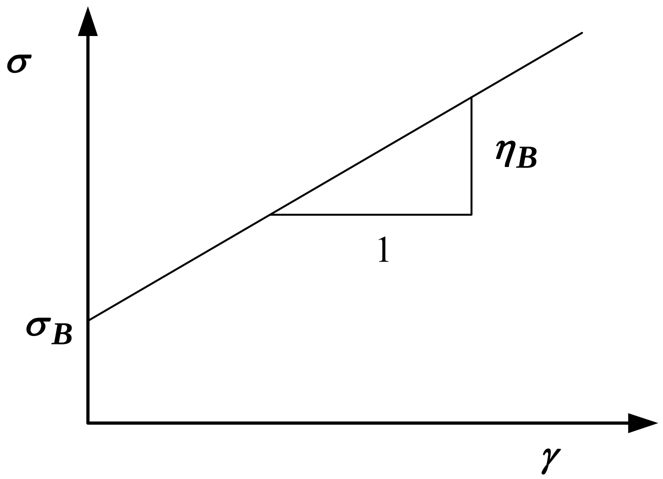

Figure 13 Flow curve according to Bingham

The viscosity of nanofluids can also be estimated with well known formulae. Nevertheless, a more reliable and direct way to calculate the viscosity is through experimental investigation [31].

4.9. Thermal conductivity of nanofluids [2, 27]

To use the Fourier's law, thermal conductivity of the material must be known. This property, which is referred to as a transport property, provides an indication of the rate at which energy is transferred by a diffusion process. This is dependent on the physical structure of: matter, atomic and molecular and is considered to be the state of the matter. This section considers various forms of matter identifying important aspects of behaviour and applying them to nanofluid thermal property valves. Fourier's Law can be defined as [32]:

$$k = -\frac{q_x^{''}}{\partial T / \partial x} \tag{36}$$

When: k is thermal conductivity, W·(m·K)-1. $q_x^{''}$ is heat flux, W·m^{-2}. Tis temperature, K.

Thermal conductivity shows a key role in the enhancement of the heat transfer performance of a heat transfer fluid. Since the thermal conductivity metals are much higher than that of fluids, the suspension containing ultra-fine metal particles are expected to show improved heat transfer properties. It was found that the thermal conductivity of a nanofluid affected the volume fraction, the size and the shape of the nanoparticle suspension in the liquid, as well as the distribution of the dispersed particle [23, 33].

4.10. Theory of nanofluids thermal conductivity [2, 27]

As the thermal conductivity of nanofluids theory is non-existent, scientists have used an existing model for estimating this theory. The Maxwell model was developed to explain the heat transfer characteristics of larger particles in nanofluids research. This Maxwell model has served as a foundation in the development and explanation of a much higher conductivity increase observed in nanofluids. The effective thermal conductivity (k_{eff}) can be defined by [34]:

$$k_{eff} = \frac{k_p + 2k_l + 2(k_p - k_l)\phi}{k_p + 2k_l - (k_p - k_l)} k_l \tag{37}$$

When: k_p is thermal conductivity of particle. k_l is thermal conductivity of liquid. ϕ is volume fraction of suspension.

Thus, the ϕ can be defined by;

$$\phi = \frac{v_p}{v_p + v_l} \tag{38}$$

When: v_p is volume of nanoparticles in fluid. v_l is defined as volume of base fluid.

The thermal conductivity plays a role in the heat transfer enhancement of fluids. It is higher in the solid metals than in liquids. The contained nanoparticles in suspension are expected to improve the thermal properties. Consequently, the Maxwell model shows that the effective thermal conductivity of fluids containing ultra-fine particles, depend on the thermal conductivity of the spherical particles, the base liquid and the volume fraction of the solid particles [23, 34].

4.11.The contact angle [2, 27]

The contact angle is the angle of liquid or vapour which meets the interface on a solid surface. It is this specific characteristic of most systems to determine the interactions across the three interfaces. The contact angle of a small liquid droplet which is resting on a flat horizontal solid surface shows the role of a boundary condition. It is measured by using a contact angle goniometry. It does not have a high boundary limitation on a liquid or a vapour interface, thus it can be equally applied between two liquids or two vapours. In the case of a molecule at or near the surface of a liquid, the attracting forces will no longer balance out and the molecule will experience a resultant force inwards. Due to this effect, the liquid will tend to take up a shape with a minimum surface area [14]. In the case of a free-falling drop in a vacuum, this would become a sphere. Due to this spontaneous tendency to contract, a liquid surface behaves like a rubber membrane under tension. In order to increase the surface area, this work must be done on the liquid. The energy associated with this work is known as the free surface energy. The corresponding free surface energy per unit surface area is given the symbol, σ_l Figure 14which shows the surface tension and the pressure difference across a curved surface. In Figure 14a, the area is increased by moving one side a distance dx and the work done is equal to Fdx, hence the increased energy is $2\sigma_l / dx$.

Factor 2 arises since the film has two free surfaces. Hence, if T is the force per unit length for each of the two surfaces $2T_l dx = 2\sigma_l / dx$ or $T = \sigma_l$ This force per unit length is known as the surface tension. It is numerically equal to the surface energy per unit area measured in any consistent set of units, e.g. N/m. Since the latent heat of vapourization, L , is a measurement of the forces of attraction between the molecules of a liquid we might expect surface energy or surface tension σ_l to be related to L . This is found to be the case. Solids will also have a free surface energy and, in the magnitude, it is found to be similar to the valve for the same material in the molten state.

Figure 14b shows that a liquid is in contact with a solid surface. Molecules in the liquid adjacent to the solid will experience forces from the molecules of the solid, in addition to the forces from other molecules in the liquid. Depending on whether these solid/liquid forces are attractive or repulsive, the liquid/solid surface will curve upwards or downwards.

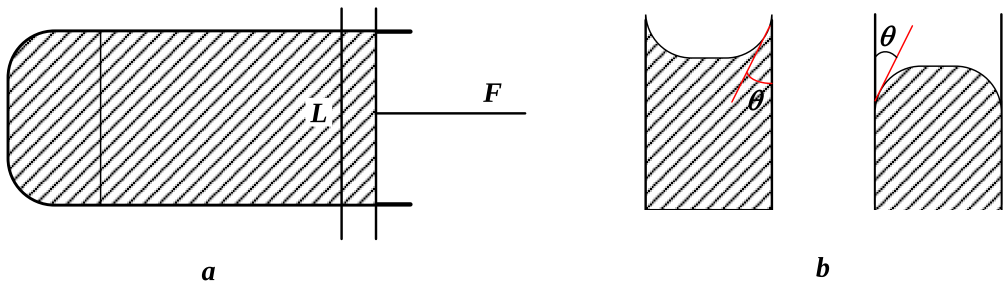

Figure 14 Surface tension and pressure difference across a curved surface [14]

For example, two attractive and repulsive forces are water and mercury. The attractive forces are the forces when the liquid is wetter than the solid. The angle of contact made by the liquid surface with the solid is known as a contact angle, θ .For wetting, θ will lie between 0 and $\frac{\pi}{2}$ and for non-wetting liquid, $0 > \frac{\pi}{2}$, as indicated in Figure 15 Wetting and non-wetting contact angle [14]

The wetting condition occurs when total surface energy is reduced by wetting;

$$\sigma_{sl} + \sigma_{lv} < \sigma_{sv} \quad (39)$$

The non-wetting will not occur is defined as;

$$\sigma_{sl} + \sigma_{lv} > \sigma_{sv} \quad (40)$$

The intermediate condition of partial wetting is defined as;

$$\sigma_{sl} + \sigma_{lv} = \sigma_{sv} \quad (41)$$

When: s is solid. l is liquid. And v is vapour.

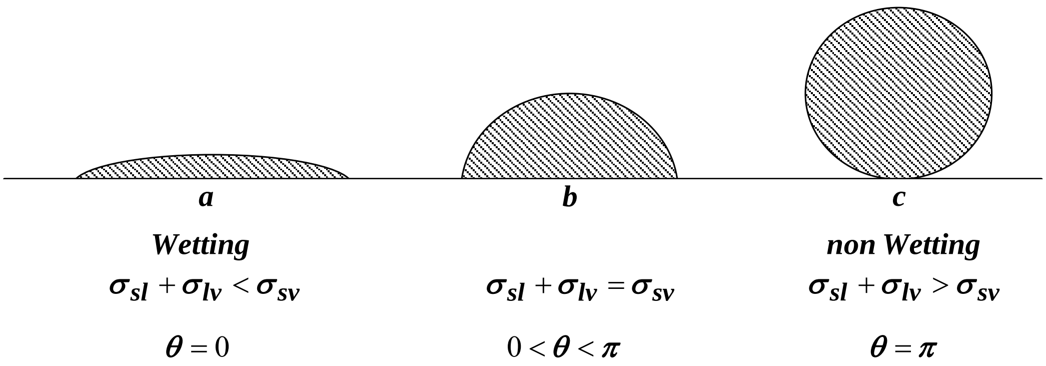

Figure 15 Wetting and non-wetting contact angle [14]

5. Surfactant [2]

Etymology - The surfactant term is a blend of surface active agent. Surfactants are usually organic compounds that are amphiphilic, meaning they contain both hydrophobic groups (their "tails") and hydrophilic groups (their "heads"). Therefore, they are soluble in both organic solvents and water. The surfactant term was coined by Antara products in 1950. In Index Medicus and the United States National Library of Medicine, "surfactant" is reserved for the meaning pulmonary surfactant. For the more general meaning, "surface active agent" is the heading as shown in Figure 16.

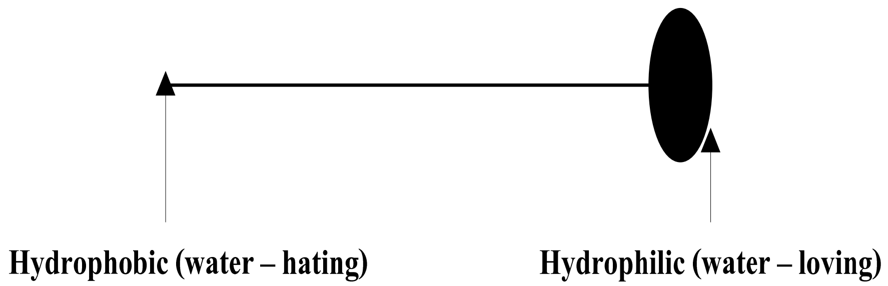

Figure 16 Surfactant[2]

Properties - Surfactants reduce the surface tension of water by adsorbing at the liquid-gas interface. They also reduce the interfacial tension between oil and water by adsorbing at the liquid-liquid interface. Many surfactants can also assemble in the bulk solution into aggregates. Examples of such aggregates are vesicles and micelles. The concentration at which surfactants begin to form micelles, is known as the critical micelle concentration or CMC. When micelles form in water, their tails form a core that can encapsulate an oil droplet and, their (ionic/polar) heads form an outer shell that maintains favorable contact with water. When surfactants assemble in oil, the aggregate is referred to as a reverse micelle. In a reverse micelle, the heads are in the core and the tails maintain favorable contact with the oil. Surfactants often classified into four primary groups; anionic, cationic, non-ionic and zwitterionic (dual charge). Thermodynamics of the surfactant systems are of great importance, theoretically and practically. This is because surfactant systems represent systems between ordered and disordered states of matter. Surfactant solutions may contain an ordered phase (micelles) and a disordered phase (free surfactant molecules and/or ions in the solution). Ordinary washing up (dish washing) detergent for example, will promote water penetration in soil, but the effect would only last a few days (many standard laundry detergent powders contain levels of chemicals such as sodium and boron, which can be damaging to plants and should not be applied to soils). Commercial soil wetting agents will continue to work for a considerable period, but they will eventually be degraded by soil micro-organisms. Some can however, interfere with the life-cycles of some aquatic organisms, so care should be taken to prevent run-off of these products into streams and excess products should not be washed down.

Oleic acid - Oleic acid (Figure 17 and Table 8) is a mono-unsaturated omega - 9 fatty acid found in various animal and vegetable sources. It has the formula CH3(CH2)7CH=CH (CH2)7COOH). The trans-isomer of oleic acid is called elaidic acid. The term oleic means related to, or derived from, oil or olive.

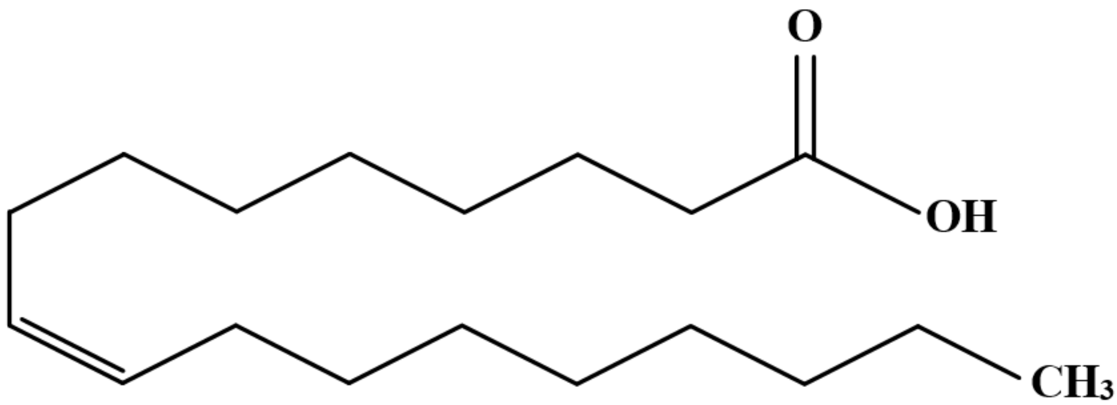

Figure 17 Chain of Oleic acids [2]

Table 8 Other names of oleic properties [2]

Oleic properties	
(9Z)-Octadecenoic acid	
(Z)-Octadec-9-enoic acid	
cis-9-Octadecenoicacid	
cis-Δ9-Octadecenoic acid	
Oleic acid	18:1cis-9
Molecular formula	C18H34O2
Molar mass	282.4614 g/mol
Density	0.895 g/mL
Melting point	13-14°C (286 K)
Boiling point	360°C (633 K) (760 mmHg)
Solubility in water	Insoluble
Solubility in methanol	Soluble

CHAPTER III SILVER NANOFLUIDS PROPERTIES

This chapter describes the results and discussions of silver nanofluids properties when preparingfor filled as working fluids in ALT/CV. It is divided into a number of sections to determine the thermal properties of silver nanofluids containing surfactant, as follows:

1. Literature review [35]

Cooling is one of the most important challenges facing numerous industrial sectors. Despite the considerable amount of research and development focusing on industrial heat transfer requirements, major improvements in cooling capability are still insufficient because conventional heat transfer fluids possess poor heat transfer properties. Nanofluids, which are engineered by suspending ultrafine metallic or non-metallic particles of nanometer dimensions in traditional cooling fluids, have shown great enhancement in thermal conductivity and convective heat transfer coefficiency [2, 11, 36, 37].

This section also contains the literature review for thermal properties. Many researchers have discussed the thermal properties points on which this study is based, together with the background of the research and explanations of the problems faced. This study highlights the theories and experiment for investigating the characteristics of thermal properties. Points of importance will be emphasized, with significance given to the properties of nanofluids and surfactants and their use in this experiment. Also included is the explanation of the characteristics of nanofluid behaviour in silver nanofluids containing surfactant. Thus, the researchers used different methods depending on the base fluids, nanofluid/nanoparticle type, etc. Recently, Thermal conductivity of 0.1 to 0.4% volume concentration silver (Ag) nanoparticles in water were investigated. The nanofluids were formulated using the ultrasonic vibration method for 3 hours and thermal conductivity enhancement showed 10% at0.4% of concentration [38]. Using a different method, the synthesis of silver nanofluids was performed using high-pressure homogenization with a volume fraction 0.1 to 0.3% in water. The highest thermal conductivity of the nanofluids showed an 18% increase at the concentration of 0.3%

[39]. Moreover, regarding the difference in base fluid, Ag nanofluids in toluene have shown 9% thermal conductivity enhancement with a very low loading of 1.10-3 vol% [40-43]. Consequently, nanofluids show better cooling capacity with respect to water in conventional heat pipes since nanoparticles can flatten the temperature gradient of the fluids and reduce the boiling limit [36, 40, 41]. In addition, the concentration of nanofluids may affect the enhancement of thermal conductivity. The studied silver nanofluids in ethylene glycol (EG) with 10,000 ppm concentrations showed 18% thermal conductivity enhancement [44]. Then, the investigated carbon black (CB) in deionized water with sodium dodecylsulfate (SDS) as well as Ag nanoparticles in silicon oil with oleic acid (OA), and with the maximum enhancement of thermal conductivity compared to the base liquid, was 9% for the wt% of the carbon black (CB) nanofluids and the wt% of the Ag nanofluids respectively [45]. The .1 wt% copper (Cu) aqueous nanofluids with 0.14 wt% of sodium dodecylbenzene sulfonate (SDBS) as surfactant can generate maximum thermal conductivity enhancement up to 10.7% [46].

The rheological behaviour of nanofluids is essential in establishing adequate application and design of processing. The 8 wt% titania nanoparticles in the EG showed Newtonian behaviour at a low shear rate, and the shear viscosity was strongly dependent on the temperature and concentration of the nanoparticles [47]. Then, the studied 1 vol% silver NP in ethanol with polyvinylpyrrolidone (PVP) was stabilized [48]. The rheological results suggest that the PVP helped to decrease the nanoparticle's size, resulting in low fluid viscosity and Newtonian fluid behaviour but remarkably high thermal conductivity. Meanwhile, the 4.38 vol% silver nanofluids in the diethylene glycol (DEG) showed Newtonian behavior at high viscosity [49]. However, different literature data have shown that nanofluids have non-Newtonian behavior, particularly at a low shear rates. The most important influence could be the effective particle concentration, the range of shear rate, and the viscosity of the base liquid [48]. Then, it was found that the TiO2 nanoparticle in the EG exhibited shear thinning behavior when the particle concentration was higher than ~2% [47]. The investigated shear thinning behaviour was 3% γ-Al_2O_3 and 10% TiO_2 in water [50]. Another main reason for the non-Newtonian behavior could be the aggregation of nanoparticles in the nanofluids. Lu reported that physical properties may change when the surfactant affects surface tension and viscosity. For instance, Al_2O_3

in water, at a 1:10 weight ratio with ammonium poly (PMAA-NH4), has demonstrated shear thinning behaviour (a decrease in viscosity with an increased shear stress rate), which yields a good dispersion rate when using PMAA suspension up to 47.5 %vol [51]. Then it was found that the 4 vol% of γ-Al_2O_3, TiO_2, and CuO nanofluids with 0.5 wt% of carboxymethyl cellulose (CMC) in deionized water containing up to 4 vol% of particle concentration showed non-Newtonian behaviour with shear thinning [52].

In this paper, 0.5 wt% silver nanoparticle-based aqueous nanofluids with oleic acid (OA) and potassium oleate surfactant (OAK^+) as surfactant were prepared by sonicating in water bath with a cooling technique for a period time of 12 hours. The effect of the additive concentration on the thermal properties was studied experimentally (Thermal conductivity, specific heat, density, viscosity, contact angle, and application of thermal enhancement), and the rheological behaviour (the correlation between shear stress and shear rate) was investigated experimentally and theoretically. Moreover, the heat enhancement cooling of the fluid (HEC) was investigated experimentally and it was confirmed that nanofluids/nanofluids containing surfactant could be used in the application of heat transfer. The methods of the experiment are briefly explained in section 2. Section 3 shows the experimental results and offers a discussion. The conclusions to the study are in section 4.

2. Materials and methods [35]

2.1. Nanofluids and thermal property study

Figure 18 shows a schematic diagram of the preparation the nanofluids. Water-based silver nanofluids were formulated with dry silver nanoparticles (Sigma-Aldrich, USA), OA, and OAK^+ (Sigma-Aldrich, USA) by using a two-step method [45, 53]. The 0.5, 1, and 1.5 wt%of OA and OAK^+ were added to the 0.5 wt% silver nanofluids, which showed controlled and variable parameters as seen in Table 1. After sonicating for 12 hours with a cooling technique, the particle size was measured using a nano-size particle analyzer (ZEN 3600 MALVERN, USA) in the range between 0.6 nm and 6.0 µm. The thermal properties of the nanofluids were measured using the hot-wire method (PSL Systemtechnik GmbH) from 20ºC to 80ºC. The rheological characteristics of the NF were analyzed using a Rheo-microscope Physica MCR301 (Anton Paar GmbH). The measurements were based on the controlled shear stress model with the stress ranging from 0.05 to 5 Pa. The maximum uncertainty was found to be 1.7% [2, 53, 54].

The rheological behaviour of the NF containing OAK^+ can be expressed with the power model in Eq. (42) with the viscosity as following the power law model indices less than n ≤ 1.

$$\eta = K\gamma^{n-1} \tag{42}$$

In Eq. (42), η is the apparent viscosity, γ is the shear rate, K is the consistency index, and n is the power law index. The power law index of the nanofluids decreases with increasing nanoparticles concentration, and increases with increasing temperature [52]. Apparently, the viscosity of the NF decreases as the shear rate increases.Thermal conductivity

The idea of thermal conductivity is non-existent in nanofluids theory scientists have used an existing model for estimated. The Maxwell model was developed to explain the heat transfer characteristics of larger particles in nanofluids research. This model has served as a foundation in the development and explanation of the much higher conductivity increase observed in nanofluids. The effective thermal conductivity (k_{eff}) can be defined by the following [34, 55]:

$$k_{eff} = \frac{k_p + 2k_l + 2\left(k_p - k_l\right)\phi}{k_p + 2k_l - \left(k_p - k_l\right)\phi} k_l \tag{43}$$

Thus, the ϕ can be defined by:

$$\phi = \frac{V_p}{V_p + V_l} \tag{44}$$

2.2. Contact angle instrument

In order to measure the contact angle of the sample fluids, the valves are required to be at room temperature. The temperature was controlled with a precision of ±1ºC. In this study, the drops of fluids were measured using a Contact Angle Meter Model: DM-CE1; Kyowa Interface Science. The accuracy was ±0.5° (repeatability described in standard deviation). The following liquids were used in the experiment: a copper plate with a diameter of 60 mm and a thickness of 0.3 mm were used as a test surface. A droplet of nanofluids was generated at a very low rate (1 μl/s) and detached from the syringe needle tip as soon as it touched the copper plate. Consecutive photographs were used to measure the contact angles. The spatial resolution was estimated to be about 50 μm on the basis of the focused area and camera pixel size. A video was taken while the droplet was spreading over the copper plate from initial contact to equilibrium position. The temporal resolution was estimated based on the frame speed of the CCD camera at 30 fps. For each concentration, three experiments were performed and the average was ascertained. The measurement settings were then adjusted and the software was initialized [16, 56].

2.3. Specific heat

The dynamic of specific heat was applied in the experiment. This was according to Rajabpour et al., [57] regarding the application of the theory model to nanofluids.

$$C_{p,\mathrm{nf}} = \phi C_{p,n} + (1-\phi) C_{p,\mathrm{bf}} \qquad (45)$$

This second model has served as a foundation in the development and explanation of the much higher specific heat observed in nanofluids from nanoparticles. The effective specific heat $(C_{p,eff})$ can be defined as follows [58]:

$$C_{p,eff} = \frac{\phi(\rho \mathrm{C}_p)_n + (1-\phi)(\rho \mathrm{C}_p)_{bf}}{\phi\rho_n + (1-\phi)_{bf}} \qquad (46)$$

The measurement uncertainty for the specific heat was calculated by propagating the precision uncertainties of all the individual measurements required to determine the specific heat in Equation (46) and can be defined as follows [58]:

$$\mu_{total} = \sqrt{\sum_{i}^{n} \left(\frac{\partial C_{p,sample}}{\partial x_i} \mu_i \right)^2} \quad (47)$$

Equation (46) and (47) should be noted that for Newtonian nanofluids. For the non-Newtonian fluid, the variation of the rheology does not depend on direct models but on the volume fractions of the nanoparticles [59, 60].

2.4. The heat transfer enhancement

Figure 19 shows a schematic diagram of the experimental apparatus, which consists of the heat enhancement cooling of the fluid (HEC) and peripheral devices. The heat enhancement cylinder was made from Stan less steel (AISI 304) with a diameter and height of 1,500 mm and 3,000 mm. The HEC was the heat source from the Stan less heater (2,000 Watt) with a diameter and height of 500 mm and 2,000 mm. The heat was supplied by circulating the Stan less through to HEC through to 20%, 40%, 60%, 80%, and 100% respectively of the heatsource. The cooling and pre-cooling section was heat sink from a cold bath. The cooling fluids are shown in

Table 2. Eighteen thermocouples were connected through a data logger (Yokogawa DX200 with ±0.1ºC accuracy, 20 channel input, and -200ºC to 1,100ºC measurement temperature range). Type K thermocouples (OMEGA with ±0.1ºC accuracy) were attached to the inlet, the outlet, and the surface of the heating and cooling as the HEC. The inlet temperature of the cooling fluids was maintained at 20ºCand a floating Rota meter (PLATON PTF2 ASS-C with a volumetric flow rate of 0.2 Liters/min - 1.5 liters/min) was used to control the flow rate of the cooling fluid during the experiments. During the experiment, the volumetric flow rate was set at 0.25 liters/min in order to calculate the heat transfer enhancement of the cooling fluid using the calorific method. The following equations (48,49 and 50) were used for calculating one of the heat-transfer rates and for error analysis [61].

$$Q = \dot{m}\, C_p \left(T_{out} - T_{in}\right) \tag{48}$$

Thus:

$$Q = f\left(\dot{m}, T_{out}, T_{in}\right) \tag{49}$$

The error analysis of the heat transfer can be obtained from [23]:

$$Q_{Error} = \left[\left(\frac{\partial Q}{\partial \dot{m}} \times \dot{m}\right)^2 + \left(\frac{\partial Q}{\partial T_{out}} \times T_{out}\right)^2 + \left(\frac{\partial Q}{\partial T_{in}} \times T_{in}\right)^2\right]^{0.5} \tag{50}$$

In order to experiment with a wide range of aspect ratios, the following parameters were corresponding set, as shown in Table 2, to formulate the heat transfer characteristics of the HEC [24].

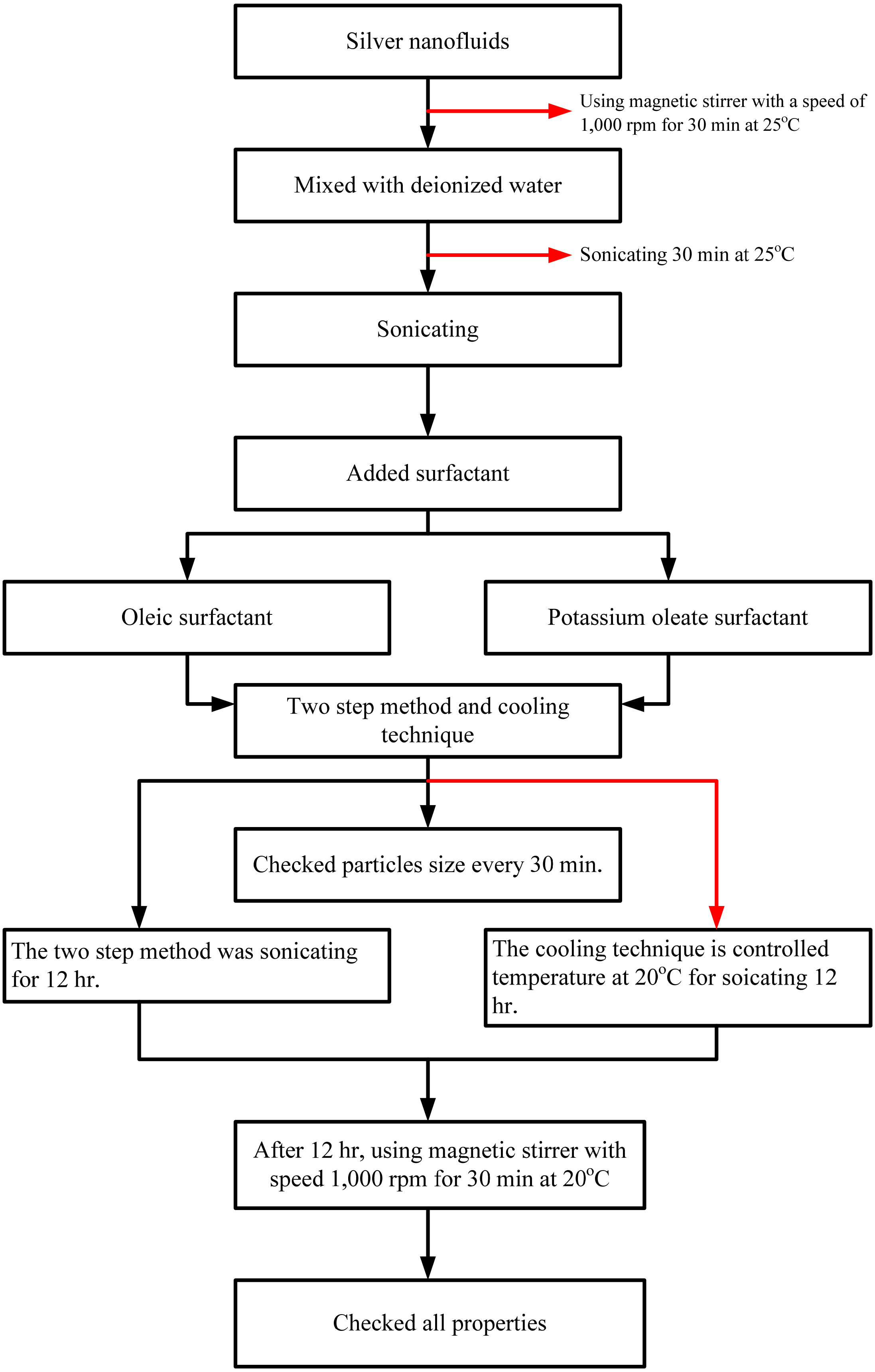

689

690 Figure 18 Shows the schematic diagram of preparation the nanofluids.

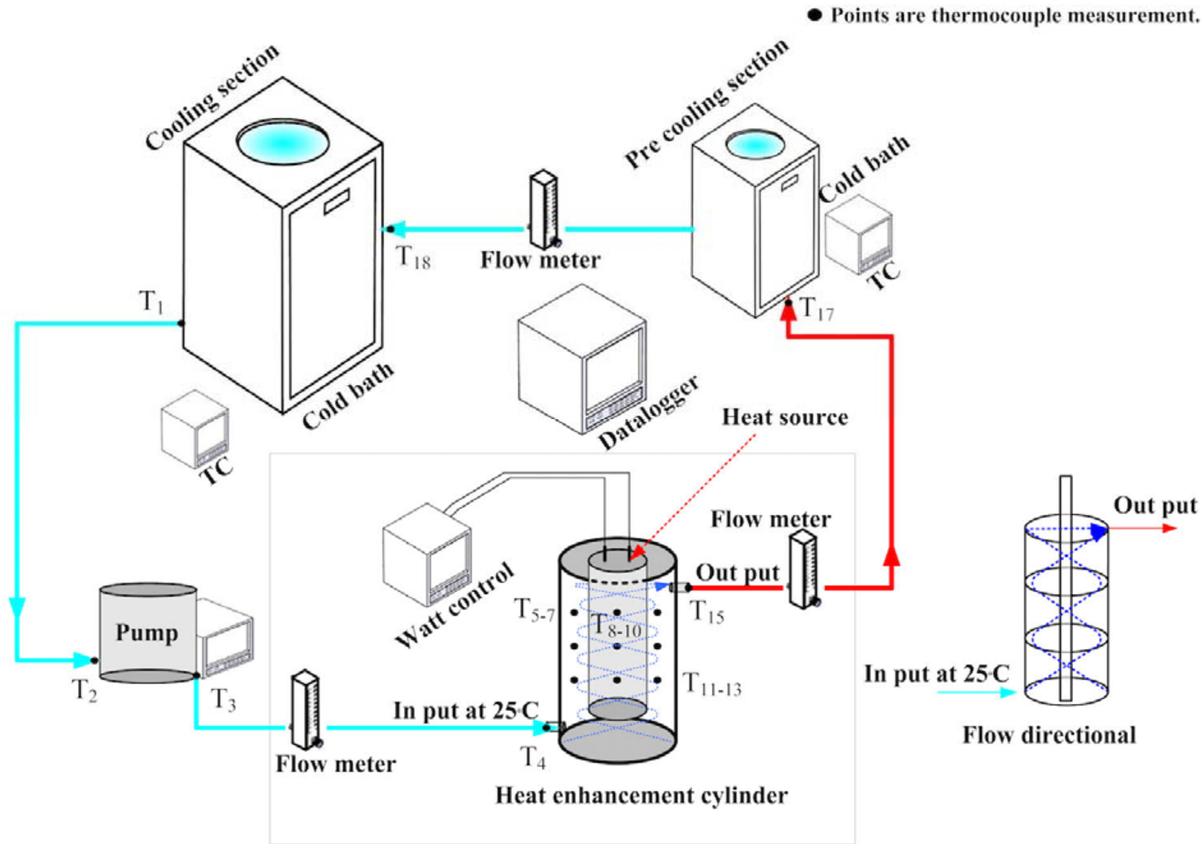

Figure 19 Schematic diagrams of the HEC experimental apparatus

3. Results and discussion

3.1. The nanoparticles size

Figure 20 shows the average particle size as a function of sonicating time. Zero point 5 wt%silver nanoparticles based nanofluids (NF) with surfactants as a stabilizer have an average particle size of ~100 and ~95 nm respectively. It can be seen that the average particle size decreases as sonicating time increases. Moreover, the red ellipse in

Figure 20a, NF+0.5OAK+ and NF+1OAK+ was seen to cause smaller particle size for a continuous period of 12 hours when compared with Figure 3b. This indicated that the two-step method and cooling technique did not break the agglomerate into primary particles [47, 62]. After sonicating for 12 hours, the sample was put into the TEM (Oxford Instruments) to check for average the particle size, as shown in

Figure 21a, suggesting that the size distribution of particles NF+1OAK+ was between 5 – 25 nm. The TEM image also shows that the long chains of potassium oleate combined with outside nanoparticles and prevented them from aggregating together [63, 64], which means that the viscosity and surface tension of the surfactant provided enough support to stabilize the dispersion of NP in deionized water [2].

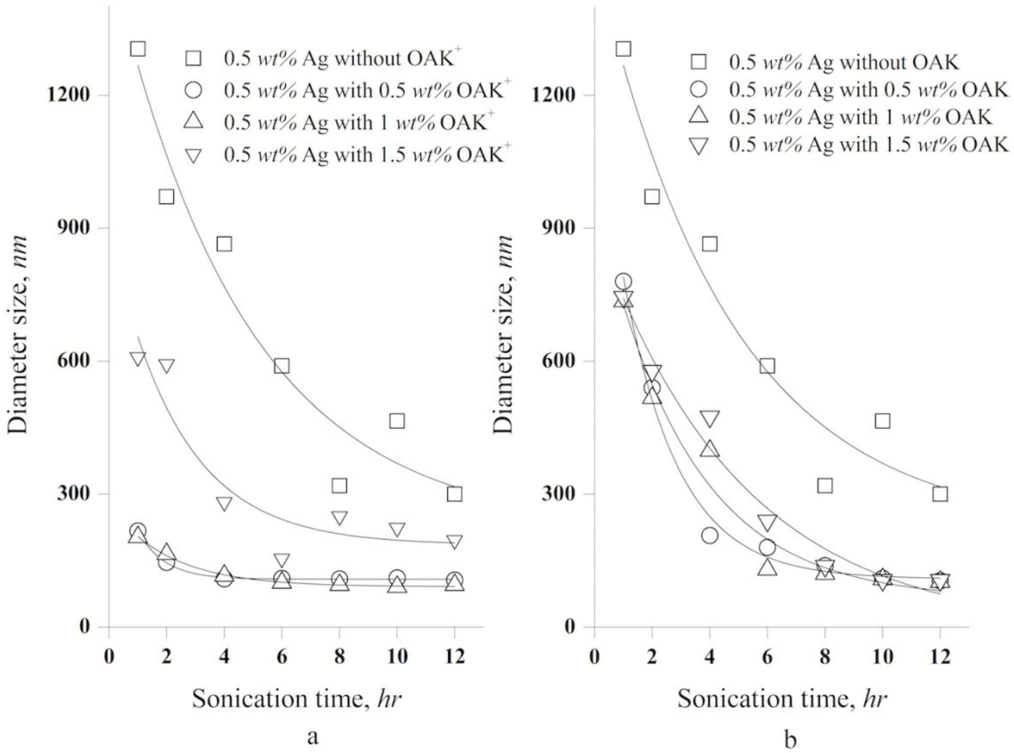

Figure 20 Relationship between sonication times and particle size

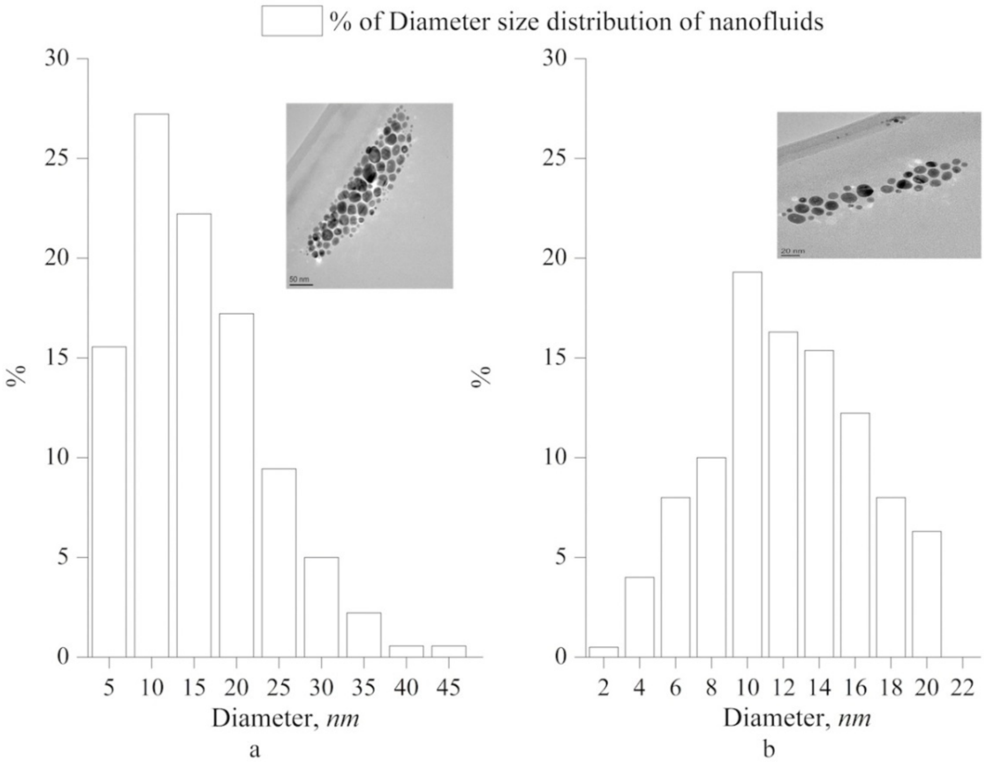

Figure 21 Relationship between Diameters with percentage of dispersed size and TEM micrograph at silver nanofluids containing surfactant at concentration 1 wt%

3.2. Rheological properties of nanofluids

The shear rate and shear stress had an effect on the rheological properties, such as viscosity. The rheological properties of the nanofluids containing surfactant are important to its thermo physical property. In this study, a surfactant was used to employ the NF's heat transfer rate. The OA and OAK+ are known for their ability to decrease viscosity and surface tension due to the organic and hydrocarbon interaction with oxygen which exists in deionized water [64, 65]. However, the case was compared with the same group of surfactant (OA and OAK^+) but with a difference in potassium salt (K^+). The potassium salt was helpful in balancing the pH valve of the liquid and dissolving the solutions of fat oil catalysis interaction with hydrogen. Thus, the OAK^+ has the ability to span the NP's random motion throughout the deionized water [2, 53, 66-68].

The rheology measurement results are shown in Figure 23 and the shear rates with the viscosity of silver nanofluids were measured at 30ºC according to Parametthanuwat et al., [2]. As shown in Figure 22, the viscosity of all samples decreased in the first 101s-1 to 103s-1 intervals and the NF showed Newtonian behaviour. This behaviour could have been caused by the change of concentration in the OA and OAK$^+$, which was 0.5, 1 and 1.5 wt%. The most preferable OAK$^+$ concentration was 1 wt%, which was sufficient to distribute the NP with the lowest and most stable viscosity. The long chain nature of the OAK$^+$ molecular structure helped to decrease the NF's surface tension. It was concluded that there was an apparent change in the viscosity of the NF and deionized water; however, the NF's viscosity was still larger than that of the deionized water when the shear rate rose [69] according to Equation (42) [52]. Thus, the NP existing in the deionized water containing OAK+, which affected the flowing behaviour of the nanofluids, was the main cause of the decrease in viscosity [70, 71]. The potassium salt which produces an effect properly surfactant was helpful in balancing the physical properties of the base liquid. As can be seen in Figure 23, along with the increasing shear rate, the nanofluids with OAK$^+$ concentration smaller or larger than 1 wt%possessed larger shear stress. From the cross point onward, all of the results of the OAK$^+$ were of almost the same valve and the R^2 was close to 1. This was in line with the study of Hojjat et al., [52], who stated that the transition metal in the same group with silver nanofluids containing OAK$^+$ produced the Newtonian fluid [2].

Figure 24 shows the viscosity of NF+1OA compared with 0.5 wt%NF+1OAK$^+$ as a function of shear rates. It was observed that for all operating temperatures and shear rate larger than 10^1s-1, the viscosity became stable and NF showed Newtonian behaviour. Thus, it was well established that for all operating temperatures, the system's rheological behaviour exhibited a similar trend. Figure 25 shows the relationship of the shear rates and shear stress in accordance with Figure 24. It could be explained that the higher temperature increased the intermolecular distances, which decreased the interaction between the molecular structures of deionized water and OAK$^+$, resulting in decreased viscosity and surface tension [47]. Obviously, the OAK$^+$ could help decrease the physical properties more than the OA. The surfactant behaved like an interfacial shell between the nanoparticles and base fluids and modified the surface tension of the nanofluids. The surface tension decreased when the concentration of surfactant increased [2, 72]. The OAK^+ exhibited good adsorption of the silver particles and the particles uniformly had a direct effect on the shear stress. The optimization of the chain length in group OA organic compounds was C18, which was effective for particle dispersing stabilization. The optimized length also improved the colloidal stability and increased the non-precipitation period for the nanoparticles to be uniformly dispersed [45, 63, 73]. Moreover, OAK^+ achieved more stable suspension than the pure NP did in the deionized water. This might be related to the Newtonian property of the nanofluids observed in this study when the rheological properties were observed at operating temperature [2, 53, 74, 75].

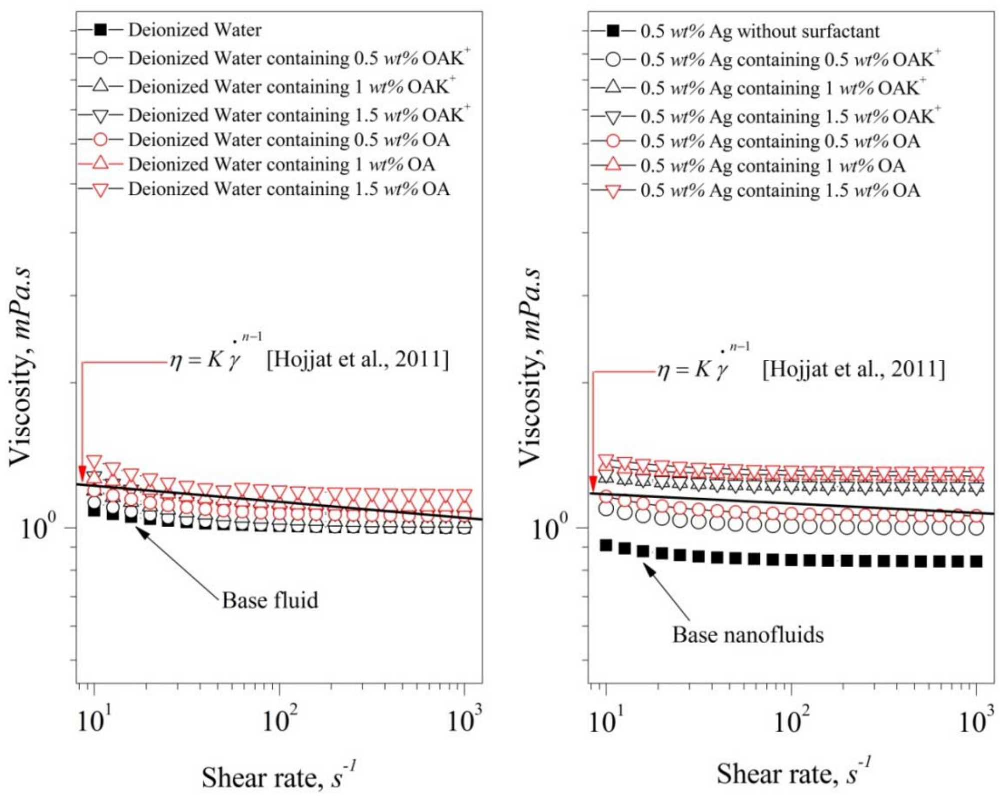

Figure 22 Relationship between shear rates with viscosity of silver nanofluids at operating temperate 30°C

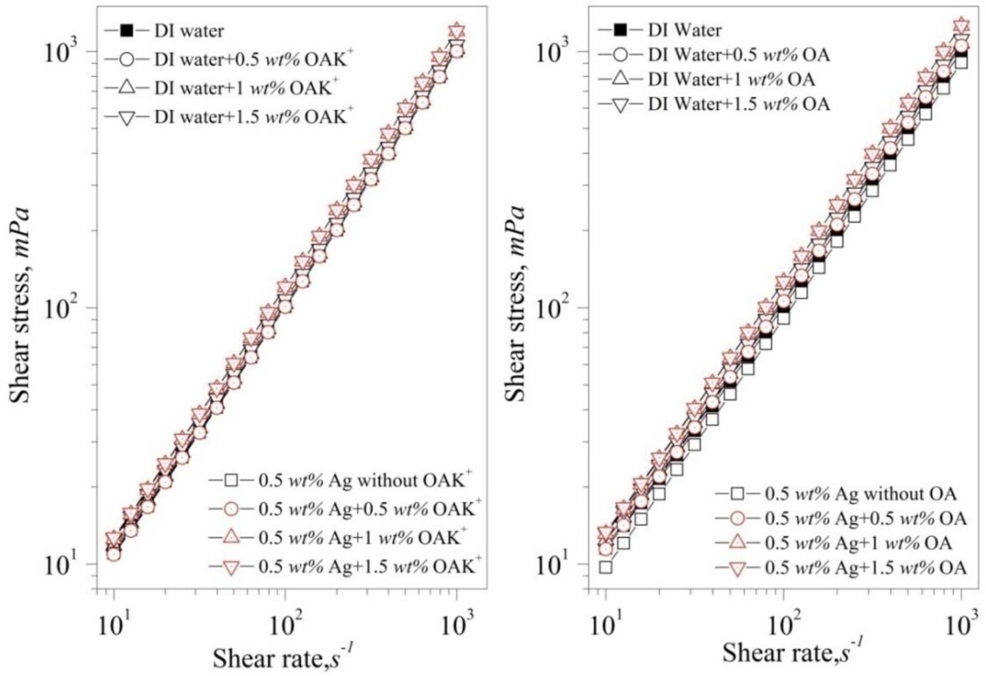

Figure 23 Relationship between shear rates with shear stress of silver nanofluids at operating temperate 30°C

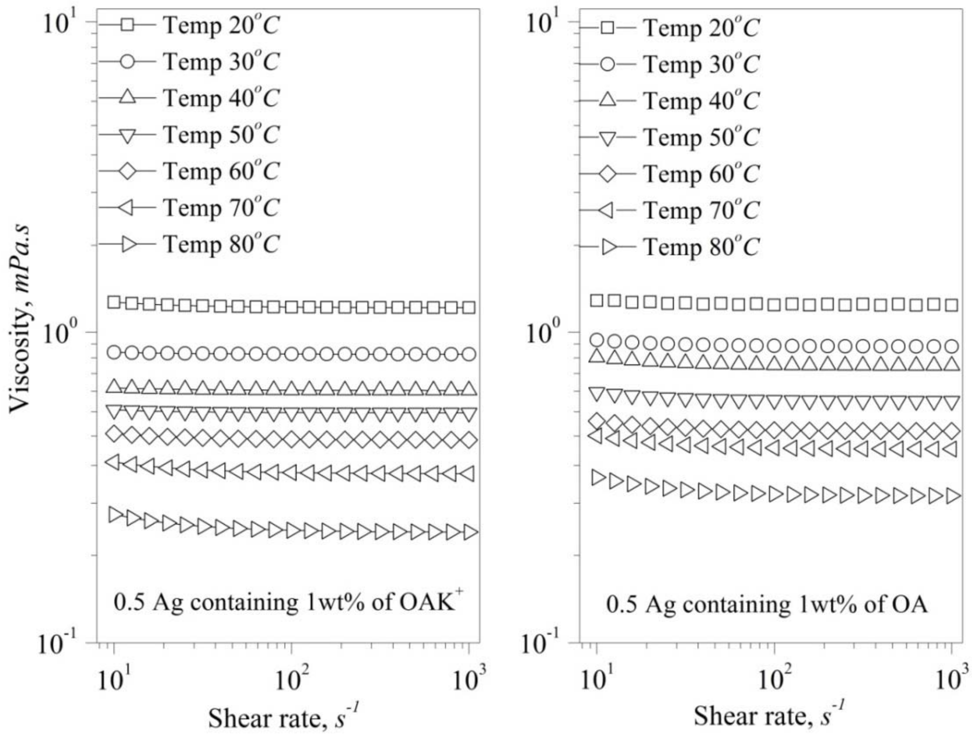

Figure 24 Relationship between shear rates with viscosity

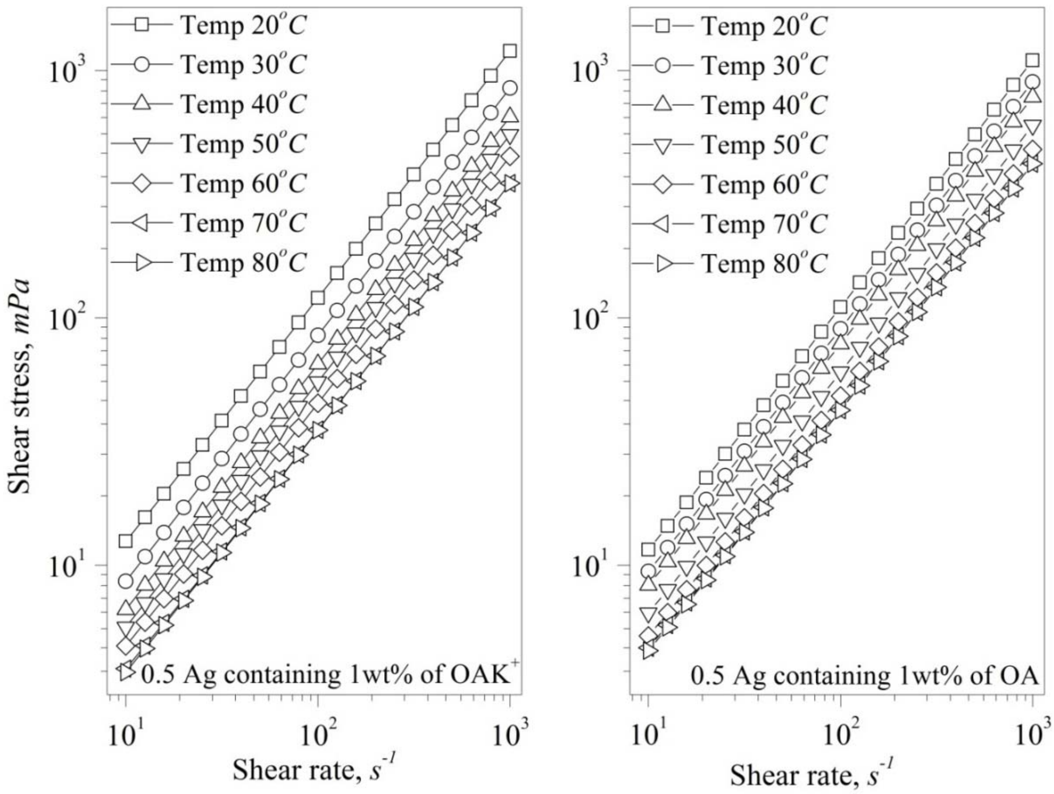

Figure 25 Relationship between shear rates and shear stress

3.3. Thermal conductivity of nanofluids

The thermal conductivity effective of the silver nanofluids containing potassium oleate (NF+OAK^+) as a function of temperature is shown in Figure 26. It can be seen that the thermal conductivity of the nanofluids depend on the linearity of the temperature, and the enhancement of the thermal conductivity of NF+OAK^+ was different when the surfactant concentration was 0.5, 1, and 1.5 wt%. In all cases the NF+OAK^+ showed superior performance to that of the water. One wt% OAK^+ showed the lower and highest increase in the thermal conductivity of 15% at 20ºC and 28% at 80ºC throughout all samples, indicating that the thermal conductivity increases independently on surfactant concentration [47]. The nanoparticles dispersed in the liquid increased the surface area for the heat absorption. In the case of NF+OAK^+, the OAK^+ decreased the surface tension of the nanoparticles, stabilized the nanoparticles by uniformly distributing them, and increased the interface area of the nanofluids with the deionized water [63]. The surface tension had a significant influence on the thermal process since the property departure and interfacial equilibrium depend on it [23]. The high OAK^+ concentration appeared to hinder the aggregation and entanglement of the NP, which was observed at the bottom of the liquid [44, 46]. According to our experimental results, 1 wt% OAK^+ was enough to homogeneously disperse the NP and produce efficient thermal transfer between the particles and deionized water, and consequently resulted in the highest thermal conductivity enhancement [43, 76-79].

However, the current experimental results contrast with those of Kang et al., [38] and Oliveira et al., [39] as shown in Figure 27. In regards to this study, the results were achieved using the same silver nanoparticles however with a difference in concentration and surfactant. The result from Kang et al., demonstrated an increase of relative thermal conductivity. Thus, it is important to note the vast differences among different experimental conditions, especially in regard to the method of preparation and nanoparticles concentration. For example, Kang et al.,[38] showed a maximum k_{nf} / k_{bf} of ~1.11 at 0.4% volume concentration with nanoparticles diameter of 8-15 nm, whilst Oliveira et al., [39] showed a maximum k_{nf} / k_{bf} of ~1.17 at 0.3% volume concentration with nanoparticles diameter of 10 and 80 nm. This contrasts significantly with the results achieved in this study of approximately 1.19 with nanoparticles of diameter 5-25 nm at NF+1OAK^+. Of particular note, the research performed by Kang et al., in 2006 and Oliveira et al., in 2014, did not specify the temperature under which the experiment was conducted. Furthermore, relative thermal conductivity was analyzed as a function of nanoparticles concentration and size. Thus, it can be determined that relative thermal conductivity is dependent upon the nanofluid's method of preparation, as well as the nanoparticles concentration and size.

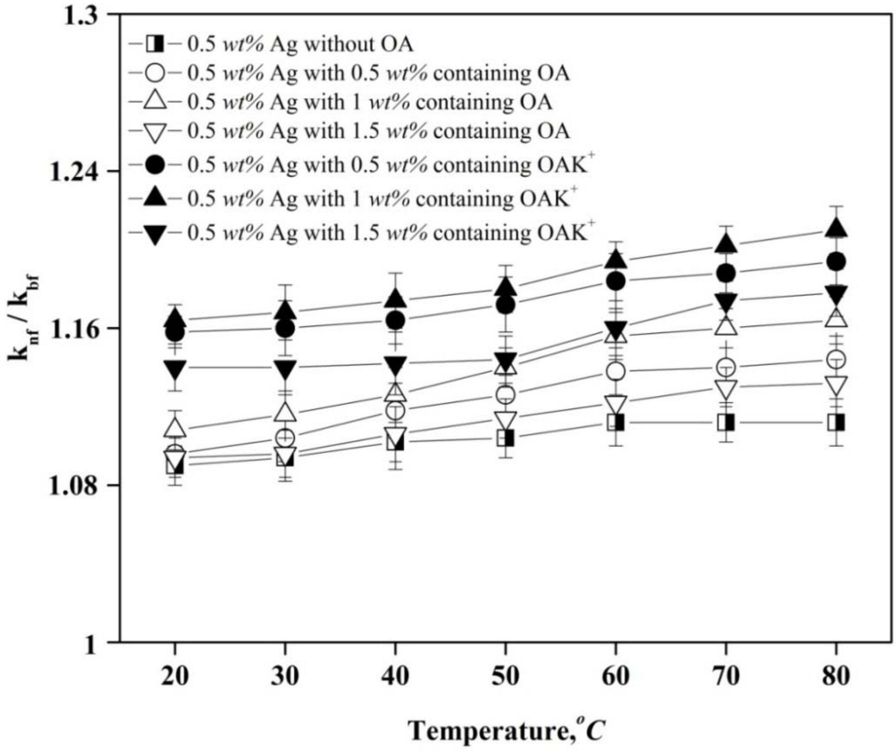

Figure 26 Relationship between temperature with k_{nf} / k_{bf}

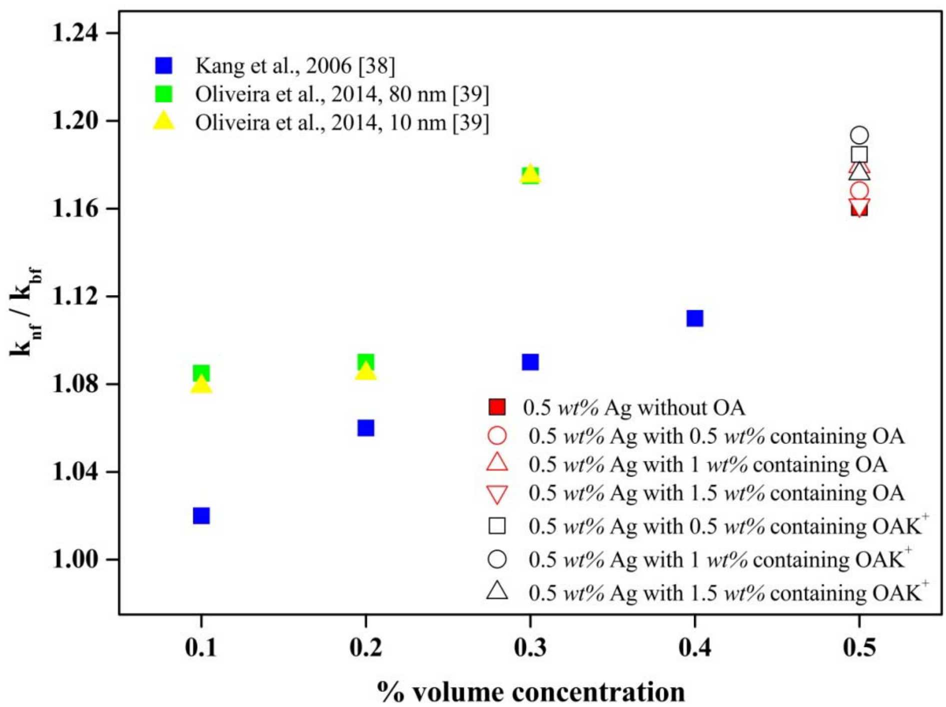

Figure 27 Comparison different experimental result

3.4. Dynamic of specific heat capacity (DSC)

The heat energy absorbed ratio is a substance to increase in temperature. Table 9 shows the dynamic of specific heat capacity: nanofluids. The DSC was used to measure the deionized water deionized water containing surfactant (OA and OAK^+) and the NF containing surfactant (OA and OAK^+) at 1 wt% respectively, which was then compared with Equation (47) according to Rajabpour et al., [57] and O'Hanley et al.,[58]. The results indicated a trend similar to that found in Rajabpour et al., [57] and O'Hanley et al., [58]. It was found that, the good resulted appeared when using OAK^+ as a surfactant. The silver nanofluids containing OAK^+ surfactant was subjected to repulsion forces between the positively-charged hydroxyl groups (OA) of the functionalized nanoparticles and the potassium salt hydroxyl groups on the silver. However, the potassium salt of the acidic group functionalizing the nanoparticles became polarized in the water solution. On the other hand, when the positivity-charged potassium cation (K^+) groups were attached to the nanoparticles, the free ends (the carboxylic groups) became negatively charged. It is possible that the particle-fluid interactions and long-range electrostatic interactions between the nanoparticles may have affected the capillary properties of the nanofluids. Therefore, the negative forces between the solid and the nanofluids induced a specific heat capacity. Both parameters were dependent on particle size and surfactant concentration.

3.5. The contact angle and surface tension

In this study, the drop contact angle of working fluids was based on the room operating temperature. Furthermore, in order to investigate the effect of adding surfactant to the nanofluids, surface wettability, the static contact angles of the sessile droplets, and the surface tension of the pendant drop (Contact Angle Meter Model: DM-CE1 ; Kyowa Interface Science) were measured on flat copper plates at room temperature as shown in Figure 28. This method was based on Khandekar et al., [36] and Rahimi et al., [80]. When the surfactant was added it caused reduced adhesion between the working fluids dropping and the metal surface and made the total surface free energy. These are the manifestations of the interaction of the different molecular forces. The effects on the bulk thermo physical properties need to be addressed and surfactant dealt with nanofluids thus according to

Radiom et al., [81]. It was further found that NF+1 OAK^+ decreased the water drop contact angle and surface tension to 38.23º and 28.69 mN/m, respectively (compared with pure water having 110° and 72.8 mN/m). Thus, the contact angle and surface tension depended on the operating temperature and time. They have an effected on the boiling phenomenon in the heat transfer application. The transfer rate improves and decreases the surface tension with wet ability and contact angle [2, 82].

3.6. Heat transfer enhancement

The experimental results clearly showed the effect of the percentage of heat supplied on the percentage of percentage of thermal heat enhancement, as shown in

Figure **29**. When comparing the percentage of heat supplied using the different working fluids, it was seen that the NF+1OAK^+ showed that the percentage of thermal enhancement was higher than with the other working fluids. Considering the case where the working fluid was NF+1OAK^+ with a heat input at 100% of heat supplied, the thermal enhancement reached 24.75±0.08%. The increase of maximum percentage of thermal enhancement with an increase in the percentage of heat supplied can be attributed to the increase in different temperatures (ΔT). In addition, the thermal motion of the nanoparticles enhanced the thermal properties of the nanofluids. The OA group helped with the homogeneous dispersion of the nanoparticles in the nanofluids. Moreover, the potassium cation (K^+) significantly contributed to accruing the thermal property increase, which had effects on the heat transfer rate mechanism more efficiently than the thermal diffusion in the fluid [34, 45, 83, 84].

Table 9 The dynamic of specific heat capacity: nanofluids

Temperature	Deionized water containing 1 wt% OA		Deionized water containing 1 wt% OAK^+		0.5 Ag containing 1 wt% OA		0.5 Ag containing 1wt% OAK^+	
(°C)	Theoretical C_p (kJ/kg·K)	Measured C_p (kJ/kg·K)	Theoretical C_p (kJ/kg·K)	Measured C_p (kJ/kg·K)	Theoretical C_p (kJ/kg·K)	Measured C_p (kJ/kg·K)	Theoretical C_p (kJ/kg·K)	Measured C_p (kJ/kg·K)
20	-	4.185±0.070 4.182±0.070	-	4.189±0.056 4.182±0.070	4.226	4.227±0.002 4.225±0.055	4.226	4.269±0.02 4.225±0.055
30	-	4.185±0.068 4.183±0.068	-	4.189±0.036 4.183±0.068	4.228	4.227±0.045 4.225±0.103	4.228	4.269±0.120 4.225±0.103
40	-	4.186±0.065 4.182±0.068	-	4.190±0.032 4.182±0.068	4.229	4.228±0.020 4.225±0.003	4.229	4.270±0.025 4.225±0.003
50	-	4.200±0.056 4.182±0.068	-	4.204±0.048 4.182±0.068	4.231	4.242±0.025 4.226±0.028	4.231	4.284±0.008 4.226±0.028
60	-	4.200±0.060 4.183±0.068	-	4.204±0.060 4.183±0.068	4.237	4.242±0.012 4.227±0.040	4.237	4.284±0.023 4.227±0.040
70	-	4.210±0.040 4.187±0.068	-	4.214±0.089 4.187±0.068	4.241	4.245±0.121 4.229±0.104	4.241	4.295±0.016 4.229±0.104
80	-	4.220±0.037 4.189±0.068	-	4.224±0.010 4.189±0.068	4.252	4.262±0.121 4.236±0.112	4.252	4.305±0.039 4.236±0.112

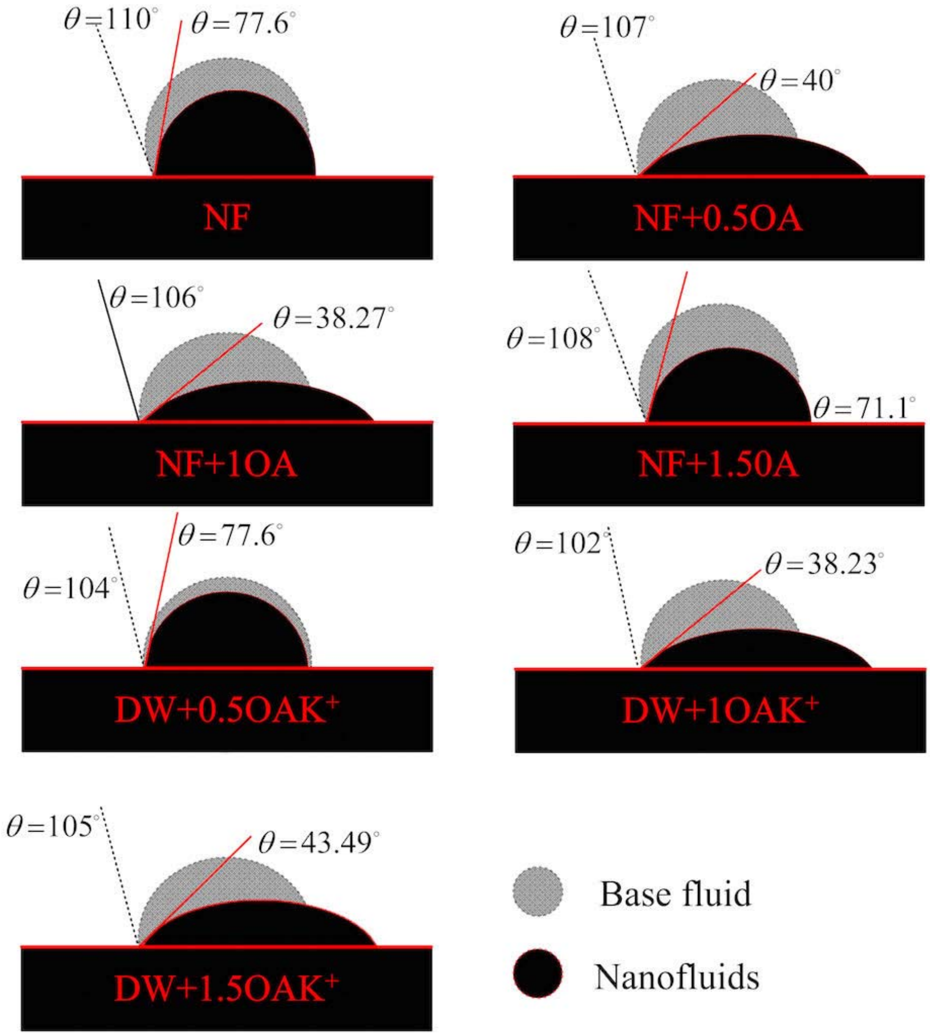

Figure 28 Wettability at room operating temperature

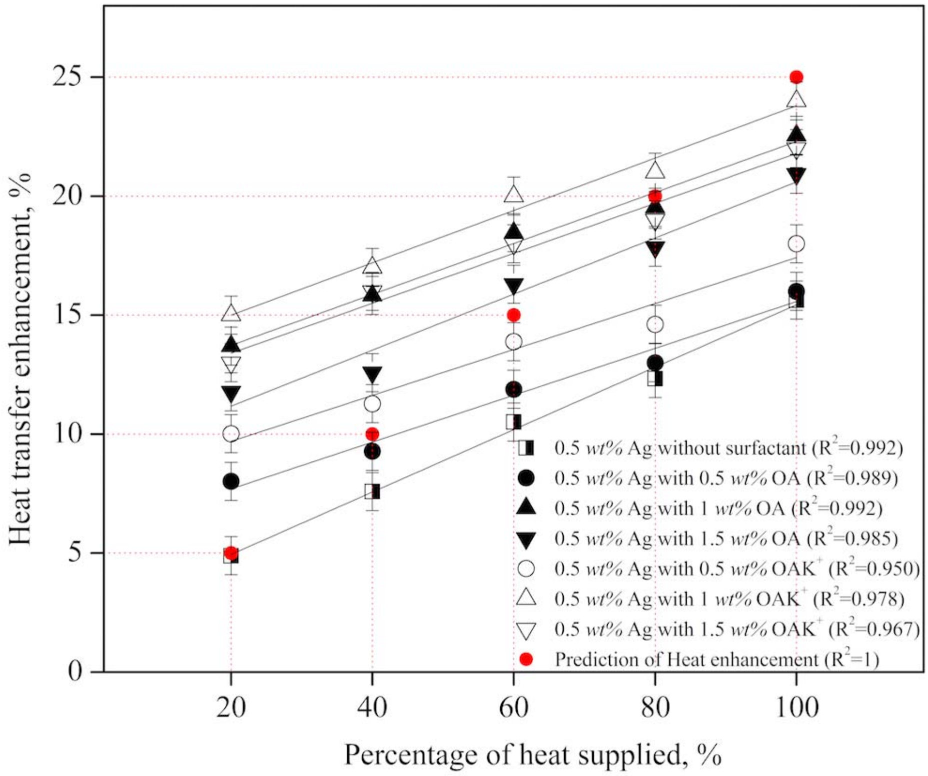

Figure 29 Thermal enhancement of working fluids

4. Conclusion

Study on NF containing surfactant is leaded tonanoparticles size, the rheological properties of the nanofluids, the thermal conductivity of nanofluids, the dynamic of specific heat capacity (DSC), wet ability (contact angle and surface tension) and heat enhancement. The important details are discussed below:

- The silver nanofluids containing OA and OAK^+ were conducted on thermal conductivity and rheological properties at various concentrations of OA and OAK^+ and operating temperatures. It was found that the NF containing 1 wt% of OAK^+ yielded better particle size ~95 nm.

- At a shear rate range of 101s-1 to 103s-1, the samples showed Newtonian behaviour, which showed Newtonian behaviour, suggesting that the shear stress and viscosity decreased the high solid loading. For a given surfactant concentration, the consistency viscosity and shear stress of the base fluid and all of the nanofluids decreased with an increase in temperature, which confirmed that temperature had a strong effect on the shear stress and viscosity of the nanofluids. The rheological produced Newtonian.

- The NF containing 1 wt%of OAK+ gave the highest thermal conductivity. It can be seen that the thermal conductivity enhancement was from 11% at 20ºC to 28 % at 80ºC when compared with the base fluids. The DSC was increased with respect to operating temperature increase. Explicitly, the thermal conductivity of the NF containing the surfactant was in respect to the operating temperature, showing increments at all concentrations.

- The specific heat of NF containing OA and OAK+was superior in specific heat capacity, over water studied in all experimental conditions. The presence of surfactant had clearly contributed to the rise in specific heat capacity.

- It was concluded that the static contact angles of the OA group surfactant used, have better wettability characteristics, dependent on the surfactant concentration. Moreover, the NF containing 1 wt% of OAK+ could be good at reducing the wettability and the OA group improved the colloidal stability which potassium cation (K+) increased the non-precipitation period for nanoparticles to be uniformly dispersed in the base fluid. The nanofluids containing 1wt% of OAK+ produced a good contact angle of 38.23°.

It could be concluded that theamount of the thermal enhancement of the nanofluids containing surfactant contributed to the greater rise of the thermal performance over the base fluid/nanofluids by approximately 80%.

CHAPTER IV THERMAL PERFORMACE OF LOOP THERMOSYPHON

This chapter is described on the heat transfer rate behaviour in of an advanced loop thermosyphon with check valve (ALT/CV) which is filled with silver nanofluids, and containing OA and OAK^+. Traditional working fluids such as water, ethanol, etc., have poor physical properties which makes it difficult to change phase [10, 11]. Silver nanoparticles were chosen to be added in the traditional working fluid because it has the highest thermal conductivity in the transition metal group and could be a good stabilizer in a base fluid compared to most solids [11]. The particles could improve thermal performance. The problem with nanofluids is agglomeration with un-dispersed nanoparticles due to the decrease in the lead time period for nanoparticles to be uniformly dispersed[85]. Consequently, this article focuses on improving working fluid properties which is achieved by adding surfactant. The OA and OAK^+ could decrease the surface tension and increase the homogeneity of the dispersed nanoparticles [48, 85]. Silver nanoparticles containing OA and OAK^+ could increase thermal conductivity and heat transfer coefficient. The purpose of the silver nanoparticles containing OA and OAK^+ in the working fluid is for filling of the TPCT was to find out the optimal OA and OAK^+ surfactant concentration in order to maximize heat transfer rate. The new working fluid has a unique characteristic where the heat transfer rate is slightly higher than the traditional working fluid, as follows:

This chapter describes the heat transfer rate behaviour of an advanced loop thermosyphon with check valve (ALT/CV) which is filled with silver nanofluids and contains OA and OAK^+. Traditional working fluids such as water, ethanol, etc., have poor physical properties, which makes it difficult to change the phase [10, 11]. Silver nanoparticles were chosen to be added tothe traditional working fluid because it has the highest thermal conductivity in the transition metal group and canbe a good stabilizer in a base fluid compared to most solids [11]. Additionally, theparticles canimprove thermal performance. The problem with nanofluids is agglomeration with un-dispersed nanoparticles due to the decrease in the lead time period for nanoparticles to be uniformly dispersed [85]. Consequently, this article focuses on improving working fluid properties, which is achieved by adding surfactant. OA and OAK^{+} can decrease the surface tension and increase the homogeneity of the dispersed nanoparticles [44, 81]. Silver nanoparticles containing OA and OAK^{+} can increase thermal conductivity and the heat transfer coefficient. The purpose of the silver nanoparticles containing OA and OAK^{+} in base fluid is filling in the ALT/CV, was to find out the optimal OA and OAK^{+} surfactant concentration in order to maximize the heat transfer rate. The new working fluid has a unique characteristic, where the heat transfer rate is slightly higher than the traditional working fluid, as discussed below.

1. Literature review

The objective of this study is based on the ALT/CV using silver particles containing OA and OAK^{+} as the working fluid. Moreover, it has proven beneficial to improve the working fluid properties as a way to allow for smaller nanoparticles which ultimately reduce the thermal resistance contained in the base fluid as the working fluid in the ALT/CV. The effects of the operating percentage of the heat supplied (heat input), the working fluids, the loop size of the thermosyphon and thermal behaviour (thermal resistance, heat transfer coefficient, relative ofthermal efficiency) under normal operating conditions were studied.

This literature review consists of a number of points to be reviewed and discussed. The requirements forthe ALT/CV and the nanofluids will be summarized, together with the existing characterization measurement and application of the online methods, which will also be reviewed. Thus, the addition of nanoparticles toa base fluid forms so-called nanofluids, as the nanoparticles can improve the heat transfer rate, which can be used in the ALT/CV or heat exchanger applications. Then, nanofluids are used as working fluids in the heat pipes. The points to be considered include the method using the nanofluids and the effect this has on the ALT/CV. Thus, the heat transfer rate behaviour of the ALT/CV is essential in establishing an adequate application and design of the processing. Payakaruk et al., [25] studied the heat transfer rate of a two phase closed thermosyphons (TPCT) made from copper tubes with diameter as 7.5,11.1 and 25.4 mmID. Five working fluids were chosen: water, ethanol, R-22, R 123, and R-134a. It was concluded that the working fluid affected the heat transfer rate at inclination angles of 20 to 70°. The filling ratios had no effect on the ratio of the heat transfer at any angle; however, the properties of the working fluids were affected. Ristoiu et al.,(2003) [86] experimentally studied the effect of inclination angles on the heat transfer of a wickless solar heat pipe (Thermosyphon). The thermosyphon used acetone, methanol, and water as working fluids. The copper heat pipe investigated here exhibited the highest heat transport rate at inclinations of around 40° - 45°. Then, the study of nanofluids wasconducted by suspending ultra-fine metallic or non-metallic particles from the nanometer dimension group in base fluids such as water, oil, and ethylene glycol. Noie (2005) [87] reported that the heat transfer performance of the TPCT with aspect ratios was 7.45, 9.8 and 11.8. The parameter had input heat transfer rates of $100 < Q < 900$ W with filled the working fluid ratios of $30\% \leq FR \leq 90\%$. It was found that, with the filling ratio at 60%,a higher heat transfer rate occurred and was lower at 90%. Moreover, adrop in temperature wasexpected due to the internal resistance of boiling and condensation. After the heat transfer coefficient measurement, it was found that the heat transfer of all the filling ratios werereasonable for finding the empirical correlationbetween the experimental results and predicted valves. Then, Noie et al., (2007) [4] studied the effect of the inclination angle from5° to 90° with different filling ratios (Distilled water as the working fluid) of 15%, 22%,and 30%. The thermal performance of a TPCT(copper tube diameter of 14.5 mmID, length 1,000 mm) was investigated experimentally under normal operating conditions. It was found that,the TPCThadthe highest thermal performance in the inclination angle range of 15° to 60°. The interesting phenomenon of geyser boiling occurred in our experiments for filling ratios equal to or greater than 30%. The geyser boiling puts no limitation onthe thermal performance of the thermosyphon; however, it should be avoided because it damages the condenser end cap due to the slug striking. Another study was applied to nanofluids in 2009 [18]. This investigation,studying Al_2O_3 in the water, showed thatthe efficiency of the TPCTwas enhancedup to 14.7% at 3 vol%. It was also found that the temperature distribution on the TPCT was at a lower level when nanofluids were used as opposed to pure water.The thermal resistance of the TPCT was less. When nanofluids was changed with the higher thermal performance of the TPCT loaded with nanofluids proved its potential as a substitute for a convectional one with pure water [20]. In 2011, Khazaee et al., [88] presented a study of the heat transfer characteristics of the TPCT made from a copper tube of 15 mmOD and a length of 2,000 mm with iron oxide-nanofluids (Averagediameter of 4–5 nm) in water as the working fluid. It was found that the effects of the TPCT inclination angle wasbetter at 90°. However, this depends on the operating temperature and nanoparticles concentration levels of the heat transfer characteristics of the TPCT. The thermal resistance of the TPCT with nanoparticles solution waslower than that with pure water. This shows that thermal resistance decreases as the volume concentration increases.However, this depends on the operating temperature and nanoparticles concentration levels of the heat transfer characteristics of the TPCT. The thermal resistance of the TPCT with nanoparticles solution is lower than that with pure water. This shows that thermal resistance decreases as the volume concentration increases. The different types of nanofluids have been investigated by Khandekar et al., [20]. This used Al_2O_3, CuO and laponite clay mean diameter < 100 nm in water. The TPCT was made from copper tubing with a filling ratio was of 100%. It was found that nanofluids show inferior thermal performance than pure water. The wet ability of all nanofluids on copper substrate, having the same average roughness as that of the TPCT, is better than pure water. A scaling analysis in an evaporator side Peclect number found this eventually leads to poor thermal performance. The condenser and evaporator were an important factor on overall performance. When studying the TPCT, the physical effects are very important.

Paramatthanuwat et al., [3] studied the heat transfer of the thermosyphon made from copper tubes with 7.5, 11.1, and 25.4 mmID, and the aspect ratios (Le/di) chosen for the study were 5, 10, and 20. The filling ratios chosen for the study were 30%, 50% , and 80% with respect to the evaporator length. Pure water and silver nanofluids were used in thermosyphon and compared with three operating temperatures of 40, 50 and 60°C.It was found that the best filling ratio was at 50% for the temperature to affect the heat transfer rate of the thermosyphon. Kang et al., (2009) [77] investigated silver nanofluids in water applied as a working fluid in a heat pipe. The silver nanofluid showed better cooling with respect to water because the nanoparticles could flatten the temperature gradient of the fluid and reduce the boiling limit because it increased theeffective liquid conductance in the heat pipe. Hence, the nanofluids aremore interesting as cooling fluids for devices because they havea higher energy density. Kim et al., (2007) [89] studied the pool boiling of dilute dispersions of alumina, zirconia, and silica in water. It was found that the nanofluids improved the layer and were important to the surface wettability, as shown by a reduction in the static contact angle on the nanofluid-boiled surfaces compared with the pure boiled water surfaces.

Thus this section focuses on the physical effects of substance based fluid functions and applications of nanofluids. However, few studies have been carried out to improve physical properties, for example decreasing surface tension or changing the structure or decreasing the viscosity of the base fluid. Hwang et al.,(2008) [45] investigated silver nanofluids in silicon oil with oleic acid (OA) produced by a one-step method (Magnetron sputtering),which showed the largest improvement in thermal conductivity over that of silicon oil. It was observed that silver nanoparticles were homogeneously dispersed and were stable for a long period of time in thesilicon oil. Li et al.,(2008) [46] investigated the thermal conductivity dependence with respect to the appropriate concentrations of an added surfactant. The work focused on the effect of pH, and the nanofluids chosen were Cu and sodium dodecylbenzenesulfonate (SDBS) as the surfactant. It was found that the surfactant was recommended to correct the thermal conductivity for practical applications of nanofluids. The maximum thermal conductivity could be enhanced by up to 10.7%. Hojjat et al., (2011) [52] reported on the γAl2O3, TiO_2 and CuOnanofluids with 0.5 wt% of carboxymethyl cellulose (CMC) in de-ionized water containing up to a 4 vol% of particle concentration. They concluded that the apparent viscosity of the base fluid and nanofluids decreasedwhen the shear rate increased. Rahimi et al., (210) [80] focused on thecontact angle and used a 1 m height TPCT with water as the working fluid with pressure operating at 0.75 and 160 mbar. It was found that the evaporator had more than the hydrophilic (4°) and the condenser had more than the hydrophobic (120°), so it was possible to raise the thermal performance to 15.27% and to decrease the thermal resistance to ×2.35 when compared with plain water. Qi et al., (2001) [90] and Hwang et al., (2008) [45] concluded that the surfactant could reduce the surface tension of the working fluid, which would improve the colloidal stability and would increase the lead time period for thenanoparticles to be uniformly dispersed. This could increase the surface area for silver nanofluids to absorb heat; thus this was found to be an enhancement for boiling fluid.

After that many researcher had trying to improve the performance of TPCT which was advanced the TPCT such as Fumito et al., (2003) investigated the loop closed thermosyphon, and showed that the heat transfer rate was better than the single tube thermosyphon[91]. Khodabandeh et al., (2010) [92] found that the maximum heat transfer flux of the loop thermosyphon was 20-44 W/cm^2 which is larger than the single tube, due to the non-countercurrent flow and non-vapour lock limit. In any application, e.g. the plate heat source, one kind of heat pipe is always applied. Then, Chang et al., (2010) investigated the thermal performance of a two-phase closed-loop thermosyphon with a thermal resistance model for electronic cooling. Results indicated that the evaporator and condenser thermal resistance decreased about 15.5% [93]. However, the heat was dissipated to the evaporator section, the saturated working fluid was vaporized to the evaporator section and then the heat was released to the condensing area. The loop thermosyphon performance was limited in receiving a heat source in the evaporator section; due to the separated tube construction. For these reasons, Jengsooksawat et al., (2008) [94] designed the loop thermosyphon with chamber (LTVC) to solve the weak points in the limitation of heat being received in the evaporator area and the limitation of the condensing area. The TPCT made adjustments to for the problems which used the LTVC. Then, Jengsooksawat et al.,(2014) [95] reported about loop thermosyphon with vapour chamber. It was found that, the data showed that the LTVC yielded the valve of the relative of thermal efficiency of about 1 at R-11, a filling ratio of 60%, a velocity of 0.5 m/s, and an aspect ratio of 2.5 in the study conditions. It was further found that the larger vapour chamber was superior in the rating of the heat transfer over other vapour chambers in all experimental conditions in this study. Moreover, It was solved the weak points in the limitation of heat being received in the evaporator area and the limitation of the condensing area with chamber.

Previous research studies on TPCT and ALT/CV have rarely focused on nanofluids containing surfactant and application of check valve. Check valve can solve problems of reverse flow in a tube. It can control direction of flow and separately manage flow of liquid and vapour. Moreover, nanofluids containing surfactant can resolve agglomeration issues and increase thermal performance of the ALT/CV.

2. Experimental apparatus and procedure

This section describes the experimental set up, theparameters of the study, and theprocedure as shown in Table 1. Thus, the total number of variables used in the experiment was 2,430 (5×3×3×3×3×6). The experiment had repeated threefold.

Nanofluidsareproduced using themethod discussed in Chapter III andare suspended in a base fluid such as water. The nanofluid preparation involves many steps, such as changing the pH valve of the suspension, and using surfactant activators and ultrasonic vibration. The nanoparticles suspended in the base fluid are stable for long periods of time. In this research, thenanofluidswereobtained using theultrasonic vibration method anda sonicator(bath type, operating frequency, and power source of the sonicator were 43 kHz and AC100 ~120V/AC220~240V 50/60 Hz, respectively) for 12 hours. The nanoparticles (Silver nanopowder is <100 nm particle size, 99.9% metals basis), oleic acid (OA), and potassium oleate(OAK^{+})were purchased from SIGMA-ALDRICH, Inc. in the USA. The silver nanoparticles were suspended in deionized water with a concentration of 0.5 wt% (NP). After that, the NP contained OA and OAK^{+} at concentrations of 0.5, 1 and 1.5 wt%, respectively.

Figure 30 shows a schematic diagram of the experimental apparatus, which consisted of an ALT/CV. Section A, as the evaporator, is the heat source with a heat supply of 2,000 Watts: section B is the adiabatic; and section C, as the condenser, is the heat sink with fresh air (controlled at 25°C). The TPCT was made from copper tubes with an internal diameter of 12.70 mm. The ALT/CV had three sections, an evaporator, adiabatic, and condenser, of equal loop size of 30 cm, 40 cm, and 50 cm, with an installation fin of 8 FPI in thecondenser section.Twenty-four temperatures were controlled and measured in the adiabatic section, which was constant at ± 4°C points of thermocouple Type K (OMEGA with ±0.1°Caccuracy). The thermocuplewere installed along with a data logger attached to the ALT/CV (Yokogawa DX200 with ±0.1°C accuracy, 24 channel input, and a -200°C to 1100°C measurement temperaturerange) with the circle symbol point shown in Figure 30. The jacket was covered with insulation. Fresh air flow and velocity werecontrolled by the use of an AC motor.

The controlled and variable parameters are shown in Table 3. During the experiment, the air velocity was set at 0.6 m/s (25°C) in order to calculate the heat transfer characteristics of the ALT/CV using the calorific method. The following equations were used for calculating of the heat transfer rates and for error analysis [58].

The following equations were used to calculate the heat transfer rate and for error analysis recently compiled by Paramatthanuwat et al., (2010) [3].

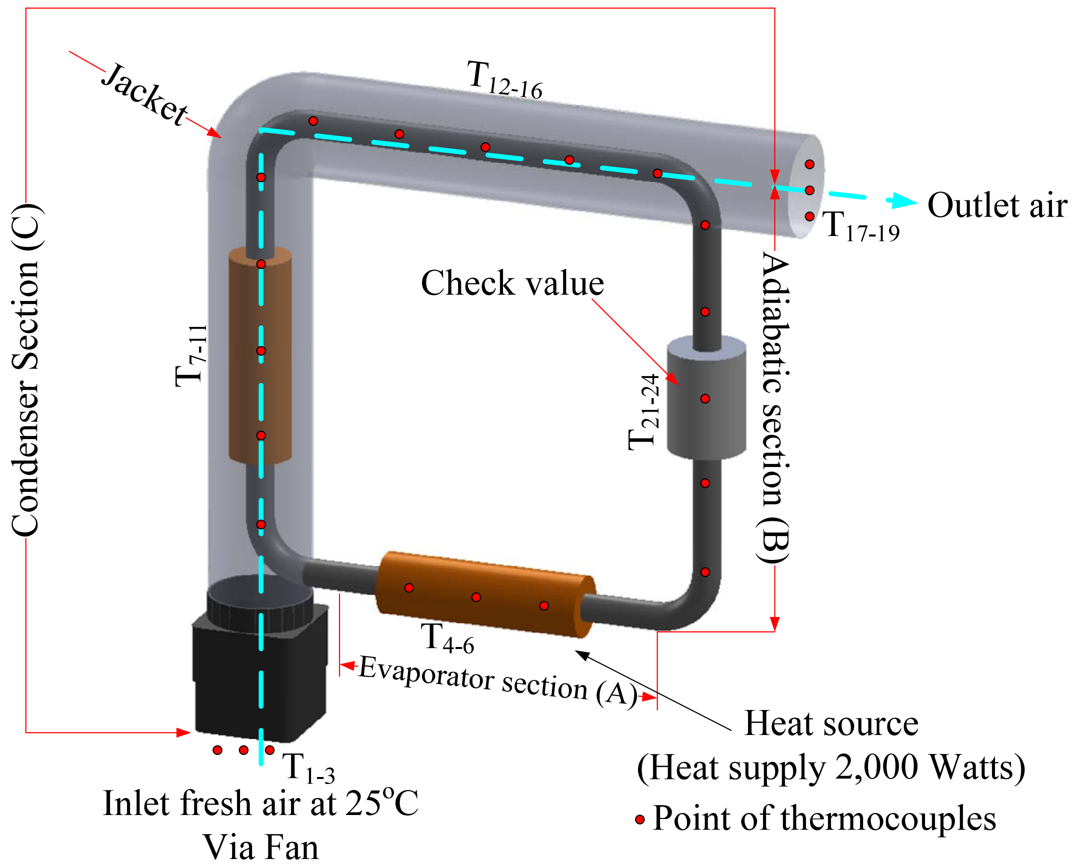

Figure 30 Schematic diagram of experimental apparatus

3. Results and discussion

3.1. Temperature distribution of loop thermosyphon

Figure 31 show the adiabatic temperature at the upper part and the side of the ALT/CV at different times, where the temperature showed a positive trend. The maximum temperature difference of both was ±5°C at T_{inlet} and T_{outlet} with NP containing 1 wt% of OAK^{+} as a working fluid and heat input at OPHS of 100%. T_{inlet} was higher than T_{outlet} and vice versa, causing higher thermal performance. The adiabatic temperature of the ALT/CV was able to reach a temperature higher than the ambient temperature, so heat transfer. The working fluid and the position of heat source were important, as they led to thermal performance [96]. In addition, the start up to 400 sec showedtransient transfer and then at 400 sec to the end showed a steady state. Accordingly, the transient transfer that occurred from the unequally-filled working fluid flow as vapour + liquid in the loop and the passed check valve of the thermosyphonresulted in the nonuniformdistribution of the temperature. The point of steady steate, the ball moving through a saturate vapour and super heat experiences a force in direction opposite to its motion. The terminal velocity is achieved when the drag force is equal in magnitude but opposite in direction to the force propelling the object. The effect of ball buoyancy in ALT/CV, the pressure acting motion ball is in upward direction, according to Eq. ((51) then the ball acting motion is downward direction according to (52). The force direction due to the pressure difference (ΔP) that flow was separated vapour with liquid. This relation was observed and defind in the heat transfer mechanism to generate pressure at evaporator section. In this case, the $P_{upward} \geq F_{ball\,total}$ caused ball buoyancy affect to T_{inlet} and T_{outlet} had a differance (ΔT). Consequently, the ALT/CV helped to regulate and control the $\Delta P \infty \Delta T$ for ALT and check valve operation,as shown in Figure 32.

$$\frac{F_{upward}}{A_{ball}} > \frac{(-\mathrm{F}_{\tau} - F_{\sigma} - \mathrm{F_g} + \mathrm{F_d})_{\mathrm{ball}}}{A_{ball}} \quad (51)$$

$$\frac{F_{downward}}{A_{ball}} < \frac{(\mathrm{F}_{\tau} + F_{\sigma} + \mathrm{F_g} - \mathrm{F_d})_{\mathrm{ball}}}{A_{ball}} \quad (52)$$

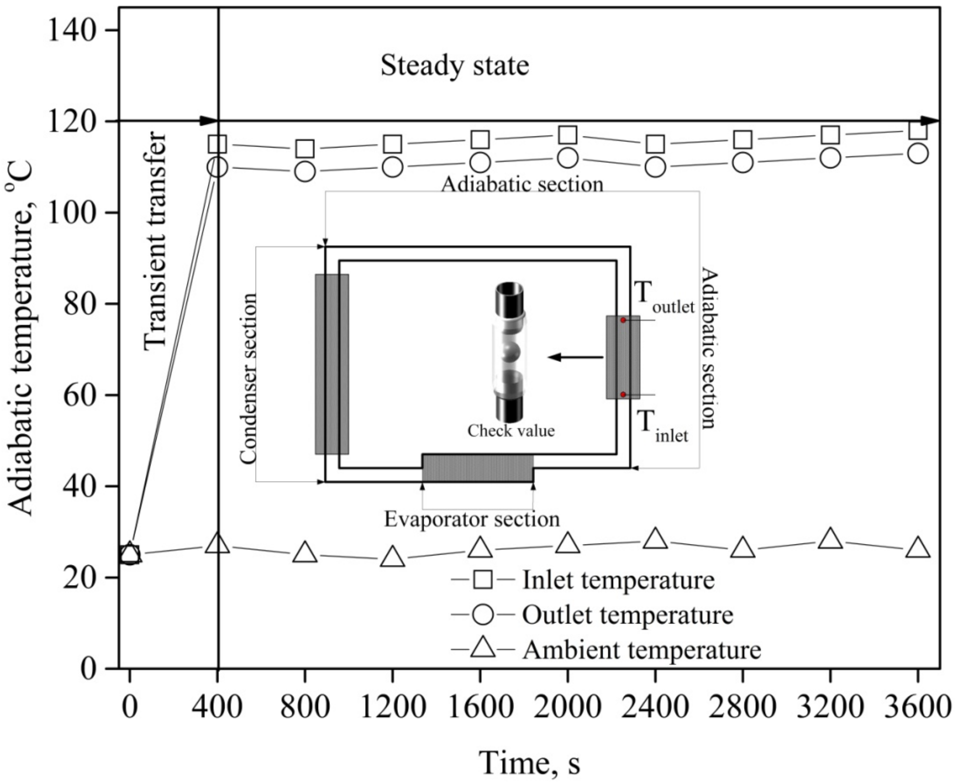

Figure 31 Temperature distribution of loop thermosyphon in the adiabatic section

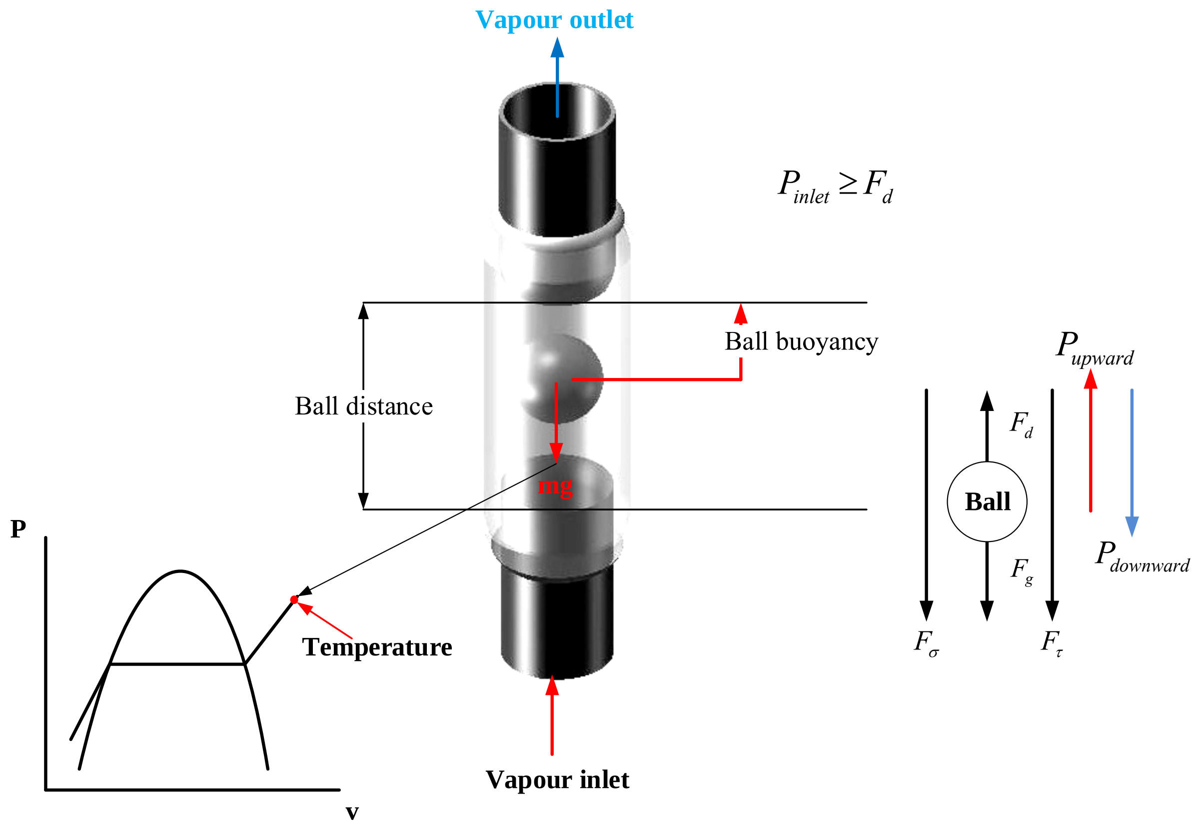

Figure 32 Check valve operation

3.2. Effect of operating percentage of heat supplied (Heat source)

Figure 33 shows the heat transfer of the ALT/CV at a loop size of 50 cm as a function of the operating percentage of the heat supplied (OPHS), filled with fourteen working fluids.The data shown correspond to the filling ratio of each working fluid of 50% of evaporator volume. The resultsindicatethat the NP contained 1 wt% of OAK^+ which produced a heat transfer rate valve of 1,150W at OPHS of 100%. Then, all of experimental data were compared with the heat transfer rate of the ALT/CV without the working fluid orbase fluid. In all cases the heat transfer rate of the NP contained 1 wt% of OAK^+ and showed superior performance over other parameters throughout all experimental conditions in this study.It can be observed that for a given working fluid, the heat transfer rate of the base fluid and all of the NP and NP containingsurfactant increased along with anincrease of the OPHS, which confirms that the OPHS had a strong effect on the heat transfer rate and the working fluid properties.It was therefore determined that the peak heat transfer rate occurs when the percentage of heat supplied is 100%. Moreover, the viscosity and surface tension were found to decrease after the introduction of OA and K^+[13, 45]. The viscosity and surface tension of the working fluids decreased as a result ofthe increase in operating temperature that theworking fluidis easier to boil. Furthermore, the OA would allow the particles to disperse uniformly within the base fluid, but high OA concentration appearedto hinder the aggregation ofthe NP, which was observed at the bottom of the liquid [44, 46]. The outcome of this experiment by raising the heat transfer rate is according to Hwang et al.,(2008) [45], Sharma et al., (2011) [44] and Li et al., (2008) [46]. In this study, the optimal concentration of OAK^+ added to the NP was 1 wt%, having the highest heat transfer rate throughout all conditions.

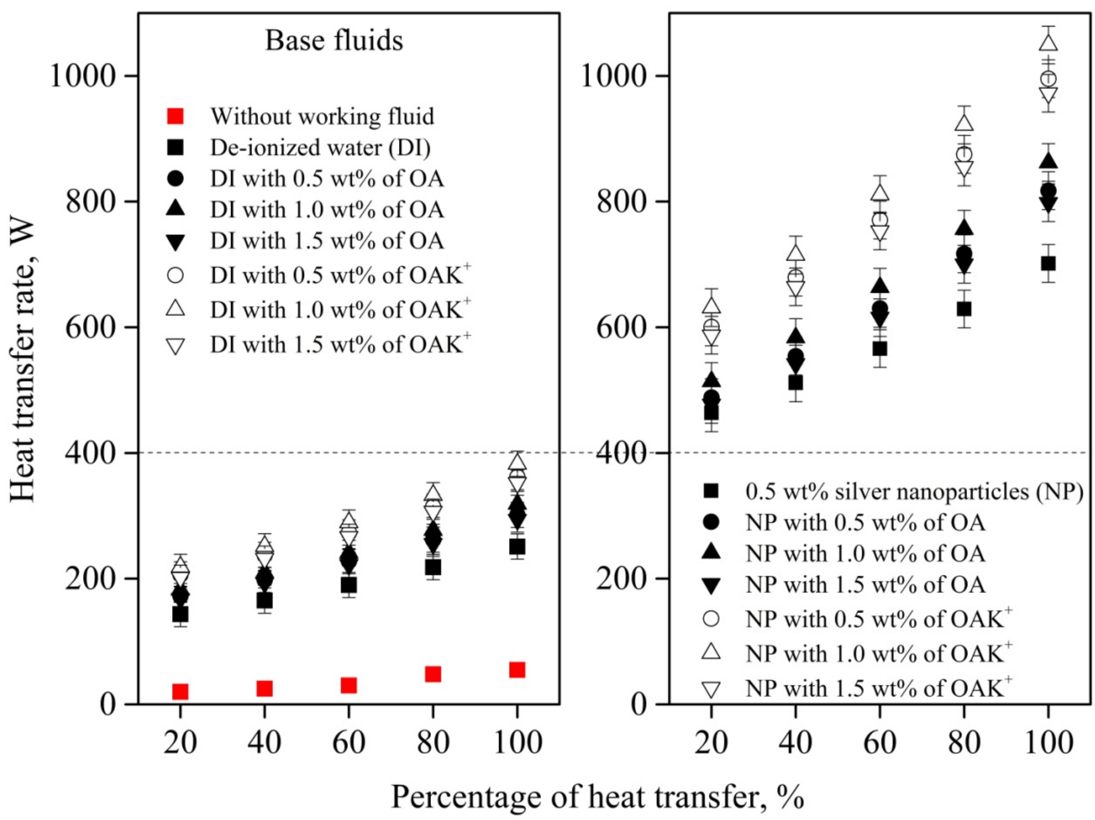

Figure 33 Effect of operating percentage of heat supplied (Heat source)

3.3. Effect of working fluid ratios

Figure 34 shows the heat transfer rate and heat flux of the filling ratio. The comparative heat transfer rate and heat flux among the 3 filling ratios weredefined by 30, 50, and 80% with the ALT/CV at a loop size of 50 cm. The result of the heat transfer rate and heat fluxshowed a maximum valve of 1,150W and 10.5 W/m^2 at the filling ratio of 50%, OPHS of 100%, and NP containing 1 wt% of OAK^+. It can be observed that the heat transfer rate and heat flux experienced a peak as a function of the filling. The optimum filling ratio for the addition of the working fluid in the ALT/CV was 50%, wherecritical film thickness occurred and the highest heat transfer rate was achieved [4, 16, 87, 97]. Moreover,the NP could be helpful for increasing thermal performance because of the particles that are increased in the base fluids. The suspension of the nanoparticles could increase the surface areas of the working fluid and heat capacity of the base fluid. Furthermore, the optimization of the chain length of the oleic acid was 18 with K^+, which was effective for particle dispersing stabilization. The optimized chain length also improved the colloidal stability and increased the non-precipitation period so that thenanoparticles could be uniformly dispersed [4, 35, 45]. The NP containing oleic acid was superior in its thermal performance over the deionized water of approximately 80% in all the experimental conditions in this study.

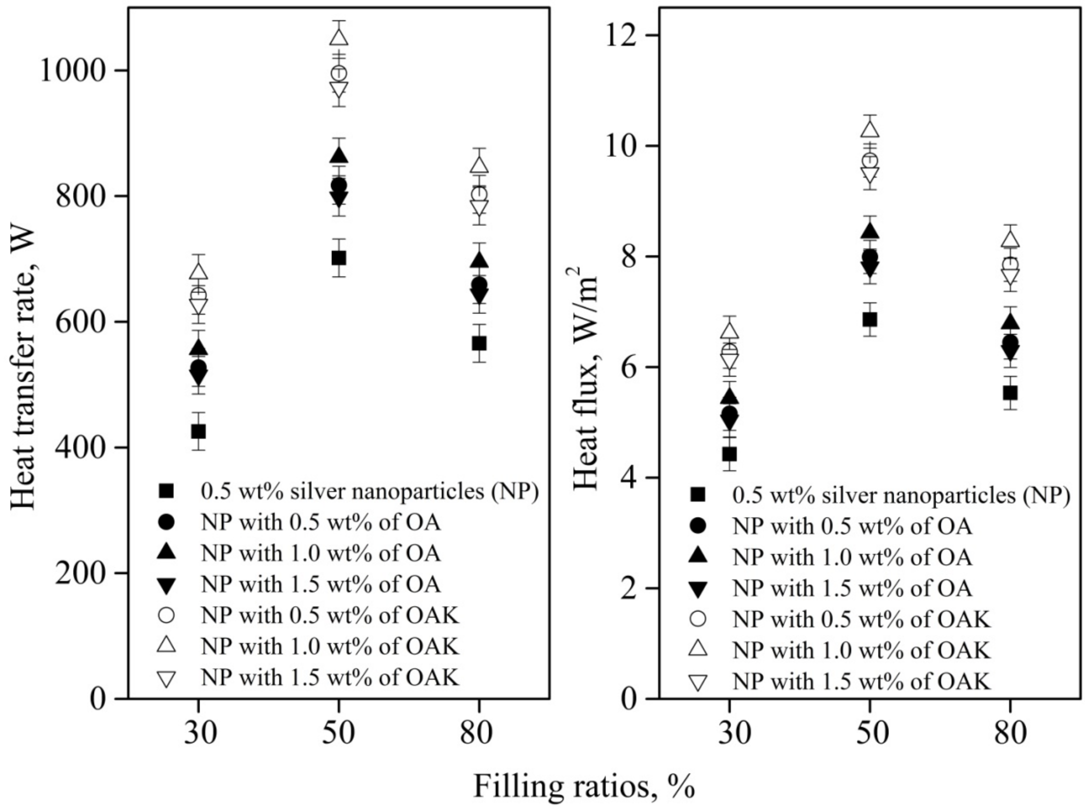

Figure 34 Effect of working fluid ratios

3.4. Effect of the loop size of the thermosyphon

Figure 35 shows the heat transfer rate and heat flux of the loop size of the thermosyphon. The experimental results clearly indicatedthe aspect ratios with the use of NP containing 1 wt% of OAK^+, producing the maximum heat transfer rate valves of 1,150 W with a loop size of 50 cmOPHS of 100%. Furthermore, the 1 wt% of OAK^+ had the highest heat transfer ratemore so than the TPCTused by Paramatthanuwat et al., (2010) with NP, $\frac{L_e}{d_i}$ = 20 ID 25.4 mm at T_v = 50°C [3] and Paramatthanuwat et al., (2017) with RTPCT from the stainless tube with NP containing1 wt% of OA at OPHS of 100% [13]. However, the current experimental results contrasted with those of Paramatthanuwat et al., (2010) and Paramatthanuwat et al., (2017). Thus, it is important to note the vast differences among different experimental conditions, especially in regard to the type of heat pipe and thermosypon. Accordingly, it can be seen that while the loop size increased from 30 cm to 50 cm, the heat transfer rate behaviour only slightly increased. Thus, the increase in the loop size is equivalent to the increase in the evaporator section size of ALT/CV,which will result in increased heat transfer rate behaviour. The larger evaporator section led to pool boiling, thus increasing theheat transfer rate [3, 16, 25]. On the other hand, the small aspect ratio led to the boiling in the confined channel, thus lowering the heat transfer rate [16]. Thus, the loop size and evaporator section was changed in terms of the ALT/CV's length, the filling ratio was changed,thus causing the thermal received valve to change that depend onthe proportion of ALT/CV's length [20]. In addition, the silver nanoparticles are very small, so when NPcontained oleic acid and K^+, the particles were dispersed uniformly in the fluid. This increased the surface area in the bubble diameter for absorbing heat [98, 99] , thus enhancing the boiling ofthe fluid. Therefore, it could be predicted that the amount of condensate was so high that it could return to the evaporator section, thereby ensuring an ample amount of working fluid for boiling and phase transition [34, 85, 100].

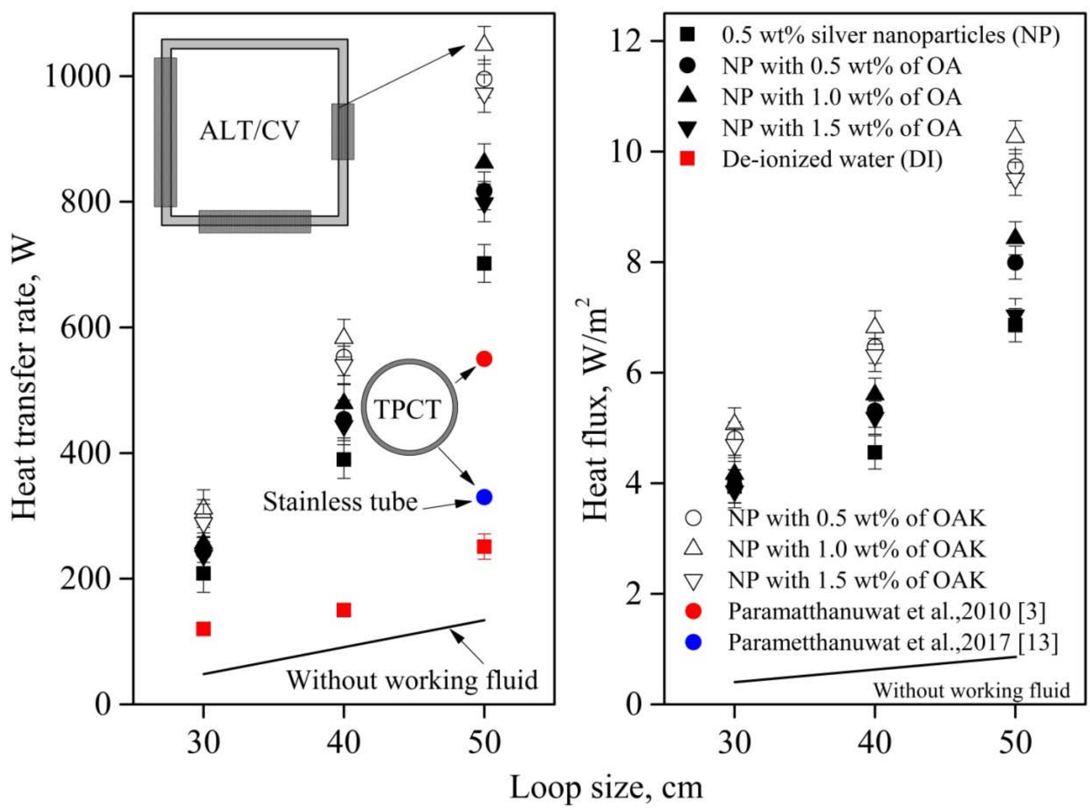

Figure 35 Effect of the loop size of the thermosyphon

3.5. Effect of Thermal resistance

The ALT/CV influenced the thermal transport to the evaporator section then boiling phenomenonoccurred. The thermal resistance contoured the pool boiling/film boiling of thermosyphoninthe evaporator section. The thermal resistance can be estimated from a number of ESDU81038 [15]. Thus, the nanoparticles existed in the base fluid containing surfactant, which affected the flow of the nanofluids, causing the surface tension and wettability to decrease but it was found thatthenanofluids containing surfactant produced high thermal property valves [35, 101]. Thus, the boiling phenomenon can be expressed according to thethermal/physical properties of the working fluids and physical of the thermosyphon, which was important for thermal resistance. Accordingly, when the cross sectional was changed it caused reduced friction loss and affected the phase transfer sophenomenon film boiling decreased [13]. However, the current experimental results contrasted with those of Noie (2005-TPCT) [87], Imura et al.,(1997-TPCT) [102], Srimuang et al., (2009-VFT and CT) [103], Amatachaya et al., (2010-FTPT) [104] and Parametthanuwat et al., (2017) [13], as shown in Figure 36, with the type of thermosyphon. In regard to this study, the results were achieved using a different heat source, working fluid, and condition. It was found that the minimum thermal resistance that occurred was 4.76×10^{-4}°C/W of a loop thermosyphon size of 50 cm, the NP containing 1 wt% of OAK+. It is obvious that while the loop size ofthethermosyphon increased, the thermal resistance only decreased. The heat source was varied by changing the percent of heat supplied. It was further found that the thermal resistance of the ALT/CV washigher when increasing the heat source because the ALT/CV is a single loopand has a higher total area. Studies cited for this result werecompared with Noie (2005-TPCT) [87], Imura et al., (1997-TPCT) [102], Srimuang et al., (2009-VFT and CT) [103], Amatachaya et al., (2010-FTPT) [104], and Parametthanuwat et al., (2017) [13] concerning thetype of thermosyphon (TPCT, CT, and VFT) according to themaximum valve of each those conditions at maximum heat source. Moreover, the type of thermosypon was approached boiling phenomenon. The pool boiling phenomenon only occurred when the lower thermal resistance which was high thermal performance was reached. On the other hand, the pool boiling phenomenonwas approached inside the confined channel, which had higher thermal resistance.

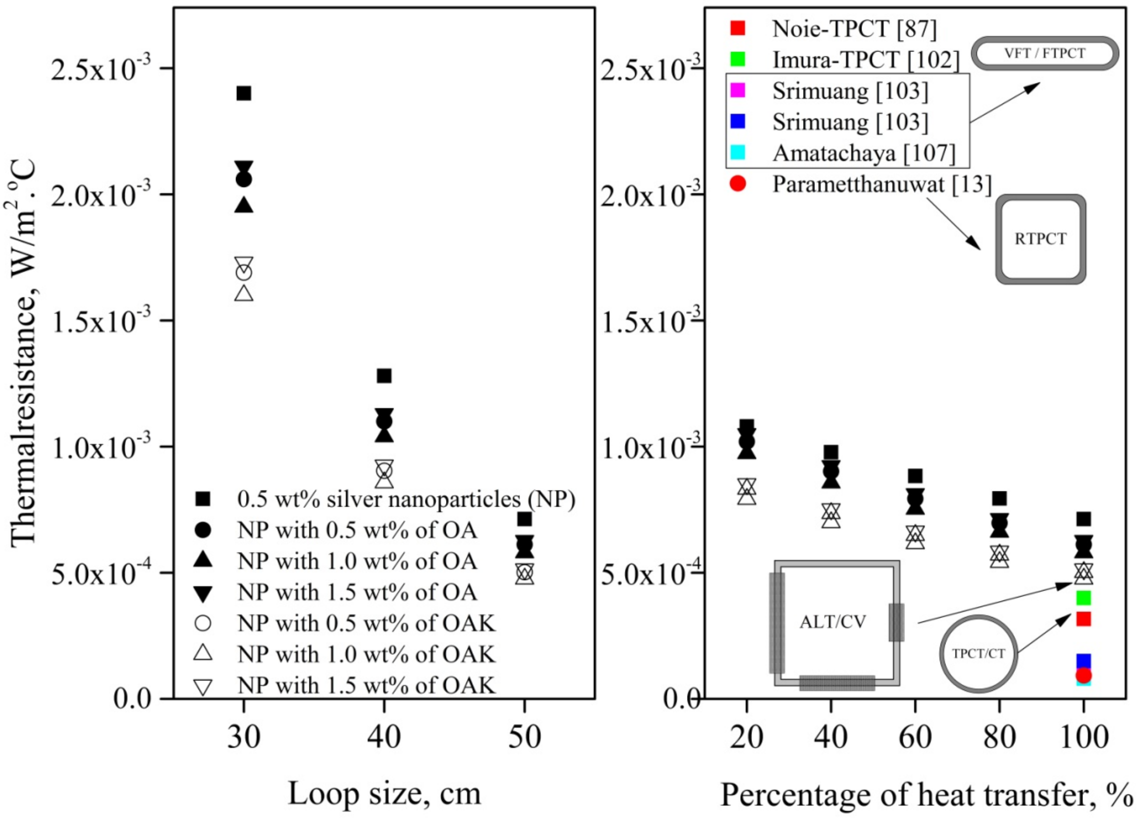

Figure 36 Effect of Thermal resistance

3.6. Effect of the heat transfer coefficient

Figure 37 shows the heat transfer coefficient (HTC). The ALT/CV was presented with a loop size 50 cm, and an OPHS of 100%. It was observed that 50% of the filling ratio of the samples showed similar positive trends. Furthermore, the HTC of the ALT/CV dependon filling ratios and NP containing OAK^+ wasdifferent when the surfactant concentration was0, 0.5, 1 and 1.5 wt%. In all cases the filling ratio of 50% with NP containing 1 wt% of OAK^+ showed superior performance than the other concentrations. The NP that contained 1 wt% of OAK^+ had the highest HTC valves of 20986.029 W/m^2K. On the other hand, the HTC seemedto have an inverse effect on the thermal resistance [10, 16]. Generally, it can be explained that the filling ratio and surfactant concentration increased when the viscosity of the working fluids changed, resulting in the movement of the nanoparticles. The Brownian motion of the nanoparticles inside the NP hada greater increase in dispersal, which in turn increasedtheconvection transfer. Consequently, the convection-like effects remarkably increased,which lead to an increased HTC [105, 106].

All of theheat transfer coefficient data increasedwith an increased percentage of heat supplied. The experimental results of this current research can be compared with the work of Parametthanuwat et al., (2017) [13], Noie (2005) [87], Imura et al., (1997) [102], Srimuang et al., (2009) [103], and Lee et al., (2003) [107]. It can be seen that the heat transfer coefficients of the ALT/CV depended linearly on the percentage of heat supplied throughout all the samples, indicating that the heat transfer coefficients increasedindependently onthesurfactant concentration. The enhancement of the heat transfer coefficients of the NP containing surfactant wasdifferent when the surfactant concentrations were0.5, 1 and 1.5 wt%. In all cases, the DI water containing surfactant and NP containing OAK^{+} showed superior performance than the base fluids. However, in all cases, the ALT/CV showed superior performance than the TPCT, CT, and VFT. The results between the five studies cited show an agreement between the difference in the thermosyhon type and cross-sectional and physical conditions. However, the heat transfer coefficients werehigher than in the five studies cited because of the ALT/CV was installed check valve for controlling the liquid and vapour, which was made those for separating. This may have beendue to the improvement pool boiling phenomenon in the evaporator section and the condensation phenomenon in the condenser section. Hence the heat transfer coefficients depend on the phase change transfer. Moreover, the nanoparticles (NP) dispersed in the liquid can increase the surface area for heat absorption. In the case of the NF containing OA and K^{+}, the OA and K^{+} will decrease the surface tension of the NP, and stabilize the NP by uniformly distributing NPand increase the interface area of the nanofluids with deionized water [39]. The surface tension has a significant influence on the thermal process since it depends on property and interfacial equilibrium [108]. A high OA and K^{+} concentration appeared to hinder aggregation, and entanglement of the NP was observed at the bottom of the liquid [44, 109]. According to our experimental results, 1 wt% OAK^{+} wasenough to homogeneously disperse the NP and produce efficient thermal transfer between the particles and de-ionized water. This consequently resulted in the highest thermal properties enhancements [43, 76, 77, 110]. NP andwasdominated by the pool boiling phenomenon due to the large number of heat transport inside the ALT/CV.

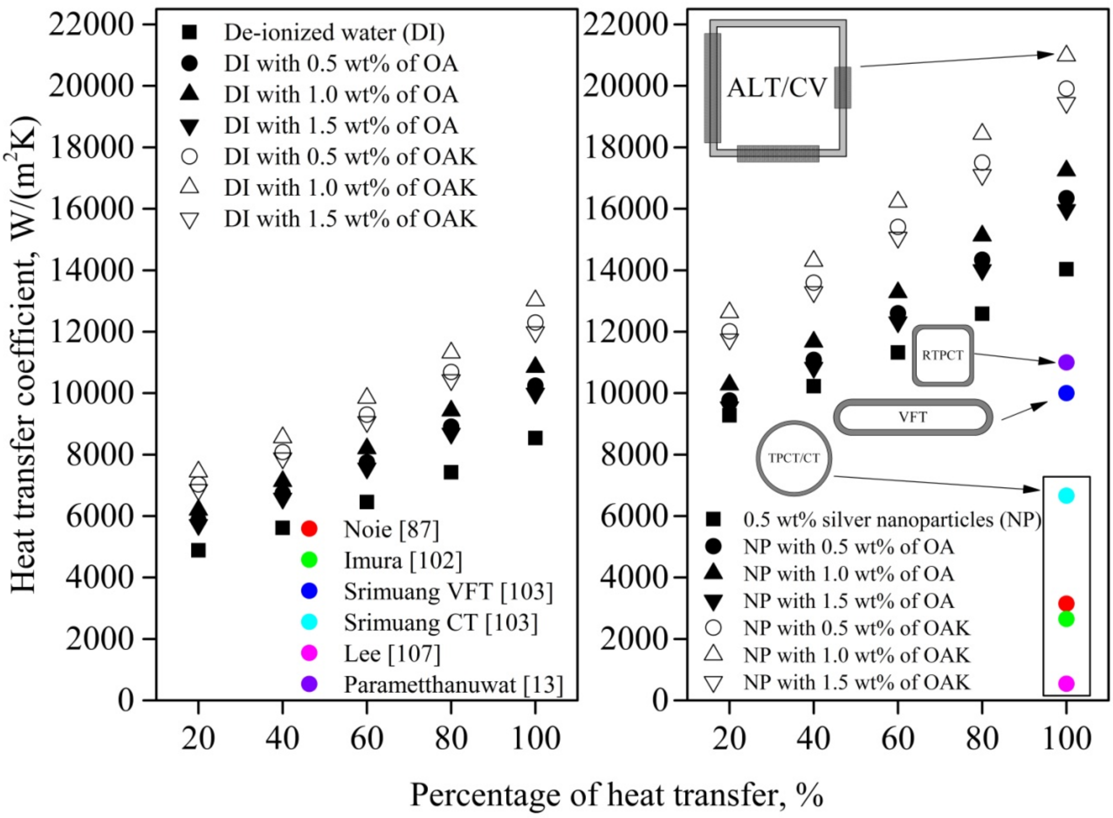

Figure 37 Effect of the heat transfer coefficient

3.7. Effect of the relative of thermal efficiency

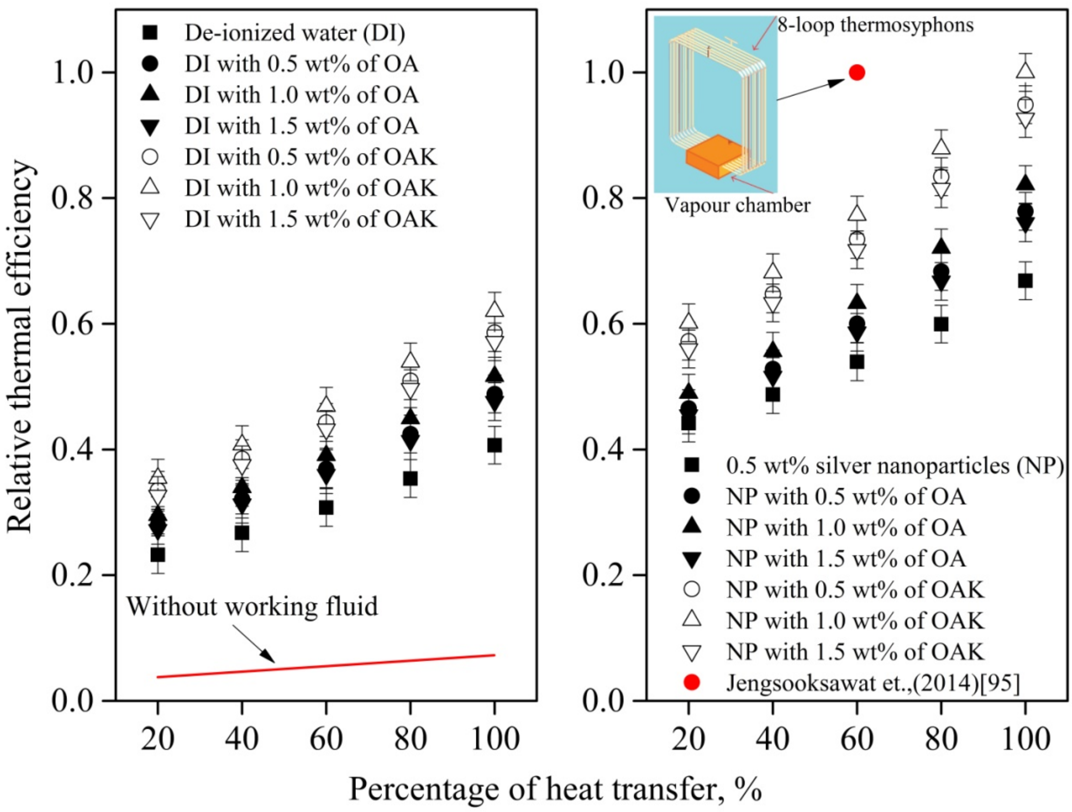

Figure 38 Effect of the relative of thermal efficiency

Figure 38 shows the relative thermal efficiency (RTE) of all working fluidsfiled. The RTE was presented with aloop size of 50 cm at a filling ratio of 50% and an OPHS of 100%. According to our experiment, the 1 wt% of OAK^{+} seemed to produce the maximum of RTE. The check valve of the loop thermosyphonwas helping the highest heat transfer behaviour as this check valve could separate and control the flow of the liquid and vapour[111-113]. However, the current experimental results contrasted with the results of Jengsooksawat et al., (2014) [95]. Studies cited for this result werecompared with Jengsooksawat et al., (2014) [95], was used 8 loop thermosyphons with OPHS of 1,200 W, an air velocity of 0.5 m/s, and a filling ratio of 60% of ethanol as a working fluid. Thus, it is important to note the vast differences among different experimental conditions, especially in regard to the type of heat pipe and thermosypon. In addition, the thermal motion of the nanoparticles enhanced the thermal conductivity of the nanofluids. The OA and K^+ helpedthe homogeneous dispersion of the nanoparticles in the nanofluids. Moreover, Brownian motion significantly contributed to the risein the thermal conductivity of the nanofluids. Thus, the thermal conductivity was superior, it had the heat transfer rate mechanism efficiently over thermal diffusion in the fluid [34, 43].

3.8. Dimensionless

3.8.1. The effect of the dimensionless group on Kutateladze number (Ku)

The dimensionless parameters on heat transfer characteristics of the ALT/CV; thus, $\frac{Lo_{size}}{D_i}$, $Pr, Bo, Ja, Co, Cd, Ga_m, Pe_m, Ar, Gr \text{ and } Z$ values can be used to formulate a correlation to predict the heat transfer rates of the ALT/CV. The standard least square curve fitting technique was adopted. The power function was found to be the best representation to formulate a correlation. Thecorrelation of the Ku number to predict the heat transferred from the ALT/CV was:

$$Ku = 3.24\left[\frac{Lo_{size}}{D_i}^{6} \cdot \frac{\mathrm{Pr}^{6.2}\cdot Bo^{6.4}\cdot Ja^{6.2}\cdot Co^{5.2}\cdot Cd^{3.8}\cdot {Ga_m}^{1.5}}{{Pe_m}^{2.7}\cdot Ar^{0.4}\cdot Z^{0.2}\cdot Gr^{0.6}}\right]^{1.57} \quad (53)$$

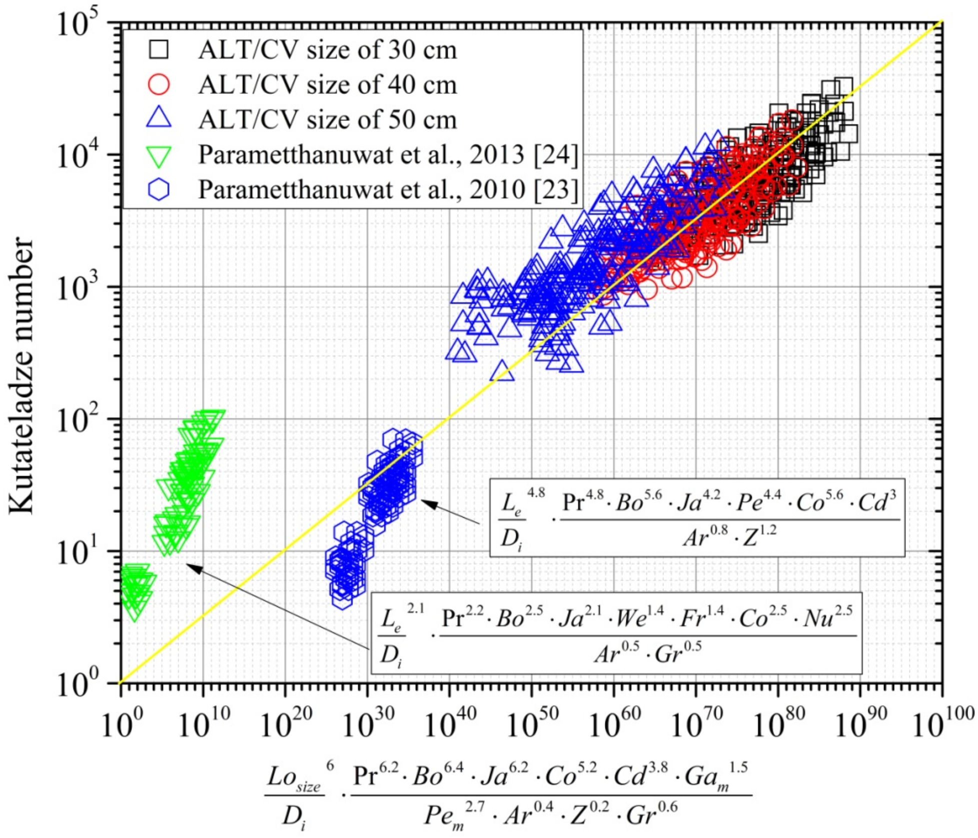

Figure 39 Relationship between the dimensionless group and Kutateladze number

The results are shown in Figure 39. It was further found that the filling ratio had no effect on the ratio of the heat transfer rates in the vertical position, but the properties of the working fluid affected the heat transfer rate. Furthermore, when the dimensionless groups were compared with the results of Parametthanuwat et al., (2013) [24] and Parametthanuwat et al., (2010) [23], it was found that the dimensionless group of the ALT/CV was higher than determined of them. In regards to this study, the results were achieved using the silver nanoparticles; however, there was a difference in the surfactant and the type of thermosyphon. Thus, it is important to note the vast differences in experiment conditions, especially in regards to the method of heat transfer rate.In addition, a correlation for predicting the heat flux for the ALT/CV in the vertical position has been established. Moreover, the coefficient of determination (R^2) of this equation was 0.8.

3.8.2.Correlation equation

From the results obtained, the heat flux of the ALT/CV positioned vertically can be evaluated from equation (54). As can be seen in Figure 40. Parametthanuwat et al., (2010) [23] used TPCT without surfactant and Parametthanuwat et al.,(2013) [24] used TPCT with OA, the heat flux was closed. Then, ALT/CV used NP containing OAK^{+}, had a heat flux similar trend with TPCT. The standard deviation (STD) of the experimental heat flux and the predicted heat flux using equation (29) was ±5%. Therefore, it can beconcluded that this equation can be used to predict the heat flux of the RTPCT and TPCT, as shown in Figure 40.

$$q = 3.24\left[\frac{Lo_{size}}{D_i}^{6} \cdot \frac{\Pr^{6.2} \cdot Bo^{6.4} \cdot Ja^{6.2} \cdot Co^{5.2} \cdot Cd^{3.8} \cdot Ga_m^{1.5}}{Pe_m^{2.7} \cdot Ar^{0.4} \cdot Z^{0.2} \cdot Gr^{0.6}}\right]^{1.57} \times \left[\rho_v h_{fg}\left(\frac{\rho_v - \rho_l}{\rho_v^{2}}\right)\right]^{0.25} \quad (54)$$

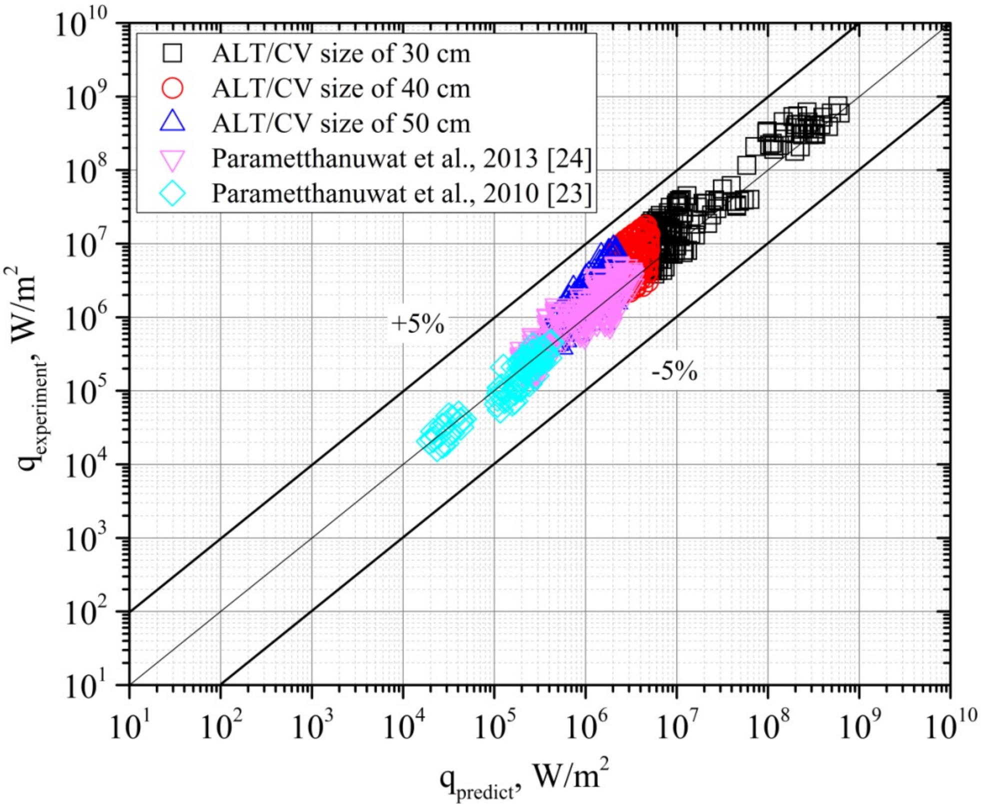

Figure 40 Comparison between $q_{predict}$ and $q_{experiment}$

4. Conclusion

This chapterexaminedthe thermal behaviour in an ALT/CV and in particular emphasizeda new “loop type of thermosyphon installed check valve” design. It wasdivided into a number of sections to demonstrate the thermal behavior, as follows:

- The ALT/CV at a loop size of 50 cmyielded better heat transfer behaviour with a filling ratio of 50% with respect to the evaporator volume when the NP with 1 wt% of OAK^+ was used as a working fluid and the percentage of the heat supplied was 100%. It was further found that the loop size of 50 cm and a filling ratio of 50% with respect to the evaporator volume were superior in thermal behaviour over other parameters throughout all experimental conditions in this study, with a relative thermal efficiency of about 1.

- In the dimensionless analysis, it was found that the filling ratio did not affect the heat transfer rate; however, the properties of the working fluid did [23, 24]. Therefore, these properties dominated the dimensionless parameters and the Ku correlation and showed that the standard deviation for predicting heat flux was ±5%.

Finally, in conclusion, the ALT/CV led to an enhancement and produced a better performance than the normal type of thermosyphon. The loop type of thermosyphon installed check valveisa new type of thermosyphon, which is appropriate for use in heat transfer engineering. The presence of OA and K^+ clearly contributed to the rise inthe heat transfer rate and the improvement of nanofluid properties.

CHAPTER V APPLICATION OF LOOP THERMOSYPHON

1. Introduction and Literature review

The dimensionless is formulated from Chapter IV to correlate and predict the heat transfer characteristic of the ALT/CV to Kutateladze number (Ku). The silver nanofluids containing OAK^+ surfactant in a prototye of oven an advanced loop thermosyphon with check valve (OALT/CV) are then applied. The OALT/CV used in this study was a special type which uses nanofluids in the loop thermosyphon to transfer heat from the evaporator to condenser without external energy requirement. The primary objective of this study is to design and test the OALT/CV so that it will increase the heat transfer to water. The heat will be helpful to distribution the temperature profile in the OALT/CV which is regularly. This OALT/CV was designed using a correlation of Kutateladza number (Ku). This review can be summarized from the challenges of the on-line characterization of thermal performance, rheological behaviour and OALT/CV.

Da Silva et al., [114] used TPCT in cooking chambers using a real size prototype. The TPCT has 1,200 *mm* of total length with water as working fluid and filling ratio of 60%. It was found that the temperature inside the prototype was shown to be highly uniform due to the large area of the condenser which was responsible for heating of the cooking chamber. Therefore, the incidence of radioactive energy over any product placed in the cooking chamber will be highly uniform, avoiding over/under cooked products. Based on that, the model shows the internal temperature and the prototype can be determined theoretically with good precision. Moreover, Milanez [115] studied TPCT heat enclosure with the dimensions 0.38×0.48×0.61 *m*, eight stainless steel, and added water as the working fluid. It was found that the enclosure heated using the TPCT had more uniform temperature and radioactive heat transfer coefficient distributions compared to the conventional approach. The conventional enclosure tends to present larger convective heat transfer coefficients than the thermosyphon assisted enclosure because of movement of the exhaust gases. The radiation field inside the thermosyphon assisted enclosure is more uniform than the conventional enclosure. A more uniform radiation field is obviously better when applying the enclosure for cooking purposes as it cooks more evenly. Nanofluid plays an important role in improving TPCT's heat transfer. In 2010, Parametthanuwat et al., [116] applied TPCT for energy conservation containing silver and gold nanofluid at the 0.5 wt% concentration. It was found that the TPCT which used silver nanofluid appeared to have uniform temperature distribution. Consequently, processing time and LPG consumption could be reduced by 10 *min*/*unit* and 1.8 *kg*/*unit*, respectively. The original oven was 37.1% more effectiveness after the installation of the TPCT and was 69.8% more effectiveness when using silver nanofluids. Obviously, the installation of the TPCT containing nanofluid was helpful to thermal distribution and improved the overall thermal effectiveness. Then, Kiniman et al., [117] improved the top heat mode closed loop oscillating heat pipe with a check valves air pre-heater (THMCLOHP/CV/AP) for chilli drying. The THMCLOHP/CV/AP showed the highest effectiveness of 0.1 at an operating temperature of 80°*C* with an air velocity of 0.5 *m/s*. The processing time used for drying chilli was 2 hours and 20 minutes. The quality of the colour measurement of the chilli exceeded the marketplace with the total colour difference (ΔE^*) being significantly different ($p \leq 0.05$). Moreover, Topuz et al., [118] studied the effect of methods and storage on the colour of paprika with the Refractance Window Drying method (RWD). Thus, the colour statistical analyses pointed out were significantly different ($p < 0.05$), according to Kiniman et al., [117]. Finally, the quality of the product such as colour, oven time and energy thrift have been important in the oven process.

2. The oridinary oven chilli

The ordinary chilli oven is usually driven by solar method, fluidized bed and etc. An oven without a heat pipe represents lower operational cost, but an oven with a heat pipe is considered economical and easier to operate. Something to note is that the chilli oven method rejects energy at high temperature, resulting in energy losses which is under moisture standard lower at 13% wet basic. Also, to guarantee reasonable temperature distribution, a ventilator, similar to the one employed to ovens with a heat pipe, is used, according to Kiniman el al., [117]. A diagram of the installation of a ALT/CV is shown in Figure 41 and process oven diagram shown in Figure 48.

3. The experimental apparatus anlysis

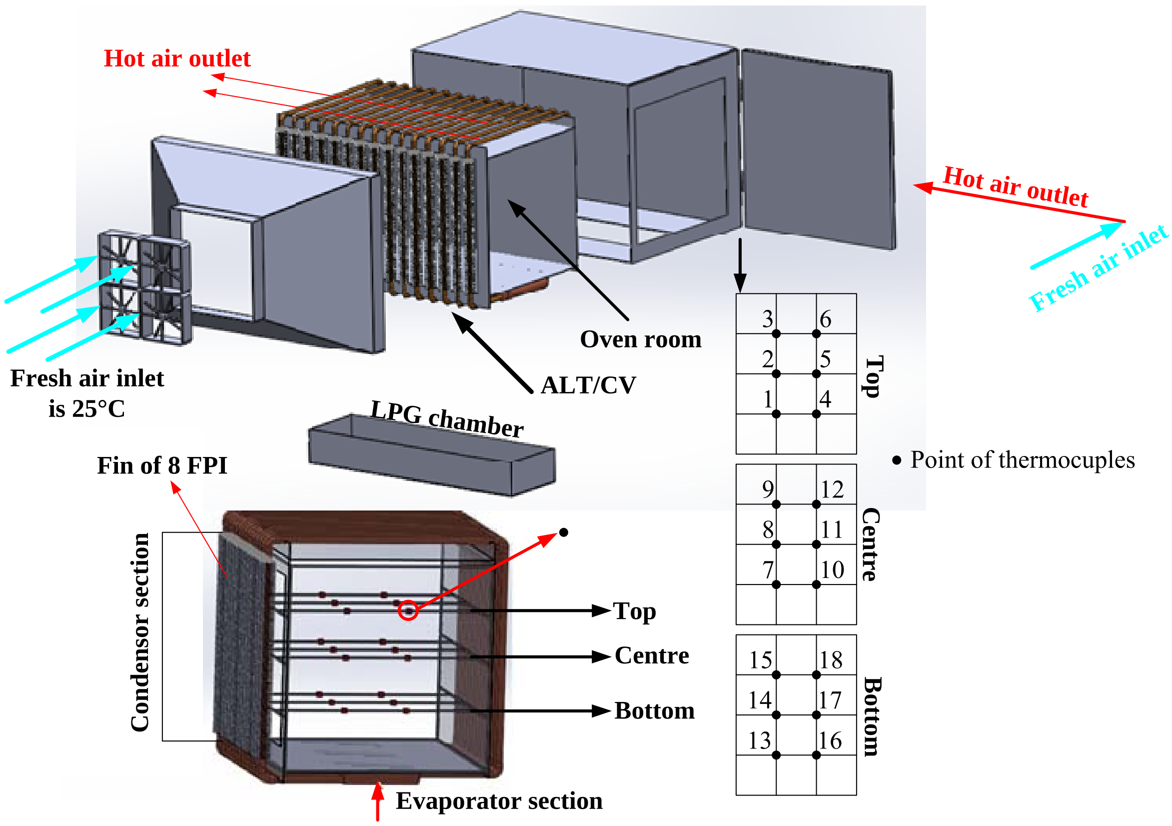

Figure 41 The prototye of oven an advanced loop thermosyphon with check valve (OALT/CV)

2.1. Chilli oven design

The prototye of oven an advanced loop thermosyphon with check valve (OALT/CV) in Figure 41 was designed using the Kutataladza number (Ku). The above-stated dimensionless numbers were correlated with Ku form Equation (54), to calculate the convection heat transfer capacity of one tube. From Equation (53), the heat flux of TPCT at a vertical position can be evaluated from Equation (54). The calculation showed that the number of tubes for OALT/CV is 15 loops.

Figure 41 shows the dimensions of the OALT/CV and Table 4 shows condittion study. The loop thermosyphon was combined with a vapour chamber that could be separated from the loop thermosyphon (adiabatic section and condenser section) and the vapour chamber (evaporator section). The fifteen loop thermosyphons with check valve were made from copper tube with an inside diameter of 12.70 mm. The OALT/CV had a dimension size of 600×600×600 mm (W×L×H) with an 15 loop thermosyphon with check valve length size of the adiabatic, condenser and evaportor sections being 1000, 500 and 500 mm respectively. The fin was assembled as 8 FPI of the area of the condenser in order to improve heat exchange. The heat was removed from the condenser sections with convective forced heat transfer that was blown through this section. Air flow and velocity was controlled by the use of an AC motor. The fifteen loop thermosyphons with check valve were connected to a vapour chamber as an evaporator section.

2.2. Temperature distribution measurement in oven room

This section focuses on temperature distribution inside the OALT/CV which uses the conventional approach as shown in Figure 41. Figure 41 presents the temperature reading points used to monitor the temperature distribution inside a baking oven. Eighteen thermocouples were installed for data collection (Yokogawa DX200 with ±0.1°C accuracy, 30 channel input and −200°C to 1,100°C measurement temperature- range) and were used with type K thermocouples (OMEGA with ±0.1°C accuracy) [116]. Then, all the data from Figure 41 inside the oven was used in a computer program to determine the temperature contour.

2.3. Quality of chilli analysis

The colour of chilli analysis was determined using Hunter lab-MiniScan EZ to measure colour in terms of *L** *a** and b*. The *L*, a*, b** model is an international standard for colour measurement developed by the Commission International d'Eclairage (CIE) in 1976. The luminance or lightness component (*L**) is value, ranging from 0 to100. The colour component green to red (*a**) and blue to yellow (*b**) is ranging from -120 to +120. Then, all components are calculated to a total colour difference (ΔE^*) in equation (55) , which has recently been compiled by Parametthanuwat et al. [116] and Kiniman et al. [117].

$$\Delta E^* = \left[\left(\Delta L^* \right)^2 + \left(\Delta a^* \right)^2 + \left(\Delta b^* \right)^2 \right]^{0.5} \tag{55}$$

The sensory of chilli was tests. All samples of ovened chili were blend into chili powder using blender Vitamix Company: USA as a model Vitamix 5200 at 5,000 rpm for 1 min. Then, the consumer acceptability of size, odor, and colour of the powder chili was evaluated by a 5-score hedonic scale sensory test [119, 120]. The categories for consumer acceptability were 1 = low, 2 = slightly low, 3 = intermediate, 4 = slightly high, and 5 = high. The number of consumers was 20. The experiment was performed in 3 replicates.

The shear force of chilli analysis was evaluated using Texture Analyzer (TA.XT plus, Stable Micro Systems, UK) to imitate the cutting and blending of chilli powder in manufacture industry. The 1 N load cell was equipped with blade set and the speed of the knife was set at 3 mm/s. The chilli sample size was a cylinder length of 30 mm and a diameter of 10 mm. Statistical analyses were based on Duncan's multiple range tests for means separation. Significant differences among the data were observed when $\alpha < 0.05$ [116, 117, 120].

4. Result and discussion

3.1. The temperature distribution

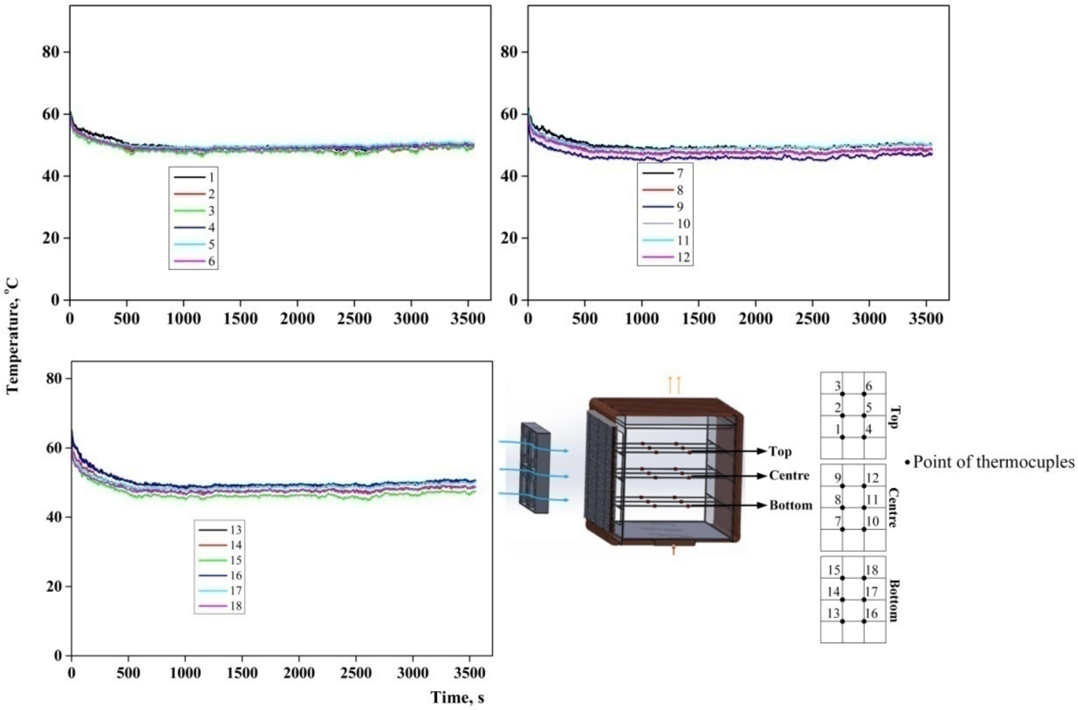

Figure 42 The distribution temperature inside the OALT/CV - Without workingfluids

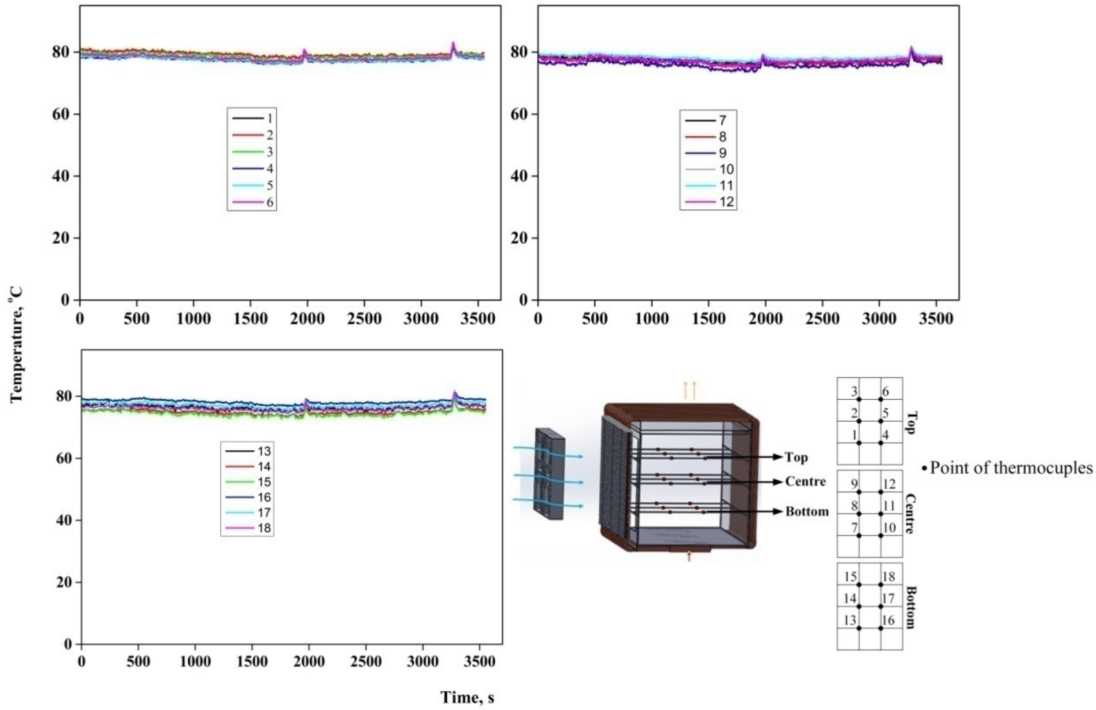

Figure 43 The distribution temperature inside the OALT/CV - Deionized water

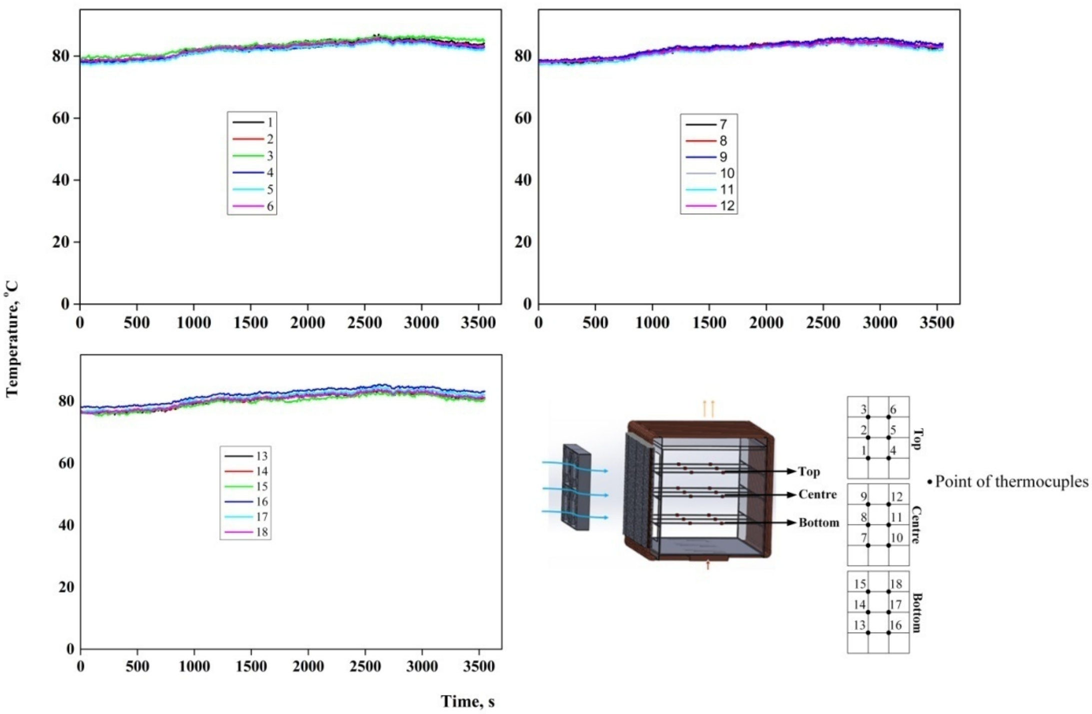

Figure 44 The distribution temperature inside the OALT/CV - 0.5 wt% silver nanoparticles (NP)

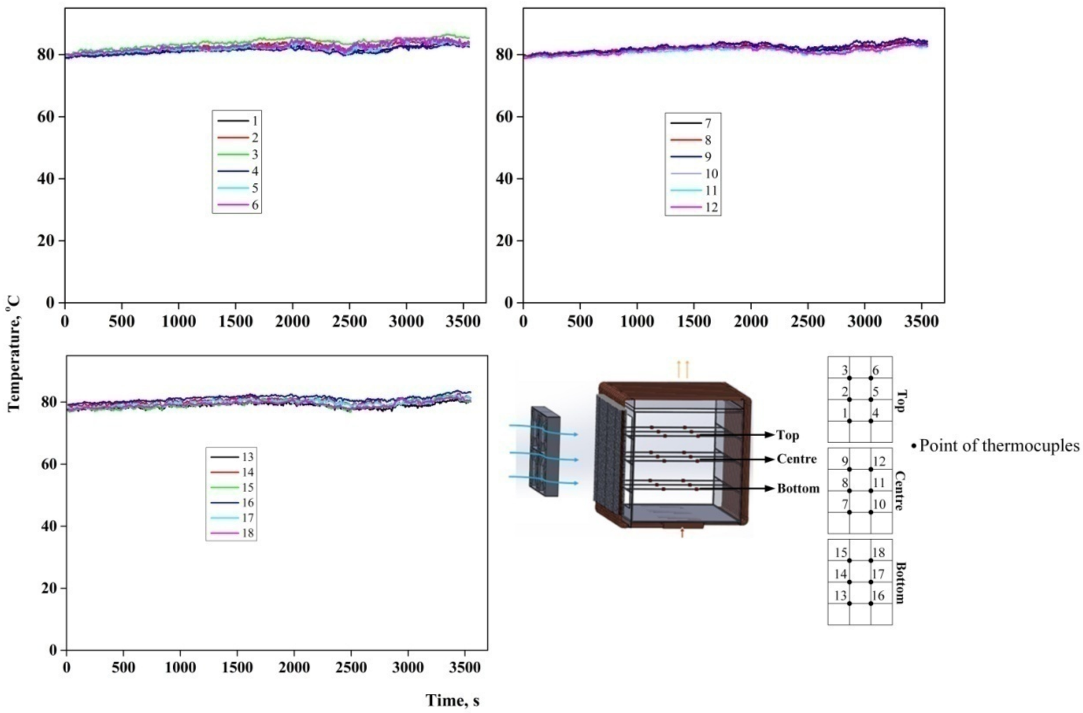

Figure 45 The distribution temperature inside the OALT/CV - NP containing 1.0 wt% of OA

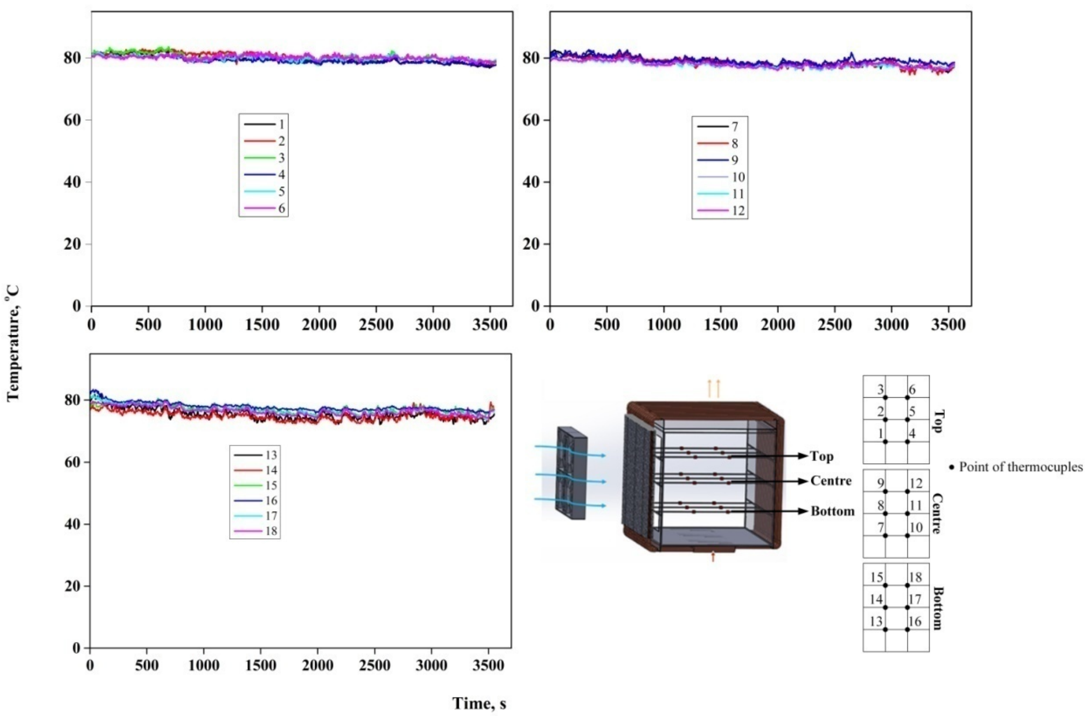

Figure 46 The distribution temperature inside the OALT/CV - NP containing 1.0 wt% of OAK+

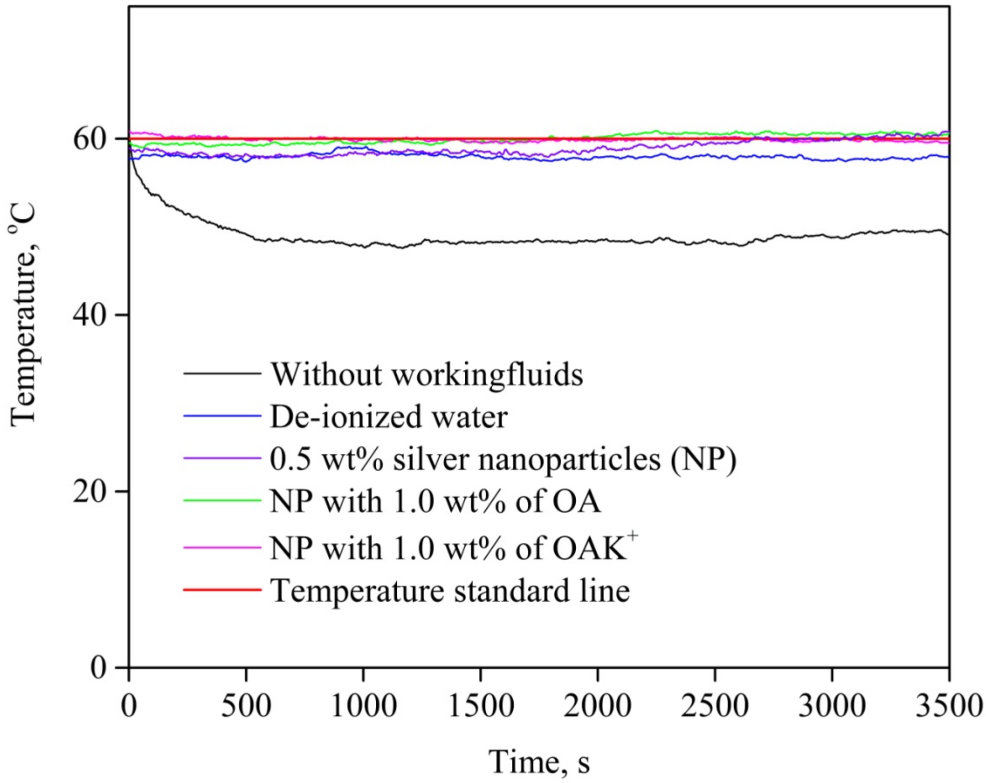

Figure 47 The distribution temperature inside the OALT/CV - Compared temerature contour

Table 10 Standard deviation of temperature inside of OALT/CV

Type of OALT/CV by workingfluids	**Standard deviation**		
	Top	**Centre**	**Bottom**
Without working fluids	±0.81	±0.67	±0.82
Deionized water	±0.50	±0.61	±0.72
0.5 wt% silver nanoparticles (NP)	±0.30	±0.30	±0.34
NP containing 1.0 wt% of OA	±0.20	±0.47	±0.33
NP containing 1.0 wt% of OAK+	±0.25	±0.33	±0.42

Figure 42, Figure 43, Figure 44, Figure 45 and Figure 46 of the OALT/CV shown temperature distribution at inside temperature controlled at 80°C with air velosity of 1 m/s. On the other hand, Figure 42 as a without working fluids was generated close inside average temperature at

$60^{o}C$ with air velosity of 1 m/s which was maximum and properly for OALT/CV- without working fluids. However, Figure 47 shown compared temperature distribution with operating temperatures at 60°C with line standard from OALT/CV- without working fluids. It was found that the temperature distribution around inside of the OALT/CV filled NP containing OAK^{+} was more regular than the other work ingfluids. The maximum temperature difference of OALT/CV was according to Table 10 in each type of OALT/CV by workingfluids. Consequently, the OALT/CV filled NP containing OAK^{+} helped temperature distribution and gave higher quality performance than the OALT/CV without a working fluids.

3.2. The Quality of chilli

A chilli quantities study can be explained as follows into 3 groups including manufacturing standards: Colour quantities, Shear force and Sensory test. All groups was controlled by moisture lower than 13% wet basic. The quality of chilli measurement diagram shown in Figure 48.

The colour measurement of chilli is shown in Figure 49. The total colour difference (ΔE*) will be according to the manufacturing standard. Thus, the statistical analysis points out that ΔE* of chilli oven were significantly different ($p \leq 0.05$). Furthermore, the colour measurement of fresh chili, dried chilli from manufacturing and OALT/CV is shown in Table 11. Thus, each oven type have produced ΔE* chilli similar to the manufacturing. Comparing both through statistical analysis points out that the colour measurement of chilli drying prepared by all conditions are significantly different ($p \leq 0.05$) which is according with Kiniman et al. [117]. The quality of colour of the chilli form OALT/CV exceeded the manufacturing standard. Definitely, the OALT/CV is confirmed as having good performance with short time.

Table 11 Total colour difference of chili

OALT/CV type	Colour quantities			
	L*	a*	b*	ΔE
Frech chili (Oven total time = N/A)	$34.02^{ab}\pm3.824$	$38.53^{cd}\pm5.61$	$24.33^{g}\pm5.23$	-
Manufacturing (Oven total time = N/A)	$26.86^{b} \pm 0.131$	$23.59^{d} \pm 0.541$	$13.03^{ab}\pm 0.39$	$28.88^{ag} \pm 0.68$
Without working fluid (Oven total time = 21 hr)	$34.96^{ca}\pm2.47$	$25.87^{de}\pm1.68$	$15.91^{cb}\pm1.40$	$26.47^{fg}\pm1.68$
Deionized water (Oven total time = 17 hr)	$30.58^{a}\pm2.59$	$26.92^{eg}\pm3.67$	$19.54^{cg}\pm4.58$	$29.78^{fb}\pm5.02$
0.5 wt% silver nanoparticles (NP) (Oven total time = 15.5 hr)	$31.86^{abc}\pm1.44$	$22.54^{efg}\pm1.13$	$15.42^{c}\pm1.05$	$25.93^{be}\pm2.32$
NP containing 1.0 wt% of OA (Oven total time = 14 hr)	$31.53^{a}\pm1.06$	$24.23^{fg}\pm4.49$	$17.06^{ag}\pm0.88$	$24.35^{ce}\pm1.56$
NP containing 1.0 wt% of OAK^{+} (Oven total time = 11)	$32.93^{ab}\pm2.42$	$22.65^{f}\pm4.49$	$14.4^{c}\pm3.59$	$27.92^{bg}\pm4.70$

Difference superscript (a,b,c,d,e,f and g) in the same column means that the values signification different ($p\leq 0.05$)

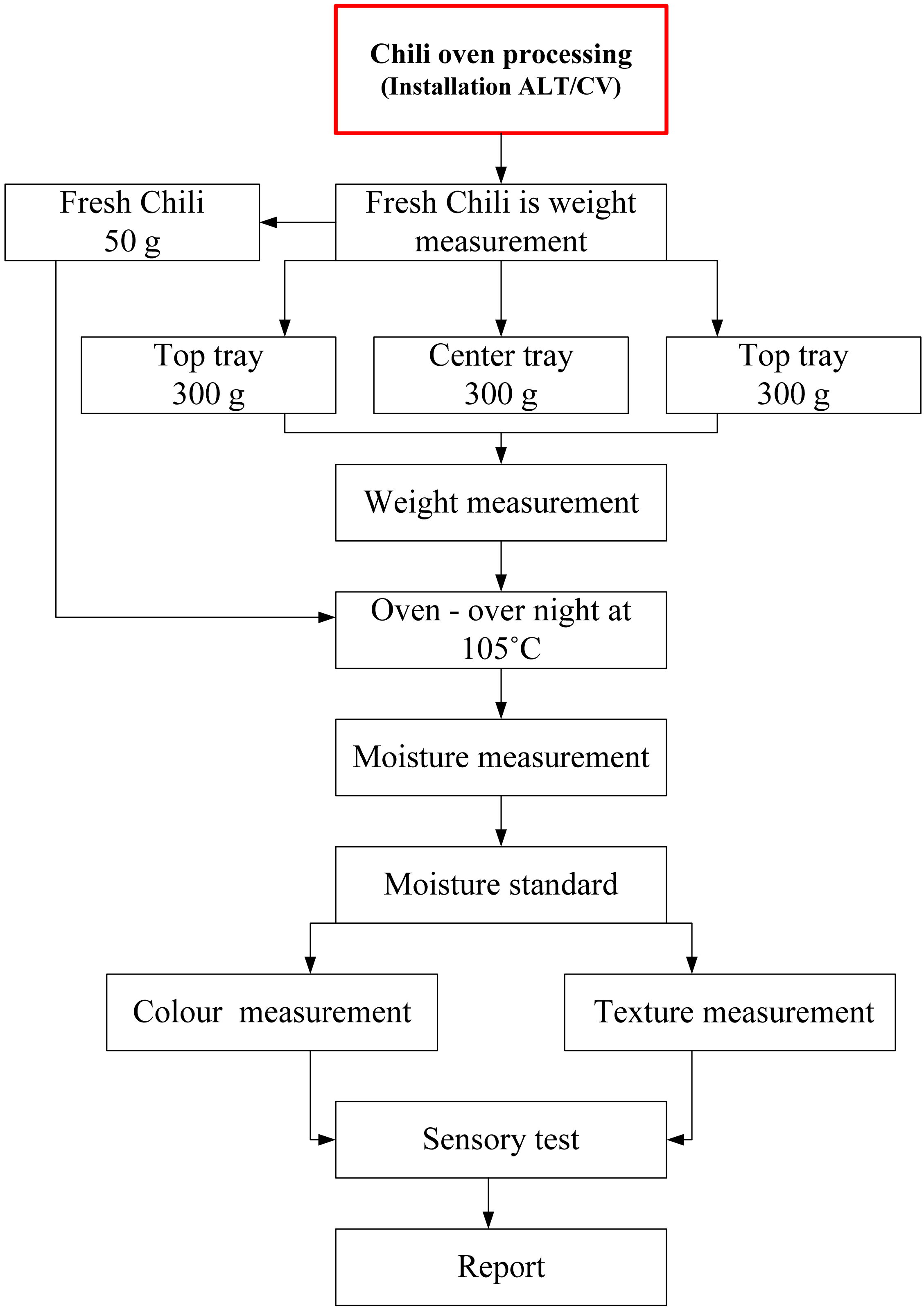

Figure 48 The quality of chilli measurement

Frech chili

Manufacturing

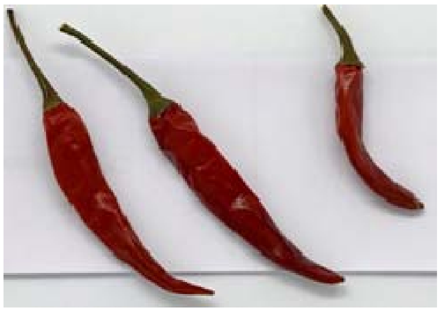

Without working fluid

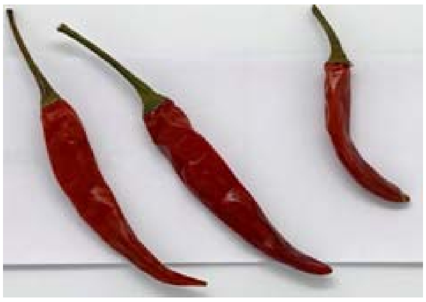

Deionized water

0.5 wt% silver nanoparticles (NP)

NP containing 1.0 wt% of OA

NP containing 1.0 wt% of OAK^+

Figure 49 The colour chilli of each type oven

The result of sear froce is shown in Table 12 and Figure 50. The values showed that shear force of OALT/CV is close the manufacturing. Moreover, shear force of OALT/CV did not significant different when comparing with that of manufacturing standard. This result revealed that blending of O/LTCV was easy and consumed less energy. The quality of chilli powder of the chilli form O/LTCV exceeded the manufacturing standard.

Table 12 Shear force (N) of dried chili

Type of OALT/CV by workingfluids	**Shear force (N)**
Manufacturing	$25.62^{a} \pm 1.11$
Without working fluids	$27.28^{a} \pm 2.36$
Deionized water	$26.48^{a} \pm 2.31$
0.5 wt% silver nanoparticles (NP)	$25.32^{a} \pm 3.25$
NP containing 1.0 wt% of OA	$26.72^{a} \pm 2.89$
NP containing 1.0 wt% of OAK^{+}	$25.78^{a} \pm 3.15$

Table 13 The result of Sensory score

Type of OALT/CV by workingfluids	**Sensory score**			
	Colour	Texture	Spicy and Smell	Odor
Manufacturing	$4.12^{a} \pm 0.65$	$4.20^{a} \pm 0.72$	N/A	N/A
Without working fluids	$4.45^{a} \pm 0.19$	$4.78^{a} \pm 0.48$	N/A	N/A
Deionized water	$4.33^{a} \pm 0.71$	$4.72^{a} \pm 0.43$	N/A	N/A
0.5 wt% silver nanoparticles (NP)	$4.39^{a} \pm 0.22$	$4.23^{a} \pm 0.59$	N/A	N/A
NP containing 1.0 wt% of OA	$4.00^{a} \pm 0.63$	$4.30^{a} \pm 0.33$	N/A	N/A
NP containing 1.0 wt% of OAK^{+}	$4.68^{a} \pm 0.12$	$4.16^{a} \pm 0.43$	N/A	N/A

Difference superscript (a and b) in the same column means that the values signification different ($p \leq 0.05$)

Manufacturing

Without working fluid

Deionized water

0.5 wt% silver nanoparticles (NP)

NP containing 1.0 wt% of OA

NP containing 1.0 wt% of OAK^{+}

Figure 50 Shear force of dried chili

Sensory test in Table 13 is normally used to indicate consumer acceptability in food product. To evaluate and compare consumer acceptability of ovened chili which were produce from different oven. Sensory test was then performed. The result presented that the sensory which were produce from different ovened chili were in the range of 4.00 - 4.46. The values of colour, texture, spicy and smell which was product from OALT/CV ovened chili and manufacturing were significant different. The consumer agreed with the results of shear force, L*, a*, b*, *ΔE**, smell and tester to check the level of spicy. This result indicated that OALT/CV oven can produce high quality of ovened chili. Consumer accepted OALT/CV oven chili similar with manufacturing.

3.3. The OALT/CV effectiveness

Table 14 The OALT/CV effectiveness

Type of OALT/CV by workingfluids	**OALTCV effectiveness (%)**		
	60	**70**	**80**
Without working fluids	-	-	-
Deionized water	18.92	25.23	35.33
0.5 wt% silver nanoparticles (NP)	28.36	30.45	444.58
NP containing 1.0 wt% of OA	37.45	46.26	52.36
NP containing 1.0 wt% of OAK^+	48.65	55.23	65.46

Table 14 shows the effectiveness of the OALT/CV with calulated form air velocity and LPG. It was found that the effectiveness dependant on air velosity and LPG. The maximum effectiveness of the OALT/CV was 65.46% with NP containing 1.0 wt% of OAK^+. Consumer accepted OALT/CV depent on condittion in oven application which was selected.

5. Conclusions

The OALT/CV gave a total colour difference similar with the chilli from the manufacturing. All chilli at each tray level in the oven from OALT/CV had a total colour, texture, spicy and smell difference with the statistical analysis pointing out significant difference ($p \leq 0.05$). However, the quality of chilli ovened will exceed the manufacturing standard. Moreover, the ALT/CV improvement in the oven was more economical in the energy consumption cost which is increasing effectiveness. In conclusion, the design and improvement of the OALT/CV led to performance in oven process The OALT/CV has maintained a quality exceeding the manufacturing while saving in energy consumption cost by a short time.

CHAPTER VI CONCLUSION

The objective of this study is based on the heat transfer rate of ALT/CV applying silver particles which containing oleic surfactant (OA) and potassium oleate surfactant (OAK^+) as working fluid. By solving the problem of traditional TPCT with advanced loop and check value will be led the heat transfer rate enhancement.

Finally, in conclusion, the thermal properties of NF containing OAK^+ was superior in thermal behaviour, over water studied in all experimental conditions. The presence of OAK^+ had clearly contributed to the rise in the heat transfer rate. By improving the properties of the working fluid with the OAK^+ this led to thermal properties enhancement, thus giving better properties than the OA. The OAK^+ showed compatibility with silver nanoparticle. The OAK+ was Newtonain fluid. The optimum concentration for the addition of OAK^+ in the working fluid was 1 wt%. Expectedly, the heat transfer rate of ALT/CV was superior in heat transfer rate over of all experimental conditions studied. The design and improvement of the OALT/CV led to performance in oven process. The OALT/CV has maintained a quality exceeding the manufacturing while saving in energy consumption cost by a short time.

REFERENCES

1. Dunn, P. and D. Reay, *Heat pipe.* Pergamong Intrnational Library, 1982.
2. Parametthanuwat, T., *Heat transfer characteristics of the two-phase closed thermosyphon (TPCT) containing silver nanofluids with oleic acid surfactant*, in *Mechanical Engineering*. 2012, Mahasarakham University Mahasarakham; Thailand.
3. Paramatthanuwat, T., et al., *Heat transfer characteristics of a two-phase closed thermosyphon using de ionized water mixed with silver nano.* Heat and Mass Transfer, 2010. **46**(3): p. 281-285.
4. Noie, S.H., M.R.S. Emami, and M. Khoshnoodi, *Effect of inclination angle and filling ratio on thermal performance of a two-phase closed thermosyphon under normal operating conditions.* Heat Transfer Engineering, 2007. **28**(4): p. 365-371.
5. Imura, H., et al., *Critical heat flux in a closed two-phase thermosyphon.* International Journal of Heat and Mass Transfer, 1983. **26**(8): p. 1181-1188.
6. Imura, H. and Y. Koito, *Heat transfer characteristics in two-phase closed thermosyphons with a tubular sinter.* Kagaku Kogaku Ronbunshu, 2003. **29**(5): p. 698-700.
7. Shiraishi, M., K. Kikuchi, and T. Yamanishi, *Investigation of heat transfer characteristics of a two-phase closed thermosyphon.* Journal of Heat Recovery Systems, 1981. **1**(4): p. 287-297.
8. Kew, P.A. and D.A. Reay, *Compact/micro-heat exchangers - Their role in heat pumping equipment.* Applied Thermal Engineering, 2011. **31**(5): p. 594-601.
9. Vajravelu, K., et al., *Convective heat transfer in the flow of viscous Ag-water and Cu-water nanofluids over a stretching surface.* International Journal of Thermal Sciences, 2011. **50**(5): p. 843-851.
10. Yu, W., et al., *Review and assessment of nanofluids technology for transportation and other application, Energy system Division,.* Argonne National, Argonne, IL60439, USA., April, 2007.
11. Choi, S.U.S. and J.A. Eastman, *Enhancing thermal conductivity of fluids with nano-particles*, in *International mechanical engineering congress and exhibition*. 1995, ASME: San Francisco, CA (United States).
12. Choi, S.U.S., *Nanofluids: A new field of scientific research and innovative applications.* Heat Transfer Engineering, 2008. **29**(5): p. 429-431.
13. Bhuwakietkumjohn, N. and T. Parametthanuwat, *Heat transfer behaviour of silver particles containing oleic acid surfactant: application in a two phase closed rectangular cross sectional thermosyphon (RTPTC).* Heat and Mass Transfer, 2017. **53**(1): p. 37-48.
14. Reay, D. and P. Kew, *Heat pipe, Theory, Design and Application Fifth edition.* Butterworth-Heinemann. Jordan Hill, Oxford, UK, 2006.
15. Anon., *Heat pipes-general information on their use, operation and design, Data Item No. 80013.* . 1980, London: Engineering Sciences Data Unit.
16. Lock, G.S.H., *The tubular thermosyphon variations on a theme*, ed. 1st. 1992, New York: United State: Oxford University Press.
17. Bhuwakietkumjohn, N. and T. Parametthanuwat, *Heat transfer behaviour of silver particles containing oleic acid surfactant: application in a two phase closed rectangular cross sectional thermosyphon (RTPTC).* Heat and Mass Transfer, 2016: p. 1-12.
18. Noie, S.H., et al., *Heat transfer enhancement using Al2O3/water nanofluid in a two-phase closed thermosyphon.* International Journal of Heat and Fluid Flow, 2009. **30**(4): p. 700-705.

19. Mehta. B and Khandekar. B, *Two-phase closed thermosyphon with nanofluids*, in *14th International Heat Pipe Conference (14th IHPC)*. 2007: Florianópolis, Brazil.

20. Khandekar, S., Y. Joshi, and B. Mehta, *Thermal performance of closed two-phase thermosyphon using nanofluids.* Thermal Science, 2008. **47**: p. 695 - 667.

21. Dewitt, F.P.I.a.D.P., *Introduction to Heat Transfer.*, ed. Forth. 2002, New York, USA: John Wiley & Sons, Inc.

22. DP, I.F.a.D., *Fundamental of Heat and Mass Transfer*. 1996, New York: Wiley.

23. Parametthanuwat, T., S. Rittidech, and A. Pattiya, *A correlation to predict heat-transfer rates of a two-phase closed thermosyphon (TPCT) using silver nanofluid at normal operating conditions.* International Journal of Heat and Mass Transfer, 2010. **53**(21-22): p. 4960-4965.

24. Parametthanuwat, T. and S. Rittidech, *Silver Nanofluid Containing Oleic Acid Surfactant As Working Fluid In The Two-Phase Closed Thermosyphon (TPCT): A Thermodynamic Study.* Nanoscale and Microscale Thermophysical Engineering, 2013. **17**(3): p. 216-235.

25. Payakaruk, T., P. Terdtoon, and S. Ritthidech, *Correlations to predict heat transfer characteristics of an inclined closed two-phase thermosyphon at normal operating conditions.* Applied Thermal Engineering, 2000. **20**(9): p. 781-790.

26. Keblinski, P., J.A. Eastman, and D.G. Cahill, *Nanofluids for thermal transport.* Materials Today, 2005. **8**(6): p. 36-44.

27. Parametthanuwat, T. and N. Bhuwakietkumjohn, *Application of Nanofluid in Thermosyphon (TPCT) - A review*, in *Nanotechnology fundamentals and applications*, J.N. Govil, Editor. 2013, Studium Press LLC.: U.S.A. p. 293-310.

28. R.P.Chhabra, *Non-Newtonian Fluids: An Introduction*, in *SERC School-cum*. 2010: Indian Institute of Technology Kanpur.

29. S. Fohanno, C.N.a.G.P., *Newtonian Nanofluids in convevtion.* Handbook of Physical, Nanoparticles and Quantum Dots, Taylor and Francis Group, LLC, 2011.

30. Buyevich, Y.A., *Fluid Dynamics in Fine Suspension Flow. In Advances in the Flow and Rheology of Non-Newtonian Fluids, Part B. 1st ed.*, D.A.D.K. Siginer, D.; Chhabra, R. P.; Amsterdam, , Editor. 1999, The Netherlands: Elsevier. p. 1237-1297.

31. Xuan, Y. and W. Roetzel, *Conceptions for heat transfer correlation of nanofluids.* International Journal of Heat and Mass Transfer, 2000. **43**(19): p. 3701-3707.

32. Frank P. Incropera and D.P. Dewitt., *Fundamental of Heat and mass transfer Fourth edition*. Fourth edition ed. 1996, New York: John Wiley & Son.

33. Xuan, Y. and Q. Li, *Heat transfer enhancement of nanofluids.* International Journal of Heat and Fluid Flow, 2000. **21**(1): p. 58-64.

34. Kwak, K. and C. Kim, *Viscosity and thermal conductivity of copper oxide nanofluid dispersed in ethylene glycol.* Korea-Australia Rheology Journal, 2005. **17**(2): p. 35-40.

35. Parametthanuwat, T., et al., *Experimental investigation on thermal properties of silver nanofluids.* International Journal of Heat and Fluid Flow, 2015. **56**: p. 80-90.

36. Khandekar, S., Y.M. Joshi, and B. Mehta, *Thermal performance of closed two-phase thermosyphon using nanofluids.* International Journal of Thermal Sciences, 2008. **47**(6): p. 659-667.

37. Sreeremya, T.S., et al., *Synthesis and characterization of cerium oxide based nanofluids: An efficient coolant in heat transport applications.* Chemical Engineering Journal, 2014. **255**(0): p. 282-289.

38. Kang, H.U., S.H. Kim, and J.M. Oh, *Estimation of thermal conductivity of nanofluid using experimental effective particle volume.* Experimental Heat Transfer, 2006. **19**(3): p. 181-191.

39. Oliveira, G.A., E.P. Bandarra Filho, and D. Wen, *Synthesis and characterization of silver/water nanofluids.* High Temperatures-High Pressures, 2014. **43**(1): p. 69-83.

40. Trisaksri, V. and S. Wongwises, *Critical review of heat transfer characteristics of nanofluids.* Renewable & Sustainable Energy Reviews, 2007. **11**(3): p. 512-523.

41. Daungthongsuk, W. and S. Wongwises, *A critical review of convective heat transfer of nanofluids.* Renewable & Sustainable Energy Reviews, 2007. **11**(5): p. 797-817.

42. Wang, X.Q. and A.S. Mujumdar, *Heat transfer characteristics of nanofluids: a review.* International Journal of Thermal Sciences, 2007. **46**(1): p. 1-19.

43. Patel, H.E., et al., *Thermal conductivities of naked and monolayer protected metal nanoparticle based nanofluids: Manifestation of anomalous enhancement and chemical effects.* Applied Physics Letters, 2003. **83**(14): p. 2931-2933.

44. Sharma, P., et al., *Enhancement of thermal conductivity of ethylene glycol based silver nanofluids.* Powder Technology, 2011. **208**(1): p. 7-19.

45. Hwang, Y., et al., *Production and dispersion stability of nanoparticles in nanofluids.* Powder Technology, 2008. **186**(2): p. 145-153.

46. Li, X., et al., *Thermal conductivity enhancement dependent pH and chemical surfactant for Cu-H2O nanofluids.* Thermochimica Acta, 2008. **469**: p. 98 - 103.

47. Chen, H.S., et al., *Rheological behaviour of ethylene glycol based titania nanofluids.* Chemical Physics Letters, 2007. **444**(4-6): p. 333-337.

48. Singh, A.K. and V.S. Raykar, *Microwave synthesis of silver nanofluids with polyvinylpyrrolidone (PVP) and their transport properties.* Colloid and Polymer Science, 2008. **286**(14-15): p. 1667-1673.

49. Tamjid, E. and B.H. Guenther, *Rheology and colloidal structure of silver nanoparticles dispersed in diethylene glycol.* Powder Technology, 2010. **197**(1-2): p. 49-53.

50. Pak, B. and Y. Cho, *Hydrodynamic and heat transfer study of dispersed fluids with submicron metallic oxide particles.* Exp Heat Tran., 1998. **11**: p. 151.

51. Lu, K. and C. Kessler, *Colloidal dispersion and rheology study of nanoparticles.* Journal of Materials Science, 2006. **41**(17): p. 5613-5618.

52. Hojjat, M., et al., *Rheological characteristics of non-Newtonian nanofluids: Experimental investigation.* Int Comm Heat Mass Tran., 2011. **38**: p. 144.

53. Moghaddam, M.B., et al., *Preparation, characterization, and rheological properties of graphene–glycerol nanofluids.* Chemical Engineering Journal, 2013. **231**(0): p. 365-372.

54. Chen, H.S., Y.L. Ding, and C.Q. Tan, *Rheological behaviour of nanofluids.* New Journal of Physics, 2007. **9**.

55. Kleinstreuer, C. and Y. Feng, *Experimental and theoretical studies of nanofluid thermal conductivity enhancement: a review.* Nanoscale Research Letters, 2011. **6**.

56. Ramesh, G. and N. Prabhu, *Review of thermo-physical properties, wetting and heat transfer characteristics of nanofluids and their applicability in industrial quench heat treatment.* Nanoscale Research Letters, 2011. **6**(1): p. 334.

57. Rajabpour, A., et al., *Molecular dynamics simulation of the specific heat capacity of water-Cu nanofluids.* International Nano Letters, 2013. **3**(1): p. 58.

58. O'Hanley, H., et al., *Measurement and Model Validation of Nanofluid Specific Heat Capacity with Differential Scanning Calorimetry.* Advances in Mechanical Engineering, 2012. **2012**: p. 6.

59. Lu, M.-C. and C.-H. Huang, *Specific heat capacity of molten salt-based alumina nanofluid.* Nanoscale Research Letters, 2013. **8**(1): p. 292.

60. Cabaleiro, D., et al., *Rheological and volumetric properties of TiO2-ethylene glycol nanofluids.* Nanoscale Research Letters, 2013. **8**(1): p. 286.

61. Parametthanuwat, T., et al., *Application of silver nanofluid containing oleic acid surfactant in a thermosyphon economizer.* Nanoscale Research Letters, 2011. **6**(1): p. 315.

62. Bönnemann, H., et al., *Monodisperse copper- and silver-nanocolloids suitable for heat-conductive fluids.* Applied Organometallic Chemistry, 2005. **19**(6): p. 768-773.

63. Vekas, L., D. Bica, and O. Marinica *Magnetic nanofluids stabilized with various chain length surfactants.* Romanian Reports in Physics, 2006. **58**: p. 257–267.

64. Salehi, H., S.Z. Heris, and S.H. Noie, *Experimental Study of a Two-Phase Closed Thermosyphon with Nanofluid and Magnetic Field Effect.* Journal of Enhanced Heat Transfer, 2011. **18**(3): p. 261-269.

65. Huminic, G. and A. Huminic, *Heat transfer characteristics of a two-phase closed thermosyphons using nanofluids.* Experimental Thermal and Fluid Science, 2011. **35**(3): p. 550-557.

66. Chiu, W.S., et al., *Synthesis of two-dimensional ZnO nanopellets by pyrolysis of zinc oleate.* Chemical Engineering Journal, 2008. **142**(3): p. 337-343.

67. Molchanov, V.S., et al., *Viscoelastic Properties of Aqueous Anionic Surfactant (Potassium Oleate) Solutions.* Colloid Journal, 2005. **67**(5): p. 606-609.

68. Mondragon, R., et al., *Determination of the packing fraction of silica nanoparticles from the rheological and viscoelastic measurements of nanofluids.* Chemical Engineering Science, 2012. **80**: p. 119-127.

69. Singh, J., V. Verma, and K.D.P. Nigam, *Flow Characteristics of Power-Law Fluids in Coiled Flow Inverter.* Industrial & Engineering Chemistry Research, 2013. **52**(1): p. 207-221.

70. Lo, C.H., T.T. Tsung, and H.M. Lin, *Preparation of silver nanofluid by the submerged arc nanoparticle synthesis system (SANSS).* Journal of Alloys and Compounds, 2007. **434**: p. 659-662.

71. Anoop, K.B., et al., *Rheological and flow characteristics of nanofluids: Influence of electroviscous effects and particle agglomeration.* Journal of Applied Physics, 2009. **106**(3).

72. Tanvir, S. and L. Qiao, *Surface tension of Nanofluid-type fuels containing suspended nanomaterials.* Nanoscale Research Letters, 2012. **7**(1): p. 1-10.

73. Li, D., et al., *Preparation of Well-Dispersed Silver Nanoparticles for Oil-Based Nanofluids.* Industrial & Engineering Chemistry Research, 2010. **49**(4): p. 1697-1702.

74. Molchanov, V.S. and O.E. Philippova, *Effects of concentration and temperature on viscoelastic properties of aqueous potassium oleate solutions.* Colloid Journal, 2009. **71**(2): p. 239-245.

75. Fohanno, S., C. Nguyen, and G. Polidori, *Newtonian Nanofluids in convevtion*. Handbook of Nanophysics Handbook of Physical, Nanoparticles and Quantum Dots, . 2011: Taylor and Francis Group, LLC.

76. Godson, L., et al., *Experimental Investigation on the Thermal Conductivity and Viscosity of Silver-Deionized Water Nanofluid.* Experimental Heat Transfer, 2010. **23**(4): p. 317-332.

77. Kang, S.W., et al., *Experimental investigation of nanofluids on sintered heat pipe thermal performance.* Applied Thermal Engineering, 2009. **29**(5-6): p. 973-979.

78. Veilleux, J. and S. Coulombe, *A dispersion model of enhanced mass diffusion in nanofluids.* Chemical Engineering Science, 2011. **66**(11): p. 2377-2384.

79. Turkyilmazoglu, M., *Exact analytical solutions for heat and mass transfer of MHD slip flow in nanofluids.* Chemical Engineering Science, 2012. **84**: p. 182-187.

80. Rahimi, M., K. Asgary, and S. Jesri, *Thermal characteristics of a resurfaced condenser and evaporator closed two-phase thermosyphon.* International Communications in Heat and Mass Transfer, 2010. **37**(6): p. 703-710.

81. Radiom, M., C. Yang, and W.K. Chan, *Dynamic contact angle of water-based titanium oxide nanofluid.* Nanoscale Research Letters, 2013. **8**(1): p. 282.

82. Kondiparty, K., et al., *Wetting and Spreading of Nanofluids on Solid Surfaces Driven by the Structural Disjoining Pressure: Statics Analysis and Experiments.* Langmuir, 2011. **27**(7): p. 3324-3335.

83. Wang, Q., et al., *Effect of Potassium Oleate on Rheological Behavior of Cationic Guar in Aqueous Solution with Varying Temperatures.* Chinese Journal of Chemical Physics, 2012. **25**(4): p. 448-456.

84. Guo, Y. and P.B. Zetterlund, *Synthesis of Nanosized (< 20 nm) Polymer Particles by Radical Polymerization in Miniemulsion Employing in situ Surfactant Formation.* Macromolecular Rapid Communications, 2011. **32**(20): p. 1669-1675.

85. Hwang, Y. and J. Lee, *Production and dispersion stability of nanoparticles in nanofluids.* Powder Technology, 2008. **186**(2): p. 145 - 153.

86. Ristoiu, D., et al. *Experimental investigation of inclination angle on heat transfer characteristics of closed two-phase thermosyphon*. in *5th General Conference of the Balkan Physical*. 2003.

87. Noie, S.H., *Heat transfer characteristics of a two-phase closed thermosyphon.* Applied Thermal Engineering, 2005. **25**(4): p. 495-506.

88. Khazaee, I., et al., *Experimental Consideration and Correlation of Heat Transfer of a Two-Phase Closed Thermosyphon Due to the Inclination Angle, Filling Ratio, and Aspect Ratio.* Journal of Enhanced Heat Transfer, 2011. **18**(1): p. 31-40.

89. Kim, S., et al., *Study of pool boiling and critical heat flux enhancement in Nanofluids.* Bull Pol Ac Tech, 2007. **55**(2): p. 211 - 216.

90. Qi, Y., Y. Kawaguchi, and Z. Lin, *Enhanced heat transfer of drag reducing surfactant solutions with fluted tube-in-tube heat exchanger.* Int J Heat Mass Transf, 2001. **44**: p. 1495 - 1505.

91. Fumito K, et al., *Heat Transfer Characteristics in an Evaporator Section of a Looped Parallel Thermosyphon*, in *The 7th International Heat pipe Symposium*. 2003: Jeju, Korea, 2003. p. 225-230.

92. Khodabandeh, R. and R. Furberg, *Heat transfer, flow regime and instability of a nano- and micro-porous structure evaporator in a two-phase thermosyphon loop.* International Journal of Thermal Sciences, 2010. **49**(7): p. 1183-1192.

93. Chang, C.C., et al., *Two-Phase Closed-Loop Thermosyphon for Electronic Cooling.* Experimental Heat Transfer, 2010. **23**(2): p. 144-156.

94. Jengsooksawat, S., et al., *Heat Transfer Characteristic of Loop Thermosyphon with Vapor Chamber*, in *The 9th International Heat pipe Symposium*. 2008: Malaysia. p. 215-218.

95. Jengsooksawat, S., K. Booddachan, and S. Rittidech, *Loop Thermosyphon with Vapour Chamber : A Thermodynamic Study.* Advances in Mechanical Engineering, 2014. **6**: p. 1-8.

96. Faghri, A., *Heat Pipe Science and Technology*. 1 ed. 1995, Washington, DC: Taylor&Francis.

97. Jiao, B., et al., *Investigation on the effect of filling ratio on the steady-state heat transfer performance of a vertical two-phase closed thermosyphon.* Applied Thermal Engineering, 2008. **28**: p. 1417 - 1426.

98. Bhuwakietkumjohn, N. and S. Rittidech, *Internal flow patterns on heat transfer characteristics of a closed-loop oscillating heat-pipe with check valves using ethanol and a silver nano-ethanol mixture.* Experimental Thermal and Fluid Science, 2010. **34**(8): p. 1000-1007.

99. Terdtoon, P., M. Chailungkar, and M. Shiraishi, *Effects of Aspect Ratios on Internal Flow Patterns of an Inclined Closed Two-Phase Thermosyphon at Normal Operating Condition.* Heat Transfer Engineering, 1998. **19**(4): p. 75-85.

100. Lin, Y., S. Kang, and H. Chen, *Effect of silver nano-fluid on pulsating heat pipe thermal performance.* Appl Ther Eng, 2008. **28**: p. 1312 - 1317.

101. Brusly Solomon, A., et al., *Thermal performance of anodized two phase closed thermosyphon (TPCT).* Experimental Thermal and Fluid Science, 2013. **48**: p. 49-57.

102. H. Imura, et al., *Heat transfer in two-phase closed-type thermosyphons.* Transactions of Japan Society of Mechanical Engineers, 1977. **22**: p. 485–493.

103. Srimuang, W., S. Rittidech, and B. Bubphachot, *Heat transfer characteristics of a vertical flat thermosyphon (VFT).* Journal of Mechanical Science and Technology, 2009. **23**(9): p. 2548-2554.

104. Amatachaya, P. and W. Srimuang, *Comparative heat transfer characteristics of a flat two-phase closed thermosyphon (FTPCT) and a conventional two-phase closed thermosyphon (CTPCT).* International Communications in Heat and Mass Transfer, 2010. **37**(3): p. 293-298.

105. Zamzamian, A., et al., *Experimental investigation of forced convective heat transfer coefficient in nanofluids of Al2O3/EG and CuO/EG in a double pipe and plate heat exchangers under turbulent flow.* Experimental Thermal and Fluid Science, 2011. **35**(3): p. 495-502.

106. Li, Z.H., *Modeling and optimization for heat exchanger networks synthesis based on expert system and genetic algorithm.* Chinese Journal of Chemical Engineering, 2002. **10**(3): p. 290-297.

107. Lee, J.S., et al., *Use of two-phase loop thermosyphons for thermoelectric refrigeration: experiment and analysis.* Applied Thermal Engineering, 2003. **23**(9): p. 1167-1176.

108. Ramesh, G. and N.K. Prabhu, *Review of thermo-physical properties, wetting and heat transfer characteristics of nanofluids and their applicability in industrial quench heat treatment.* Nanoscale Research Letters, 2011. **6**.

109. Li, X.F., et al., *Thermal conductivity enhancement dependent pH and chemical surfactant for Cu-H2O nanofluids.* Thermochimica Acta, 2008. **469**(1-2): p. 98-103.

110. Buongiorno, J., et al., *A benchmark study on the thermal conductivity of nanofluids.* Journal of Applied Physics, 2009. **106**(9).

111. Rittidech, S., N. Pipatpaiboon, and P. Terdtoon, *Heat-transfer characteristics of a closed-loop oscillating heat-pipe with check valves.* Applied Energy, 2007. **84**(5): p. 565-577.

112. Dangeton, W., et al., *Flow Visualization of a Miniature Loop Thermosyphon.* Experimental Heat Transfer, 2012. **26**(4): p. 329-342.

113. Rittidech, S. and S. Sangiamsuk, *Internal Flow Patterns on Heat Transfer Performance of a Closed-Loop Oscillating Heat Pipe with Check Valves.* Experimental Heat Transfer, 2012. **25**(1): p. 48-57.

114. da Silva, A.K. and M.B.H. Mantelli, *Thermal applicability of two-phase thermosyphons in cooking chambers--experimental and theoretical analysis.* Applied Thermal Engineering, 2004. **24**(5-6): p. 717-733.

115. Milanez, F.H. and M.B.H. Mantelli, *Thermal characteristics of a thermosyphon heated enclosure.* International Journal of Thermal Sciences, 2006. **45**(5): p. 504-510.

116. Parametthanuwat, T., S. Rittidech, and K. Booddachan, *Thermosyphon installation for energy thrift in a smoked fish sausage oven (TISO).* Energy, 2010. **35**(7): p. 2836-2842.

117. Kiniman A, Rittidech S, and Bubphachot B, *Application of the top heat mode closed-loop oscillating heat-pipe with check valves (THMCLOHP/CV) air preheater for chili drying.* Journal of Applied Sciences Research, 2012. **8**(3): p. 1699-1706.

118. Topuza A, Fengb H, and K. M, *The effect of drying method and storage on color characteristics of paprika.* LWT - Food Science and Technology, 2009. **42**: p. 1667-1673.

119. Seo, H.-S., et al., *Impacts of sensory attributes and emotional responses on the hedonic ratings of odors in dairy products.* Appetite, 2009. **53**(1): p. 50-55.

120. Lim, J., *Hedonic scaling: A review of methods and theory.* Food Quality and Preference, 2011. **22**(8): p. 733-747.

NOMENCLATURE

A_{eo}	outside wall area of evaporator section	m^2
A_{co}	outside wall area of condenser section	m^2
A	Surface area	m^2
C_p	Specific heat capacity constant	kJ/kg°C
C_{pl}	Specific heat capacity of the working fluid at liquid phase	kJ/kg°C
D_o	outside diameter of the pipe	m
D_i	inside diameter of the pipe	m
g	Gravity	m/s^2
h	Heat transfer coefficient	W/m^2
h_{eo}	Heat transfer coefficient at the evaporator section	$W/°C \cdot m^2$
h_{co}	Heat transfer coefficient at the condenser section	$W/°C \cdot m^2$
k_x	thermal conductivity of the material	W/°C·m
k_l	thermal conductivity of the working fluid at liquid phase	W/°C·m
L	Latent heat of working fluid	kJ/kg
L_e	Evaporator length	m
L_c	Condensor length	m
$\dot{m}$	Mass flow rate	kg/s
N	Number of fin	
NP	Silver nanoparticles 0.5 wt% contained in ethanol	
OA	Oleic acid surfactant	
P_v	Vapour pressure of the working fluid	Pa
P_a	Atmospheric pressure 101.3 kPa	
Q	Heat transfer rate	W
R_h	Radius of hydraulic	m
RT	relative thermal efficiency	
T_{out}	Outlet temperature of the condenser section	°C
T_{inlet}	Inlet temperature of the condenser section	°C
V_l	Volume of the working fluid	m^3
$W_{Perimeter}$	Wetted perimeter	m
X	Section width of RTPCT	m
Y	Section length of RTPCT	m
ρ_l	Density of the working fluid at liquid phase	Kg/m^3
ρ_v	Density of the working fluid at vapour phase	Kg/m^3
μ_l	Viscosity of the working fluid at liquid phase	N/m
η	Fin efficiency	
θ	Eccess temperature	
ΔE^*	total colour difference	
l^*	Sample are lighter and darker standard	
a^*	Sample are redder and greener standard	
b^*	Sample are yellower and bluer standard	

APPENDIX

Journal publication

Parametthanuwat, T.; Bhuwakietkumjohn, N.; Rittidech, S.; Ding, Y. Experimental investigation on thermal properties of silver nanofluids. International Journal of Heat and Fluid Flow, 2015. 56: p. 80-90.

International Journal of Heat and Fluid Flow 56 (2015) 80–90

Contents lists available at ScienceDirect

International Journal of Heat and Fluid Flow

journal homepage: www.elsevier.com/locate/ijhff

Experimental investigation on thermal properties of silver nanofluids

T. Parametthanuwat [a,*], N. Bhuwakietkumjohn [a], S. Rittidech [b], Y. Ding [c]

[a] Heat Pipe and Nanofluid Technology Research Unit, King Mongkut's University of Technology North Bangkok, Thailand
[b] Heat Pipe and Thermal Tool Design Research Unit (HTDR), Division of Mechanical Engineering, Faculty of Engineering, Mahasarakham University, Thailand
[c] Birmingham Centre for Thermal Energy Storage, School of Chemical Engineering, University of Birmingham, UK

ARTICLE INFO

Article history:
Received 13 January 2015
Received in revised form 11 May 2015
Accepted 9 July 2015
Available online 23 July 2015

Keywords:
Silver nanofluids
Rheological
Thermal conductivity
Potassium oleate surfactant
Newtonian behavior

ABSTRACT

This paper reports on an experimental investigation of the thermal properties behavior of 0.5 wt% silver nanoparticle-based nanofluids (NF) containing oleic acid (OA) and potassium oleate surfactant (OAK^+) with concentrations of 0.5, 1, and 1.5 wt% respectively. The experiments were conducted from 20 °C to 80 °C. It was shown that the NF with 1 wt% OAK^+ yielded the highest thermal behavior enhancement of about 28% at 80 °C compared to deionized water. The thermal performance had higher than the base fluid/nanofluids at approximately 80%. Moreover, the NF containing OAK^+ showed higher thermal conductivity and dynamics of specific heat capacity than deionized water in all of the experimental conditions in this study. The rheological experiment showed that viscosity of NF was significantly dependant on temperature. As shear rate increased, the shear stress of the NF increased; however, the viscosity of the nanofluids decreased first and then stabilized. It was further found that NF containing OAK^+ at a range of operating temperatures produced Newtonian behavior.

1. Introduction

Cooling is one of the most important challenges facing numerous industrial sectors. Despite the considerable amount of research and development focusing on industrial heat transfer requirements, major improvements in cooling capability are still insufficient because conventional heat transfer fluids possess poor heat transfer properties. Nanofluids, which are engineered by suspending ultrafine metallic or non-metallic particles of nanometer dimensions in traditional cooling fluids, have shown great enhancement in thermal conductivity and convective heat transfer coefficiency (Choi and Eastman, 1995; Khandekar et al., 2008; Parametthanuwat, 2012; Sreeremya et al., 2014).

This section also contains the literature review for thermal properties. Many researchers have discussed the thermal properties points on which this study is based, together with the background of the research and explanations of the problems faced. This study highlights the theories and experiment for investigating the characteristics of thermal properties. Points of importance will be emphasized, with significance given to the properties of nanofluids and surfactants and their use in this experiment. Also included is the explanation of the characteristics of nanofluid behavior in silver nanofluids containing surfactant. Thus, the researchers used different methods depending on the base fluids, nanofluid/nanoparticle type, etc. Recently, Thermal conductivity of 0.1–0.4% volume concentration silver (Ag) nanoparticles in water were investigated. The nanofluids were formulated using the ultrasonic vibration method for 3 h and thermal conductivity enhancement showed 10% at 0.4% of concentration (Kang et al., 2006). Using a different method, the synthesis of silver nanofluids was performed using high-pressure homogenization with a volume fraction 0.1–0.3% in water. The highest thermal conductivity of the nanofluids showed an 18% increase at the concentration of 0.3% (Oliveira et al., 2014). Moreover, regarding the difference in base fluid, Ag nanofluids in toluene have shown 9% thermal conductivity enhancement with a very low loading of 1.10–3 vol% (Daungthongsuk and Wongwises, 2007; Patel et al., 2003; Trisaksri and Wongwises, 2007; Wang and Mujumdar, 2007). Consequently, nanofluids show better cooling capacity with respect to water in conventional heat pipes since nanoparticles can flatten the temperature gradient of the fluids and reduce the boiling limit (Daungthongsuk and Wongwises, 2007; Khandekar et al., 2008; Trisaksri and Wongwises, 2007). In addition, the concentration of nanofluids may affect the enhancement of thermal conductivity. The studied silver nanofluids in ethylene glycol (EG) with 10,000 ppm concentrations showed 18% thermal conductivity enhancement (Sharma et al., 2011). Then, the investigated carbon black (CB) in deionized water with sodium dodecylsulfate (SDS) as well as Ag nanoparticles in silicon oil with

* Corresponding author.
E-mail address: thanya.p@fitm.kmutnb.ac.th (T. Parametthanuwat).

http://dx.doi.org/10.1016/j.ijheatfluidflow.2015.07.005
0142-727X/

Nomenclature

NF	silver nanofluids
NP	silver nanoparticles
OAK$^+$	potassium oleate surfactant
OA	oleic acid
K and n	consistency index and low power index
k_{eff}	the effective thermal conductivity
k_p	thermal conductivity of particle, W(m K)$^{-1}$
k_l	Thermal conductivity of liquid, W(m K)$^{-1}$
V_p	volume of nanoparticles in fluid, m^3
V_l	volume of base fluid, m^3
$C_{p,nf}$	specific heat capacity of nanofluids, J(kg °C)$^{-1}$
$C_{p,n}$	specific heat capacity of nanoparticles, J(kg °C)$^{-1}$
$C_{p,bf}$	specific heat capacity of base fluid, J(kg °C)$^{-1}$
$C_{p,eff}$	the effective specific heat capacity, J(kg °C)$^{-1}$
x_i	the independent variable to be estimated
μ_i	the manufacturer reported precision of the measurement
Q	heat transfer rate, W
T_{out}	outlet temperature at condenser section, °C
T_{in}	inlet temperature at condenser section, °C
$\dot{m}$	mass flow rate, kg s^{-1}

Greek symbols

ρ_n	density of nanoparticles, kg m^{-3}
ρ_{bf}	density of base fluid, kg m^{-3}
η	apparent viscosity
$\dot{\gamma}$	shear rate
ϕ	volume fraction of suspension

oleic acid (OA), and with the maximum enhancement of thermal conductivity compared to the base liquid, was 9% for the wt% of the carbon black (CB) nanofluids and the wt% of the Ag nanofluids respectively (Hwang et al., 2008). The .1 wt% copper (Cu) aqueous nanofluids with 0.14 wt% of sodium dodecylbenzene sulfonate (SDBS) as surfactant can generate maximum thermal conductivity enhancement up to 10.7% (Li et al., 2008).

The rheological behavior of nanofluids is essential in establishing adequate application and design of processing. The 8 wt% titania nanoparticles in the EG showed Newtonian behavior at a low shear rate, and the shear viscosity was strongly dependent on the temperature and concentration of the nanoparticles (Chen et al., 2007a). Then, the studied 1 vol% silver NP in ethanol with polyvinylpyrrolidone (PVP) was stabilized (Singh and Raykar, 2008). The rheological results suggest that the PVP helped to decrease the nanoparticle's size, resulting in low fluid viscosity and Newtonian fluid behavior but remarkably high thermal conductivity. Meanwhile, the 4.38 vol% silver nanofluids in the diethylene glycol (DEG) showed Newtonian behavior at high viscosity (Tamjid and Guenther, 2010). However, different literature data have shown that nanofluids have non-Newtonian behavior, particularly at a low shear rates. The most important influence could be the effective particle concentration, the range of shear rate, and the viscosity of the base liquid (Singh and Raykar, 2008). Then, it was found that the TiO_2 nanoparticle in the EG exhibited shear thinning behavior when the particle concentration was higher than ~2% (Chen et al., 2007a). The investigated shear thinning behavior was 3% γ-Al_2O_3 and 10% TiO_2 in water (Pak and Cho, 1998). Another main reason for the non-Newtonian behavior could be the aggregation of nanoparticles in the nanofluids. Lu reported that physical properties may change when the surfactant affects surface tension and viscosity. For instance, Al_2O_3 in water, at a 1:10 weight ratio with ammonium poly (PMAA-NH4), has demonstrated shear thinning behavior (a decrease in viscosity with an increased shear stress rate), which yields a good dispersion rate when using PMAA suspension up to 47.5 vol% (Lu and Kessler, 2006). Then it was found that the 4 vol% of γ-Al_2O_3, TiO_2, and CuO nanofluids with 0.5 wt% of carboxymethyl cellulose (CMC) in deionized water containing up to 4 vol% of particle concentration showed non-Newtonian behavior with shear thinning (Hojjat et al., 2011).

In this paper, 0.5 wt% silver nanoparticle-based aqueous nanofluids with oleic acid (OA) and potassium oleate surfactant (OAK$^+$) as surfactant were prepared by sonicating in water bath with a cooling technique for a period time of 12 h. The effect of the additive concentration on the thermal properties was studied experimentally (thermal conductivity, specific heat, density, viscosity, contact angle, and application of thermal enhancement), and the rheological behavior (the correlation between shear stress and shear rate) was investigated experimentally and theoretically. Moreover, the heat enhancement cooling of the fluid (HEC) was investigated experimentally and it was confirmed that nanofluids/-nanofluids containing surfactant could be used in the application of heat transfer. The methods of the experiment are briefly explained in Section 2. Section 3 shows the experimental results and offers a discussion. The conclusions to the study are in Section 4.

2. Materials and methods

2.1. Nanofluids and thermal property study

Fig. 1 shows a schematic diagram of the preparation the nanofluids. Water-based silver nanofluids were formulated with dry silver nanoparticles (Sigma–Aldrich, USA), OA, and OAK$^+$ (Sigma–Aldrich, USA) by using a two-step method (Hwang et al., 2008; Moghaddam et al., 2013). The 0.5, 1, and 1.5 wt% of OA and OAK$^+$ were added to the 0.5 wt% silver nanofluids, which showed controlled and variable parameters as seen in Table.1. After sonicating for 12 h with a cooling technique, the particle size was measured using a nano-size particle analyzer (ZEN 3600 MALVERN, USA) in the range between 0.6 nm and 6.0 μm. The thermal properties of the nanofluids were measured using the hot-wire method (PSL Systemtechnik GmbH) from 20 °C to 80 °C. The rheological characteristics of the NF were analyzed using a Rheo-microscope Physica MCR301 (Anton Paar GmbH). The measurements were based on the controlled shear stress model with the stress ranging from 0.05 to 5 Pa. The maximum uncertainty was found to be 1.7% (Chen et al., 2007b; Moghaddam et al., 2013; Paramethanuwat, 2012).

The rheological behavior of the NF containing OAK$^+$ can be expressed with the power model in Eq. (1) with the viscosity as following the power law model indices less than $n \leqslant 1$.

$$\eta = K\gamma^{n-1} \tag{1}$$

In Eq. (1), η is the apparent viscosity, $\dot{\gamma}$ is the shear rate, K is the consistency index, and n is the power law index. The power law index of the nanofluids decreases with increasing nanoparticle concentration, and increases with increasing temperature (Hojjat et al., 2011). Apparently, the viscosity of the NF decreases as the shear rate increases.

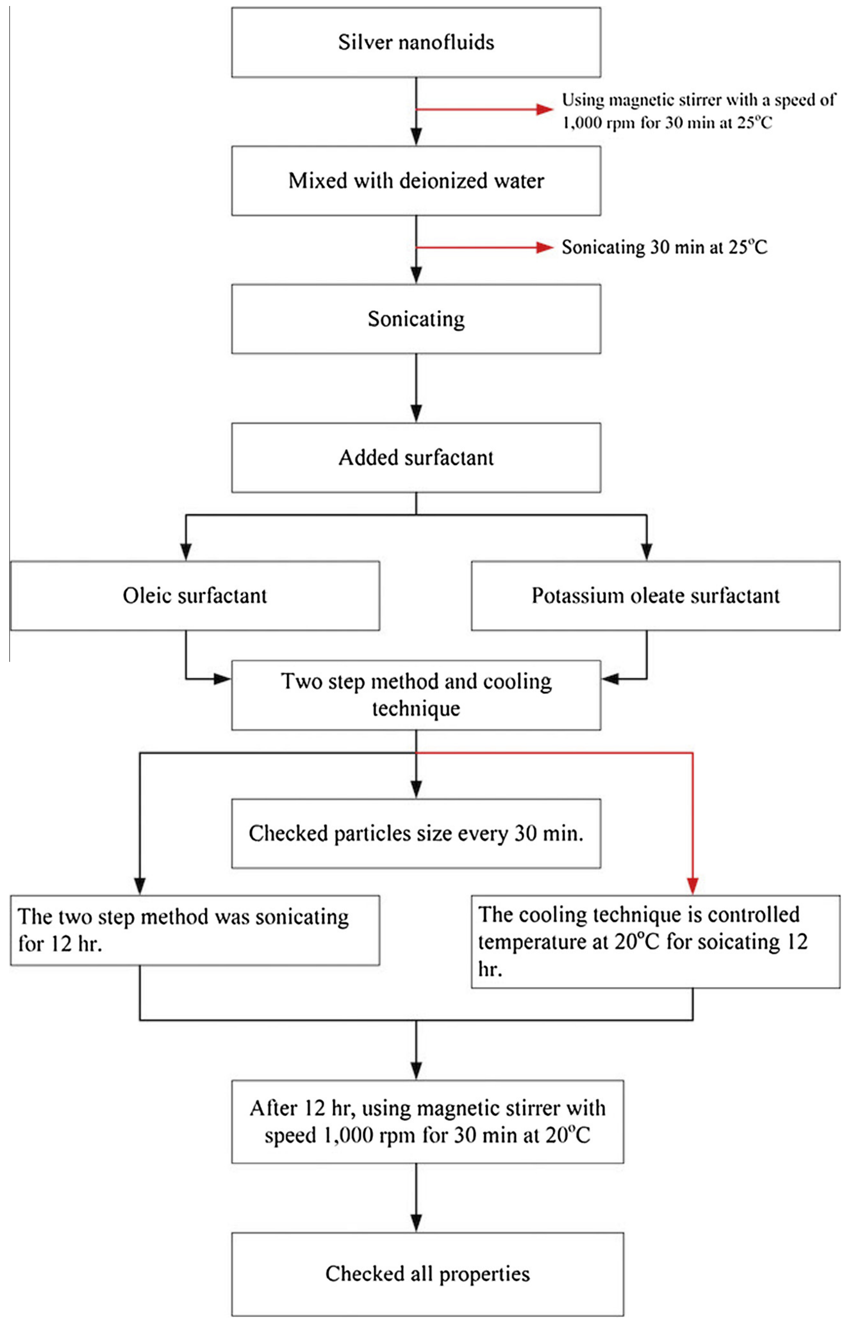

Fig. 1. The schematic diagram of preparation the nanofluids.

2.2. Thermal conductivity

The idea of thermal conductivity is non-existent in nanofluids theory scientists have used an existing model for estimated. The Maxwell model was developed to explain the heat transfer characteristics of larger particles in nanofluids research. This model has served as a foundation in the development and explanation of the much higher conductivity increase observed in nanofluids. The effective thermal conductivity (k_{eff}) can be defined by the following (Kleinstreuer and Feng, 2011; Kwak and Kim, 2005):

$$k_{eff} = \frac{k_p + 2k_l + 2(k_p - k_l)\phi}{k_p + 2k_l - (k_p - k_l)\phi} k_l \quad (2)$$

Thus, the ϕ can be defined by:

$$\phi = \frac{V_p}{V_p + V_l} \quad (3)$$

2.3. Contact angle instrument

In order to measure the contact angle of the sample fluids, the values are required to be at room temperature. The temperature was controlled with a precision of ±1 °C. In this study, the drops of fluids were measured using a Contact Angle Meter Model: DM-CE1; Kyowa Interface Science. The accuracy was ±0.5° (repeatability described in standard deviation). The following liquids were used in the experiment: a copper plate with a diameter of 60 mm and a thickness of 0.3 mm were used as a test surface. A droplet of nanofluid was generated at a very low rate (1 μl/s) and detached from the syringe needle tip as soon as it touched the copper plate. Consecutive photographs were used to measure the contact angles. The spatial resolution was estimated to be about 50 μm on the basis of the focused area and camera pixel size. A video was taken while the droplet was spreading over

Table 1
Controlled and variable parameters.

The controlled parameters	Silver nanofluid concentration of 0.5 wt% (NF) Operating temperature of 20–80 °C Shear rate ranges were $10^0\ s^{-1}$ to $10^3\ s^{-1}$
The variable parameters	Working fluid was: • Deionized water • Deionized water containing surfactant • NF • NF containing surfactant Surfactant were: • Concentration of Oleic acid was 0.5, 1, and 1.5 wt% • Concentration of Potassium oleate was 0.5, 1, and 1.5 wt%
Dependent variable	The dependent variable was: • Thermal conductivity, specific heat, density, viscosity, contact angle and application of thermal enhancement • Rheological behavior

the copper plate from initial contact to equilibrium position. The temporal resolution was estimated based on the frame speed of the CCD camera at 30 fps. For each concentration, three experiments were performed and the average was ascertained. The measurement settings were then adjusted and the software was initialized (Lock, 1992; Ramesh and Prabhu, 2011).

2.4. Specific heat

The dynamic of specific heat was applied in the experiment. This was according to Rajabpour et al. (2013) regarding the application of the theory model to nanofluids.

$$C_{p,nf} = \phi C_{p,n} + (1-\phi)C_{p,bf} \tag{4}$$

This second model has served as a foundation in the development and explanation of the much higher specific heat observed in nanofluids from nanoparticles. The effective specific heat ($C_{p,eff}$) can be defined as follows (O'Hanley et al., 2012):

$$C_{p,eff} = \frac{\phi(\rho C_p)_n + (1-\phi)(\rho C_p)_{bf}}{\phi\rho_n + (1-\phi)_{bf}} \tag{5}$$

The measurement uncertainty for the specific heat was calculated by propagating the precision uncertainties of all the individual measurements required to determine the specific heat in Eq. (5) and can be defined as follows (O'Hanley et al., 2012):

$$\mu_{total} = \sqrt{\sum_i^n \left(\frac{\partial C_{p,sample}}{\partial x_i}\mu_i\right)^2} \tag{6}$$

Eqs. (5) and (6) should be noted that for Newtonian nanofluids. For the non-Newtonian fluid, the variation of the rheology does not depend on direct models but on the volume fractions of the nanoparticles (Cabaleiro et al., 2013; Lu and Huang, 2013).

2.5. The heat transfer enhancement

Fig. 2 shows a schematic diagram of the experimental apparatus, which consists of the heat enhancement cooling of the fluid (HEC) and peripheral devices. The heat enhancement cylinder was made from Stan less steel (AISI 304) with a diameter and height of 1500 mm and 3000 mm. The HEC was the heat source from the Stan less heater (2000 W) with a diameter and height of 500 mm and 2000 mm. The heat was supplied by circulating the Stan less through to HEC through to 20%, 40%, 60%, 80%, and 100% respectively of the heat source. The cooling and pre-cooling section was heat sink from a cold bath. The cooling fluids are shown in Table 2. Eighteen thermocouples were connected through a data logger (Yokogawa DX200 with ±0.1 °C accuracy, 20 channel input, and −200 °C to 1100 °C measurement temperature range). Type K thermocouples (OMEGA with ±0.1 °C accuracy) were attached to the inlet, the outlet, and the surface of the heating and cooling as the HEC. The inlet temperature of the cooling fluids was maintained at 20 °C and a floating Rota meter (PLATON PTF2 ASS-C with a volumetric flow rate of 0.2–1.5 l/min) was used to control the flow rate of the cooling fluid during the experiments. During the experiment, the volumetric flow rate was set at 0.25 l/min in order to calculate the heat transfer enhancement of the cooling fluid using the calorific method. The following Eqs. (7) and (8) were used for calculating one of the heat-transfer rates and for error analysis (Paramethanuwat et al., 2011).

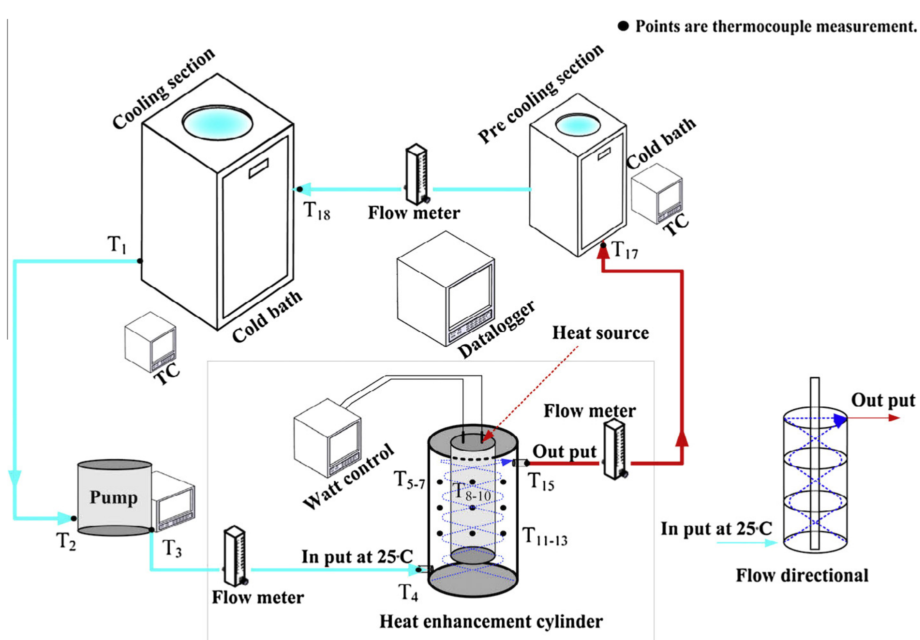

Fig. 2. Schematic diagrams of the HEC experimental apparatus.

Table 2
Controlled and variable parameters.

The controlled parameters	• Cylinder diameter and height of 1500 mm and 3000 mm. • Heater (2000 W) with diameter and height of 500 mm and 2000 mm. • The heat was supplied of 20%, 40%, 60%, 80% and 100% of heater.
The variable parameters	The cooling fluids were: • Deionized water • Deionized water containing surfactant • NF • NF containing surfactant Surfactants were: • Concentration of Oleic acid was 0.5, 1, and 1.5 wt% • Concentration of Potassium oleate was 0.5, 1, and 1.5 wt%
Dependent variable	Heat transfer enhancement

$$Q = \dot{m}C_p(T_{out} - T_{in}) \tag{7}$$

Thus:

$$Q = f(\dot{m}, T_{out}, T_{in}) \tag{8}$$

The error analysis of the heat transfer can be obtained from (Paramethanuwat et al., 2010):

$$Q_{Error} = \left[\left(\frac{\partial Q}{\partial \dot{m}} \times \dot{m}\right)^2 + \left(\frac{\partial Q}{\partial T_{out}} \times T_{out}\right)^2 + \left(\frac{\partial Q}{\partial T_{in}} \times T_{in}\right)^2\right]^{0.5} \tag{9}$$

In order to experiment with a wide range of aspect ratios, the following parameters were corresponding set, as shown in Table 2, to formulate the heat transfer characteristics of the HEC (Parametthanuwat and Rittidech, 2013).

3. Results and discussion

3.1. The nanoparticle size

Fig. 3 shows the average particle size as a function of sonicating time. Zero point 5 wt% silver nanoparticles based nanofluids (NF) with surfactants as a stabilizer have an average particle size of ~100 and ~95 nm respectively. It can be seen that the average particle size decreases as sonicating time increases. Moreover, the red ellipse in Fig. 3a, NF+0.5OAK$^+$ and NF+1OAK$^+$ was seen to cause smaller particle size for a continuous period of 12 h when compared with Fig. 3b. This indicated that the two-step method and cooling technique did not break the agglomerate into primary particles (Bönnemann et al., 2005; Chen et al., 2007a). After sonicating for 12 h, the sample was put into the TEM (Oxford Instruments) to check for average the particle size, as shown in Fig. 4a, suggesting that the size distribution of particles NF+1OAK+was between 5 and 25 nm. The TEM image also shows that the long chains of potassium oleate combined with outside nanoparticles and prevented them from aggregating together (Salehi et al., 2011; Vekas et al., 2006), which means that the viscosity and surface tension of the surfactant provided enough support to stabilize the dispersion of NP in deionized water (Parametthanuwat, 2012).

3.2. Rheological properties of nanofluids

The shear rate and shear stress had an effect on the rheological properties, such as viscosity. The rheological properties of the nanofluids containing surfactant are important to its thermo physical property. In this study, a surfactant was used to employ the NF's heat transfer rate. The OA and OAK$^+$ are known for their ability to decrease viscosity and surface tension due to the organic and hydrocarbon interaction with oxygen which exists in deionized water (Huminic and Huminic, 2011; Salehi et al., 2011). However, the case was compared with the same group of surfactant (OA and OAK$^+$) but with a difference in potassium salt (K$^+$). The potassium salt was helpful in balancing the pH value of the

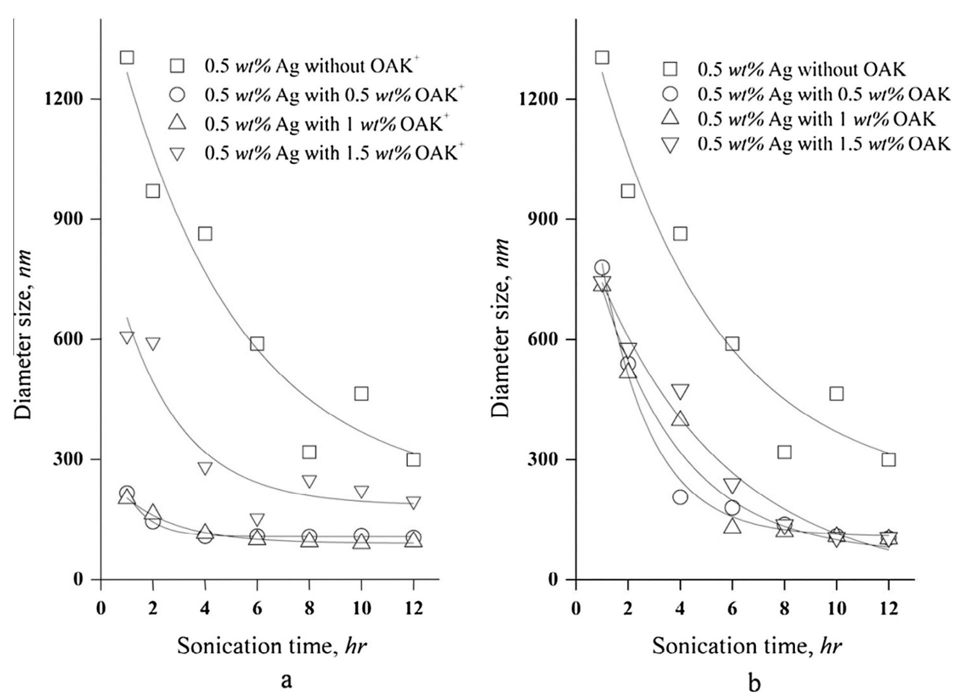

Fig. 3. Relationship between sonication times and particle size.

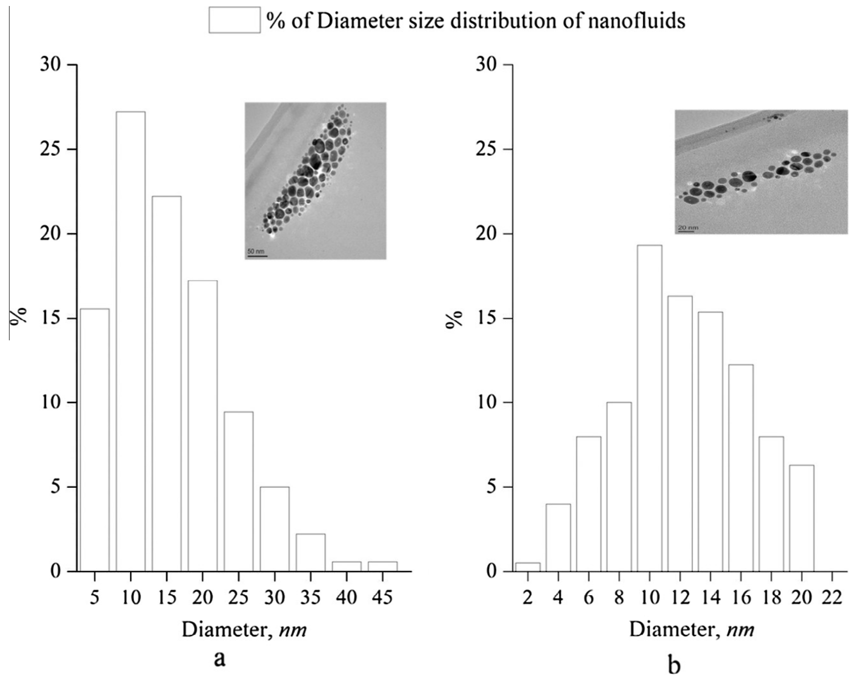

Fig. 4. Relationship between Diameters with percentage of dispersed size and TEM micrograph at silver nanofluids containing surfactant at concentration 1 wt%.

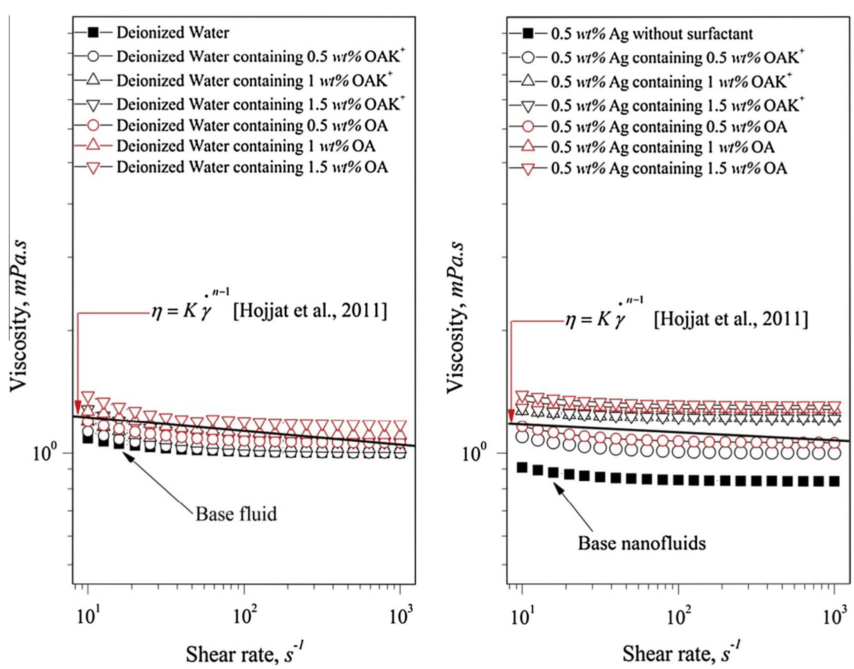

Fig. 5. Relationship between shear rates with viscosity of silver nanofluids at operating temperate 30 °C.

liquid and dissolving the solutions of fat oil catalysis interaction with hydrogen. Thus, the OAK^+ has the ability to span the NP's random motion throughout the deionized water (Chiu et al., 2008; Moghaddam et al., 2013; Molchanov et al., 2005; Mondragon et al., 2012; Paramethanuwat, 2012).

The rheology measurement results are shown in Fig. 6 and the shear rates with the viscosity of silver nanofluids were measured at 30 °C according to Paramethanuwat (2012). As shown in Fig. 5, the viscosity of all samples decreased in the first $10^1\ s^{-1}$ to $10^3\ s^{-1}$ intervals and the NF showed Newtonian behavior. This behavior could have been caused by the change of concentration in the OA and OAK^+, which was 0.5, 1 and 1.5 wt%. The most preferable OAK^+ concentration was 1 wt%, which was sufficient to distribute the NP with the lowest and most stable viscosity. The long chain nature of the OAK^+ molecular structure helped to decrease the NF's surface tension. It was concluded that there was an apparent change in the viscosity of the NF and deionized water; however, the NF's viscosity was still larger than that of the deionized water when the shear rate rose (Singh et al., 2013) according to Eq. (1) (Hojjat et al., 2011). Thus, the NP existing in the deionized water containing OAK^+, which affected the flowing behavior of the nanofluids, was the main cause of the decrease in

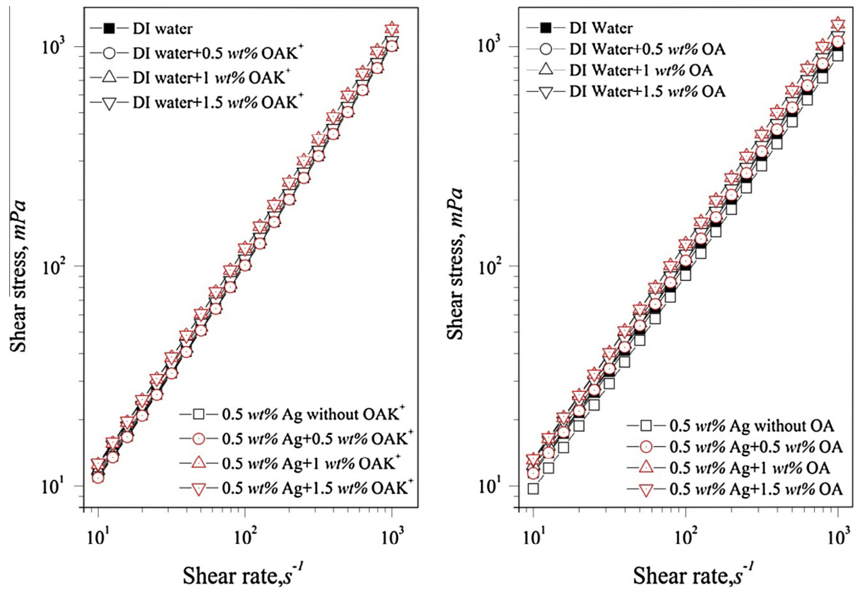

Fig. 6. Relationship between shear rates with shear stress of silver nanofluids at operating temperate 30 °C.

viscosity (Anoop et al., 2009; Lo et al., 2007). The potassium salt which produces an effect properly surfactant was helpful in balancing the physical properties of the base liquid. As can be seen in Fig. 6, along with the increasing shear rate, the nanofluids with OAK+ concentration smaller or larger than 1 wt% possessed larger shear stress. From the cross point onward, all of the results of the OAK+ were of almost the same value and the R^2 was close to 1. This was in line with the study of Hojjat et al. (2011), who stated that the transition metal in the same group with silver nanofluids containing OAK+ produced the Newtonian fluid (Paramethanuwat, 2012).

Fig. 7 shows the viscosity of NF+1OA compared with 0.5 wt% NF+1OAK+ as a function of shear rates. It was observed that for all operating temperatures and shear rate larger than 10^1 s^{-1}, the viscosity became stable and NF showed Newtonian behavior. Thus, it was well established that for all operating temperatures, the system's rheological behavior exhibited a similar trend. Fig. 8 shows the relationship of the shear rates and shear stress in accordance with Fig. 7. It could be explained that the higher temperature increased the intermolecular distances, which decreased the interaction between the molecular structures of deionized water and OAK+, resulting in decreased viscosity and surface tension (Chen et al., 2007a). Obviously, the OAK+ could help decrease the physical properties more than the OA. The surfactant behaved like an interfacial shell between the nanoparticles and base fluids and modified the surface tension of the nanofluids. The surface tension decreased when the concentration of surfactant increased (Paramethanuwat, 2012; Tanvir and Qiao, 2012). The OAK+ exhibited good adsorption of the silver particles and the particles uniformly had a direct effect on the shear stress. The optimization of

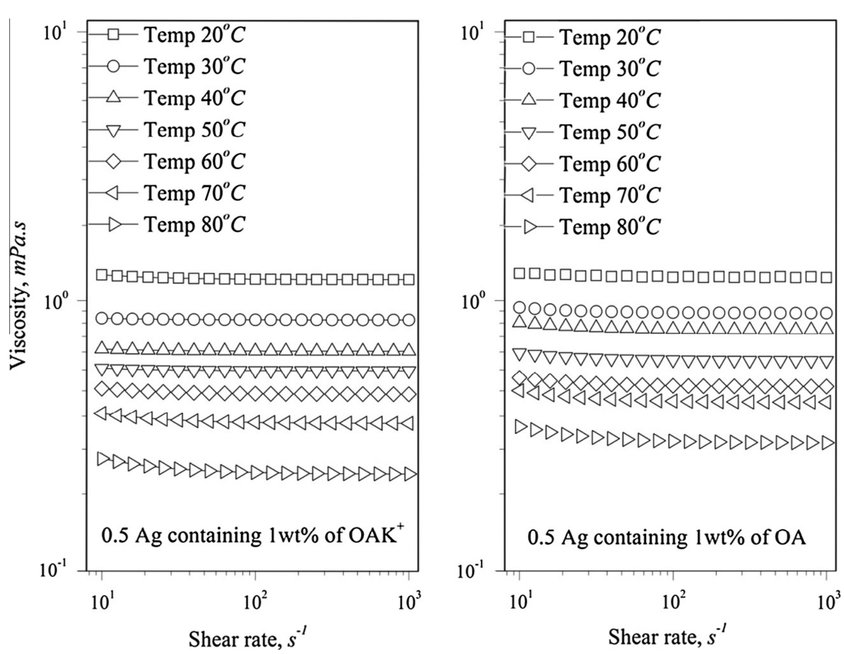

Fig. 7. Relationship between shear rates with viscosity.

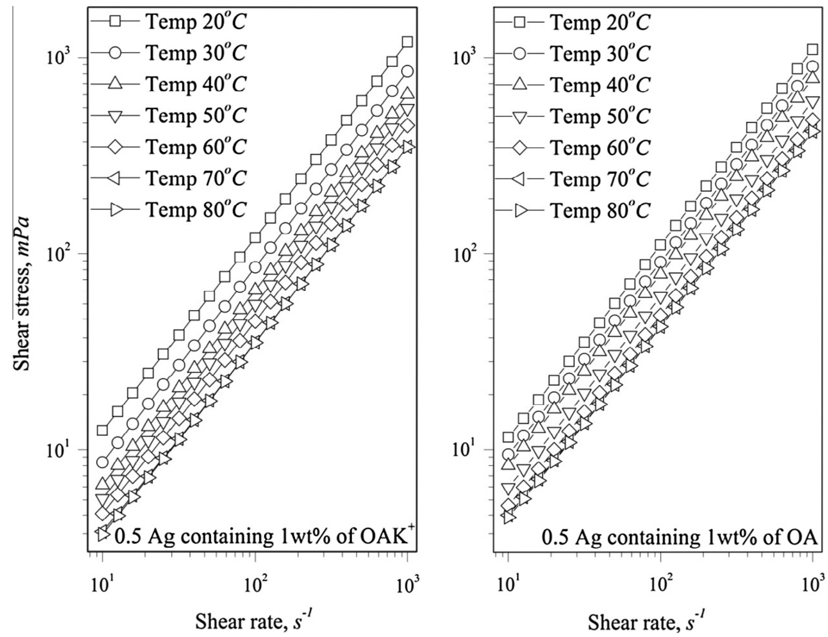

Fig. 8. Relationship between shear rates and shear stress.

the chain length in group OA organic compounds was C18, which was effective for particle dispersing stabilization. The optimized length also improved the colloidal stability and increased the non-precipitation period for the nanoparticles to be uniformly dispersed (Hwang et al., 2008; Li et al., 2010; Vekas et al., 2006). Moreover, OAK^+ achieved more stable suspension than the pure NP did in the deionized water. This might be related to the newtonian property of the nanofluids observed in this study when the rheological properties were observed at operating temperature (Moghaddam et al., 2013; Molchanov and Philippova, 2009; Paramethanuwat, 2012; Fohanno et al., 2011).

3.3. Thermal conductivity of nanofluids

The thermal conductivity of the silver nanofluids containing potassium oleate ($NF+OAK^+$) as a function of temperature is shown in Fig. 9. It can be seen that the thermal conductivity of the nanofluids depend on the linearity of the temperature, and the

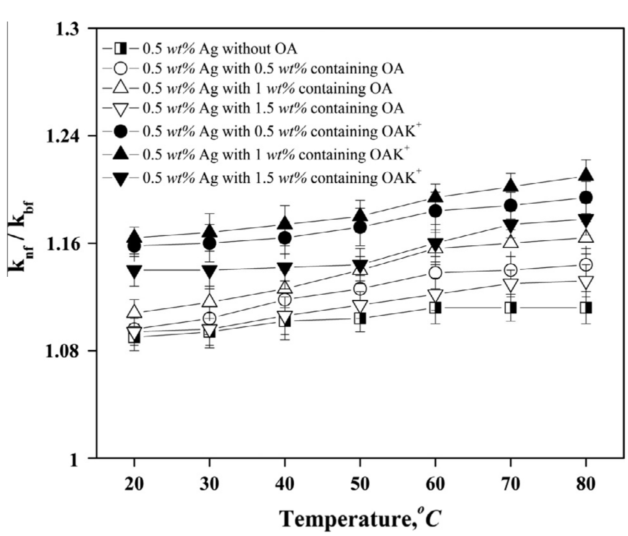

Fig. 9. Relationship between temperature with k_{nf}/k_{bf}.

enhancement of the thermal conductivity of $NF+OAK^+$ was different when the surfactant concentration was 0.5, 1, and 1.5 wt%. In all cases the $NF+OAK^+$ showed superior performance to that of the water. One wt% OAK^+ showed the lower and highest increase in the thermal conductivity of 15% at 20 °C and 28% at 80 °C throughout all samples, indicating that the thermal conductivity increases independently on surfactant concentration (Chen et al., 2007a). The nanoparticles dispersed in the liquid increased the surface area for the heat absorption. In the case of $NF+OAK^+$, the OAK^+ decreased the surface tension of the nanoparticles, stabilized the nanoparticles by uniformly distributing them, and increased the interface area of the nanofluids with the deionized water (Vekas et al., 2006). The surface tension had a significant influence on the thermal process since the property departure and interfacial equilibrium depend on it (Paramethanuwat et al., 2010). The high OAK^+ concentration appeared to hinder the aggregation and entanglement of the NP, which was observed at the bottom of the liquid (Li et al., 2008; Sharma et al., 2011). According to our experimental results, 1 wt% OAK^+ was enough to homogeneously disperse the NP and produce efficient thermal transfer between the particles and deionized water, and consequently resulted in the highest thermal conductivity enhancement (Godson et al., 2010; Kang et al., 2009; Patel et al., 2003; Turkyilmazoglu, 2012; Veilleux and Coulombe, 2011).

However, the current experimental results contrast with those of Kang et al. (2006) and Oliveira et al. (2014), as shown in Fig. 10. In regards to this study, the results were achieved using the same silver nanoparticles however with a difference in concentration and surfactant. The result from Kang et al., demonstrated an increase of relative thermal conductivity. Thus, it is important to note the vast differences among different experimental conditions, especially in regard to the method of preparation and nanoparticle concentration. For example, Kang et al. (2006) showed a maximum k_{nf}/k_{bf} of ~1.11 at 0.4% volume concentration with nanoparticles diameter of 8–15 nm, while Oliveira et al. (2014) showed a maximum k_{nf}/k_{bf} of ~1.17 at 0.3% volume concentration with nanoparticles diameter of 10 and 80 nm. This contrasts significantly with the results achieved in this study of approximately 1.19 with nanoparticles of diameter 5–25 nm at $NF+1OAK^+$. Of particular note, the research performed by Kang et al. (2006) and Oliveira

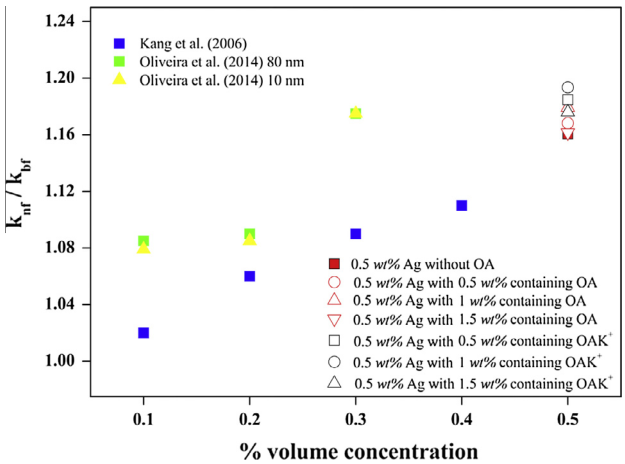

Fig. 10. Comparison different experimental result.

et al. (2014), did not specify the temperature under which the experiment was conducted. Furthermore, relative thermal conductivity was analyzed as a function of nanoparticle concentration and size. Thus, it can be determined that relative thermal conductivity is dependent upon the nanofluid's method of preparation, as well as the nanoparticle concentration and size.

3.4. Dynamic of specific heat capacity (DSC)

The heat energy absorbed ratio is a substance to increase in temperature. Table 3 shows the dynamic of specific heat capacity: nanofluids. The DSC was used to measure the deionized water deionized water containing surfactant (OA and OAK^+) and the NF containing surfactant (OA and OAK^+) at 1 wt% respectively, which was then compared with Eq. (6) according to Rajabpour et al. (2013) and O'Hanley et al. (2012). The results indicated a trend similar to that found in Rajabpour et al. (2013) and O'Hanley et al. (2012). It was found that, the good resulted appeared when using OAK^+ as a surfactant. The silver nanofluids containing OAK^+ surfactant was subjected to repulsion forces between the positively-charged hydroxyl groups (OA) of the functionalized nanoparticles and the potassium salt hydroxyl groups on the silver. However, the potassium salt of the acidic group functionalizing the nanoparticles became polarized in the water solution. On the other hand, when the positivity-charged potassium cation (K^+) groups were attached to the nanoparticles, the free ends (the carboxylic groups) became negatively charged. It is possible that the particle–fluid interactions and long-range electrostatic interactions between the nanoparticles may have affected the capillary properties of the nanofluids. Therefore, the negative forces between the solid and the nanofluids induced a specific heat capacity. Both parameters were dependent on particle size and surfactant concentration.

3.5. The contact angle and surface tension

In this study, the drop contact angle of working fluids was based on the room operating temperature. Furthermore, in order to investigate the effect of adding surfactant to the nanofluids, surface wettability, the static contact angles of the sessile droplets, and the surface tension of the pendant drop (Contact Angle Meter Model: DM-CE1; Kyowa Interface Science) were measured on flat copper plates at room temperature as shown in Fig. 11. This method was based on Khandekar et al. (2008) and Rahimi et al. (2010). When the surfactant was added it caused reduced adhesion between the working fluids dropping and the metal surface and made the total surface free energy. These are the manifestations of the interaction of the different molecular forces. The effects on the bulk thermo physical properties need to be addressed and surfactant dealt with nanofluids thus according to Radiom et al. (2013). It was further found that NF+1OAK^+ decreased the water drop contact angle and surface tension to 38.23° and 28.69 mN/m, respectively (compared with pure water having 110° and 72.8 mN/m). Thus, the contact angle and surface tension depended on the operating temperature and time. They have an effected on the boiling phenomena in the heat transfer application. The transfer rate improves and decreases the surface tension with wet ability and contact angle (Kondiparty et al., 2011; Paramethanuwat, 2012).

3.6. Heat transfer enhancement

The experimental results clearly showed the effect of the percentage of heat supplied on the percentage of percentage of thermal heat enhancement, as shown in Fig. 12. When comparing the percentage of heat supplied using the different working fluids, it was seen that the NF+1OAK^+ showed that the percentage of thermal enhancement was higher than with the other working fluids. Considering the case where the working fluid was NF+1OAK^+ with a heat input at 100% of heat supplied, the thermal enhancement reached 24.75 ± 0.08%. The increase of maximum percentage of

Table 3
The dynamic of specific heat capacity: nanofluids.

Temperature (°C)	Deionized water containing 1 wt% OA		Deionized water containing 1 wt% OAK^+		0.5 Ag containing 1 wt% OA		0.5 Ag containing 1 wt% OAK^+	
	Theoretical C_p (kJ/kg K)	Measured C_p (kJ/kg K)	Theoretical C_p (kJ/kg K)	Measured C_p (kJ/kg K)	Theoretical C_p (kJ/kg K)	Measured C_p (kJ/kg K)	Theoretical C_p (kJ/kg K)	Measured C_p (kJ/kg K)
20	–	4.185 ± 0.070	–	4.189 ± 0.056	4.226	4.227 ± 0.002	4.226	4.269 ± 0.02
		4.182 ± 0.070		**4.182 ± 0.070**		**4.225 ± 0.055**		**4.225 ± 0.055**
30	–	4.185 ± 0.068	–	4.189 ± 0.036	4.228	4.227 ± 0.045	4.228	4.269 ± 0.120
		4.183 ± 0.068		**4.183 ± 0.068**		**4.225 ± 0.103**		**4.225 ± 0.103**
40	–	4.186 ± 0.065	–	4.190 ± 0.032	4.229	4.228 ± 0.020	4.229	4.270 ± 0.025
		4.182 ± 0.068		**4.182 ± 0.068**		**4.225 ± 0.003**		**4.225 ± 0.003**
50	–	4.200 ± 0.056	–	4.204 ± 0.048	4.231	4.242 ± 0.025	4.231	4.284 ± 0.008
		4.182 ± 0.068		**4.182 ± 0.068**		**4.226 ± 0.028**		**4.226 ± 0.028**
60	–	4.200 ± 0.060	–	4.204 ± 0.060	4.237	4.242 ± 0.012	4.237	4.284 ± 0.023
		4.183 ± 0.068		**4.183 ± 0.068**		**4.227 ± 0.040**		**4.227 ± 0.040**
70	–	4.210 ± 0.040	–	4.214 ± 0.089	4.241	4.245 ± 0.121	4.241	4.295 ± 0.016
		4.187 ± 0.068		**4.187 ± 0.068**		**4.229 ± 0.104**		**4.229 ± 0.104**
80	–	4.220 ± 0.037	–	4.224 ± 0.010	4.252	4.262 ± 0.121	4.252	4.305 ± 0.039
		4.189 ± 0.068		**4.189 ± 0.068**		**4.236 ± 0.112**		**4.236 ± 0.112**

*The bold font second line shows base fluid (Deionized water) and base nanofluids (0.5 Ag without surfactant).

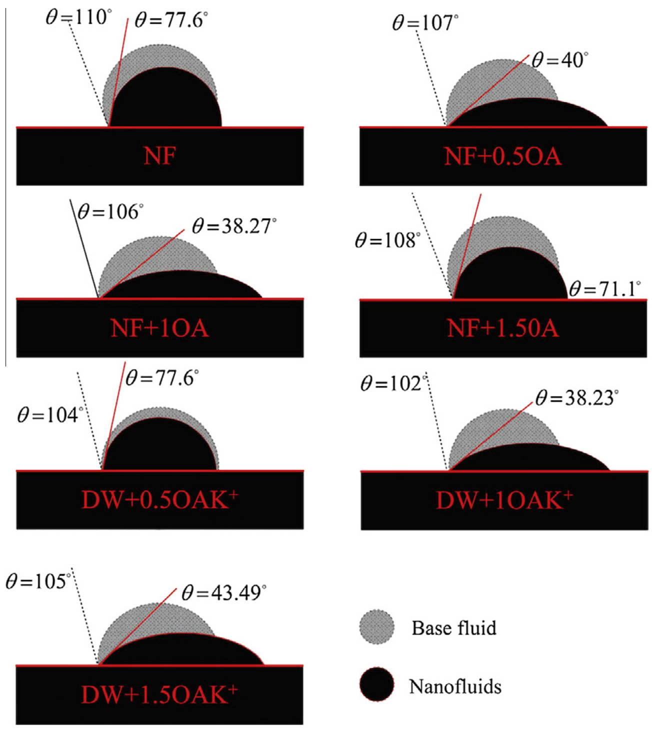

Fig. 11. Wettability at room operating temperature.

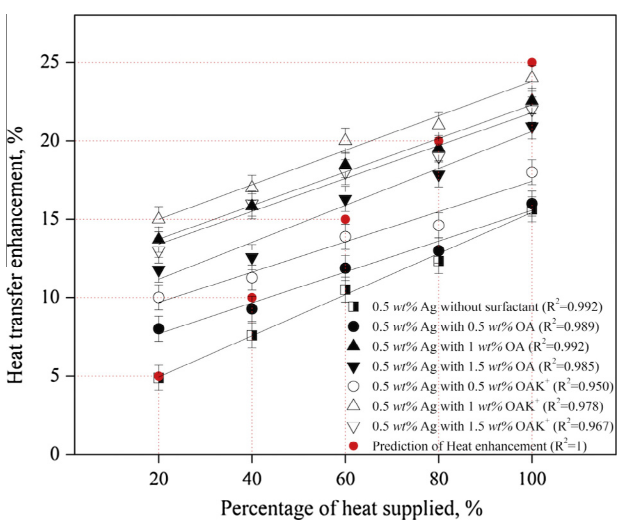

Fig. 12. Thermal enhancement of working fluids.

thermal enhancement with an increase in the percentage of heat supplied can be attributed to the increase in different temperatures (ΔT). In addition, the thermal motion of the nanoparticles enhanced the thermal properties of the nanofluids. The OA group helped with the homogeneous dispersion of the nanoparticles in the nanofluids. Moreover, the potassium cation (K^+) significantly contributed to accruing the thermal property increase, which had effects on the heat transfer rate mechanism more efficiently than the thermal diffusion in the fluid (Guo and Zetterlund, 2011; Hwang et al., 2008; Kwak and Kim, 2005; Wang et al., 2012).

4. Conclusion

Study on NF containing surfactant is leaded to nanoparticles size, the rheological properties of the nanofluids, the thermal conductivity of nanofluids, the dynamic of specific heat capacity (DSC), wet ability (contact angle and surface tension) and heat enhancement. The important details are discussed below:

- The silver nanofluids containing OA and OAK^+ were conducted on thermal conductivity and rheological properties at various concentrations of OA and OAK^+ and operating temperatures. It was found that the NF containing 1 wt% of OAK^+ yielded better particle size ∼95 nm.
- At a shear rate range of $10^1\ s^{-1}$ to $10^3\ s^{-1}$, the samples showed Newtonian behavior, which showed Newtonian behavior, suggesting that the shear stress and viscosity decreased the high solid loading. For a given surfactant concentration, the consistency viscosity and shear stress of the base fluid and all of the nanofluids decreased with an increase in temperature, which confirmed that temperature had a strong effect on the shear stress and viscosity of the nanofluids. The rheological produced Newtonian.
- The NF containing 1 wt% of OAK^+ gave the highest thermal conductivity. It can be seen that the thermal conductivity enhancement was from 11% at 20 °C to 28% at 80 °C when compared with the base fluids. The DSC was increased with respect to operating temperature increase. Explicitly, the thermal conductivity of the NF containing the surfactant was in respect to the operating temperature, showing increments at all concentrations.
- The specific heat of NF containing OA and OAK^+ was superior in specific heat capacity, over water studied in all experimental conditions. The presence of surfactant had clearly contributed to the rise in specific heat capacity.
- It was concluded that the static contact angles of the OA group surfactant used, have better wettability characteristics, dependent on the surfactant concentration. Moreover, the NF containing 1 wt% of OAK^+ could be good at reducing the wettability and the OA group improved the colloidal stability which potassium cation (K^+) increased the non-precipitation period for nanoparticles to be uniformly dispersed in the base fluid. The nanofluids containing 1 wt% of OAK^+ produced a good contact angle of 38.23°.
- It could be concluded that the amount of the thermal enhancement of the nanofluids containing surfactant contributed to the greater rise of the thermal performance over the base fluid/-nanofluids by approximately 80%.

Finally, in conclusion, the thermal properties of NF containing OA was superior in thermal behavior, over water studied in all experimental conditions. The presence of OA had clearly contributed to the rise in the heat transfer rate. By improving the properties of the working fluid with the OAK^+ this led to thermal properties enhancement, thus giving better properties than the OA. The OAK^+ showed compatibility with silver nanoparticle. The OAK^+ was Newtonian fluid. The optimum concentration for the addition of OA and OAK^+ in the working fluid was 1 wt%.

Acknowledgments

Financial supports were provided for T. Parametthanuwat from (1) the Thailand Research Fund (2) the Faculty of Industrial Technology and Management and (3) King Mongkut's University of Technology North Bangkok through Grant No. TRG5780179. S. Rittidech and Y. Ding provided technical support to T. Paramethamuwat and N. Bhuwakietkunjohn.

References

Anoop, K.B., Kabelac, S., Sundararajan, T., Das, S.K., 2009. Rheological and flow characteristics of nanofluids: influence of electroviscous effects and particle agglomeration. J. Appl. Phys. 106.

Bönnemann, H., Botha, S.S., Bladergroen, B., Linkov, V.M., 2005. Monodisperse copper- and silver-nanocolloids suitable for heat-conductive fluids. Appl. Organomet. Chem. 19, 768–773.
Cabaleiro, D., Pastoriza-Gallego, M., Gracia-Fernandez, C., Pineiro, M., Lugo, L., 2013. Rheological and volumetric properties of TiO_2-ethylene glycol nanofluids. Nanoscale Res. Lett. 8, 286.
Chen, H.S., Ding, Y.L., He, Y.R., Tan, C., 2007a. Rheological behaviour of ethylene glycol based titania nanofluids. Chem. Phys. Lett. 444, 333–337.
Chen, H.S., Ding, Y.L., Tan, C.Q., 2007b. Rheological behaviour of nanofluids. New J. Phys. 9.
Chiu, W.S., Khiew, P.S., Isa, D., Cloke, M., Radiman, S., Abd-Shukor, R., Abdullah, M.H., Huang, N.M., 2008. Synthesis of two-dimensional ZnO nanopellets by pyrolysis of zinc oleate. Chem. Eng. J. 142, 337–343.
Choi, S.U.S., Eastman, J.A., 1995. Enhancing thermal conductivity of fluids with nano-particles. In: International Mechanical Engineering Congress and Exhibition. ASME, San Francisco, CA (United States).
Daungthongsuk, W., Wongwises, S., 2007. A critical review of convective heat transfer of nanofluids. Renew. Sust. Energy Rev. 11, 797–817.
Fohanno, S., Nguyen, C., Polidori, G., 2011. Newtonian nanofluids in convection. Handbook of Physical, Nanoparticles and Quantum Dots, Taylor and Francis Group, LLC.
Godson, L., Raja, B., Lal, D.M., Wongwises, S., 2010. Experimental investigation on the thermal conductivity and viscosity of silver-deionized water nanofluid. Exp. Heat Transfer 23, 317–332.
Guo, Y., Zetterlund, P.B., 2011. Synthesis of nanosized (<20 nm) polymer particles by radical polymerization in miniemulsion employing in situ surfactant formation. Macromol. Rapid Commun. 32, 1669–1675.
Hojjat, M., Etemad, S., Bagheri, R., Thibault, J., 2011. Rheological characteristics of non-Newtonian nanofluids: experimental investigation. Int. Commun. Heat Mass Transfer 38, 144.
Huminic, G., Huminic, A., 2011. Heat transfer characteristics of a two-phase closed thermosyphons using nanofluids. Exp. Thermal Fluid Sci. 35, 550–557.
Hwang, Y., Lee, J.-K., Lee, J.-K., Jeong, Y.-M., Cheong, S.-I., Ahn, Y.-C., Kim, S.H., 2008. Production and dispersion stability of nanoparticles in nanofluids. Powder Technol. 186, 145–153.
Kang, H.U., Kim, S.H., Oh, J.M., 2006. Estimation of thermal conductivity of nanofluid using experimental effective particle volume. Exp. Heat Transfer 19, 181–191.
Kang, S.W., Wei, W.C., Tsai, S.H., Huang, C.C., 2009. Experimental investigation of nanofluids on sintered heat pipe thermal performance. Appl. Thermal Eng. 29, 973–979.
Khandekar, S., Joshi, Y.M., Mehta, B., 2008. Thermal performance of closed two-phase thermosyphon using nanofluids. Int. J. Thermal Sci. 47, 659–667.
Kleinstreuer, C., Feng, Y., 2011. Experimental and theoretical studies of nanofluid thermal conductivity enhancement: a review. Nanoscale Res. Lett. 6.
Kondiparty, K., Nikolov, A., Wu, S., Wasan, D., 2011. Wetting and spreading of nanofluids on solid surfaces driven by the structural disjoining pressure: statics analysis and experiments. Langmuir 27, 3324–3335.
Kwak, K., Kim, C., 2005. Viscosity and thermal conductivity of copper oxide nanofluid dispersed in ethylene glycol. Korea–Australia Rheol. J. 17, 35–40.
Li, D., Hong, B.Y., Fang, W.J., Guo, Y.S., Lin, R.S., 2010. Preparation of well-dispersed silver nanoparticles for oil-based nanofluids. Ind. Eng. Chem. Res. 49, 1697–1702.
Li, X., Zhua, D., Wang, X., Wanga, N., Gaoa, J., Lia, H., 2008. Thermal conductivity enhancement dependent pH and chemical surfactant for Cu–H_2O nanofluids. Thermochim. Acta 469, 98–103.
Lo, C.H., Tsung, T.T., Lin, H.M., 2007. Preparation of silver nanofluid by the submerged arc nanoparticle synthesis system (SANSS). J. Alloy. Compd. 434, 659–662.
Lock, G.S.H., 1992. The Tubular Thermosyphon Variations on a Theme. Oxford University Press, New York, United State.
Lu, K., Kessler, C., 2006. Colloidal dispersion and rheology study of nanoparticles. J. Mater. Sci. 41, 5613–5618.
Lu, M.-C., Huang, C.-H., 2013. Specific heat capacity of molten salt-based alumina nanofluid. Nanoscale Res. Lett. 8, 292.
Moghaddam, M.B., Goharshadi, E.K., Entezari, M.H., Nancarrow, P., 2013. Preparation, characterization, and rheological properties of graphene–glycerol nanofluids. Chem. Eng. J. 231, 365–372.
Molchanov, V.S., Philippova, O.E., 2009. Effects of concentration and temperature on viscoelastic properties of aqueous potassium oleate solutions. Colloid J. 71, 239–245.
Molchanov, V.S., Shashkina, Y.A., Philippova, O.E., Khokhlov, A.R., 2005. Viscoelastic properties of aqueous anionic surfactant (potassium oleate) solutions. Colloid J+ 67, 606–609.
Mondragon, R., Julia, J.E., Barba, A., Jarque, J.C., 2012. Determination of the packing fraction of silica nanoparticles from the rheological and viscoelastic measurements of nanofluids. Chem. Eng. Sci. 80, 119–127.
O'Hanley, H., Buongiorno, J., McKrell, T., Hu, L.-W., 2012. Measurement and model validation of nanofluid specific heat capacity with differential scanning calorimetry. Adv. Mech. Eng. 2012, 6.
Oliveira, G.A., Bandarra Filho, E.P., Wen, D., 2014. Synthesis and characterization of silver/water nanofluids. High Temp.-High Press. 43, 69–83.
Pak, B., Cho, Y., 1998. Hydrodynamic and heat transfer study of dispersed fluids with submicron metallic oxide particles. Exp. Heat Transfer 11, 151.
Parametthanuwat, T., 2012. Heat Transfer Characteristics of the Two-Phase Closed Thermosyphon (TPCT) Containing Silver Nanofluids with Oleic Acid Surfactant, Mechanical Engineering. Mahasarakham University Mahasarakham; Thailand.
Parametthanuwat, T., Rittidech, S., 2013. Silver nanofluid containing oleic acid surfactant as working fluid in the two-phase closed thermosyphon (TPCT): a thermodynamic study. Nanoscale Microscale Thermophys. Eng. 17, 216–235.
Parametthanuwat, T., Rittidech, S., Pattiya, A., 2010. A correlation to predict heat-transfer rates of a two-phase closed thermosyphon (TPCT) using silver nanofluid at normal operating conditions. Int. J. Heat Mass Transfer 53, 4960–4965.
Parametthanuwat, T., Rittidech, S., Pattiya, A., Ding, Y., Witharana, S., 2011. Application of silver nanofluid containing oleic acid surfactant in a thermosyphon economizer. Nanoscale Res. Lett. 6, 315.
Patel, H.E., Das, S.K., Sundararajan, T., Sreekumaran Nair, A., George, B., Pradeep, T., 2003. Thermal conductivities of naked and monolayer protected metal nanoparticle based nanofluids: manifestation of anomalous enhancement and chemical effects. Appl. Phys. Lett. 83, 2931–2933.
Radiom, M., Yang, C., Chan, W.K., 2013. Dynamic contact angle of water-based titanium oxide nanofluid. Nanoscale Res. Lett. 8, 282.
Rahimi, M., Asgary, K., Jesri, S., 2010. Thermal characteristics of a resurfaced condenser and evaporator closed two-phase thermosyphon. Int. Commun. Heat Mass Transfer 37, 703–710.
Rajabpour, A., Akizi, F., Heyhat, M., Gordiz, K., 2013. Molecular dynamics simulation of the specific heat capacity of water–Cu nanofluids. Int. Nano Lett. 3, 58.
Ramesh, G., Prabhu, N., 2011. Review of thermo-physical properties, wetting and heat transfer characteristics of nanofluids and their applicability in industrial quench heat treatment. Nanoscale Res. Lett. 6, 334.
Salehi, H., Heris, S.Z., Noie, S.H., 2011. Experimental study of a two-phase closed thermosyphon with nanofluid and magnetic field effect. J. Enhanced Heat Transfer 18, 261–269.
Sharma, P., Baek, I.-H., Cho, T., Park, S., Lee, K.B., 2011. Enhancement of thermal conductivity of ethylene glycol based silver nanofluids. Powder Technol. 208, 7–19.
Singh, A.K., Raykar, V.S., 2008. Microwave synthesis of silver nanofluids with polyvinylpyrrolidone (PVP) and their transport properties. Colloid Polym. Sci. 286, 1667–1673.
Singh, J., Verma, V., Nigam, K.D.P., 2013. Flow characteristics of power-law fluids in coiled flow inverter. Ind. Eng. Chem. Res. 52, 207–221.
Sreeremya, T.S., Krishnan, A., Peer Mohamed, A., Hareesh, U.S., Ghosh, S., 2014. Synthesis and characterization of cerium oxide based nanofluids: an efficient coolant in heat transport applications. Chem. Eng. J. 255, 282–289.
Tamjid, E., Guenther, B.H., 2010. Rheology and colloidal structure of silver nanoparticles dispersed in diethylene glycol. Powder Technol. 197, 49–53.
Tanvir, S., Qiao, L., 2012. Surface tension of nanofluid-type fuels containing suspended nanomaterials. Nanoscale Res. Lett. 7, 1–10.
Trisaksri, V., Wongwises, S., 2007. Critical review of heat transfer characteristics of nanofluids. Renew. Sust. Energy Rev. 11, 512–523.
Turkyilmazoglu, M., 2012. Exact analytical solutions for heat and mass transfer of MHD slip flow in nanofluids. Chem. Eng. Sci. 84, 182–187.
Veilleux, J., Coulombe, S., 2011. A dispersion model of enhanced mass diffusion in nanofluids. Chem. Eng. Sci. 66, 2377–2384.
Vekas, L., Bica, D., Marinica, O., 2006. Magnetic nanofluids stabilized with various chain length surfactants. Roman. Rep. Phys. 58, 257–267.
Wang, Q., Li, H.-Z., Xie, Y.-J., Li, H.-Y., Yang, H.-Y., 2012. Effect of potassium oleate on rheological behavior of cationic guar in aqueous solution with varying temperatures. Chin. J. Chem. Phys. 25, 448–456.
Wang, X.Q., Mujumdar, A.S., 2007. Heat transfer characteristics of nanofluids: a review. Int. J. Thermal Sci. 46, 1–19.

Curriculum vitae

Personal Bio

General

I am Assistant Professor. Dr. Parametthanuwat. I have been working on several applications of heat pipes, nanofluid and renewable energy for many years. I also got several research funds from Thai government and Thai industrial companies. One of them is the Royal Golden Jubilee PhD Program (RGJ) in which Professor Dr Rittidech is supervisor; Assistant Professor Dr Pattiya and Professor Yulong Ding is an associate supervisor of an outstanding me. According to the RGJ program, I am study abroad to gain experiences from a high quality university in Institute of Particle Science & Engineering, University of Leeds. I am fully funded by the RGJ program and University of Leeds.

Address

Department of Agricultural Engineering for Industry

Faculty of Industrial and Technology Management

King Mongkut's University of Technology North Bangkok Prachinburi Campus

129 Moo 21, Tambon Noenhom, Amphoe Mueang, Prachinburi 25230, Thailand

E-mail: thanya.p@fitm.kmutnb.ac.th

Tel +6681-8649-682

External Academic Staff:

Heat-Pipe and Thermal Tools Design Research Laboratory

Faculty of Engineering Mahasarakham University

Kamriang,Kantarawichai DistrictMahasarakham

44150; Thailand

http://www.esan-htdr.com/index.html

Educational

Ph.D. (Doctor of Philosophy (Mechanical Engineering, 2012)

Faculty of Engineering Mahasarakham University ; Thailand

M.Eng (Master of Mechanical Engineering, 2009)

B.Ind.Tech (Agricultural Machinery Technology, 2007)

King Mongkut’s Institute of Technology North Bangkok,Thailand

Ph.D-cooperation with

Institute of Particle Science & Engineering School of Process, Environmental and Materials Engineering University of Leeds, Leeds: UK

Scholarship

The Royal Golden Jubilee Ph.D Program

Thailand Research Fund And University of Leeds, Leeds: UK

Area of Expertise

Rheological behaviour of nanofluids, Nanofluids Properties

Heat and mass transfer, Thermodynamic, Thermosyphon

Process engineering

Food plant design

Publication

1. Bhuwakietkumjohn, N. and T. Parametthanuwat, Heat transfer behaviour of silver particles containing oleic acid surfactant: application in a two phase closed rectangular cross sectional thermosyphon (RTPTC). Heat and Mass Transfer, 2017. 53(1): p. 37-48.
2. Parametthanuwat, T.; Bhuwakietkumjohn, N.; Rittidech, S.; Ding, Y. Experimental investigation on thermal properties of silver nanofluids. International Journal of Heat and Fluid Flow, 2015. 56: p. 80-90.
3. Bhuwakietkumjohn, N. and T. Parametthanuwat, Application of silver nanoparticles contained in ethanol as a working fluid in an oscillating heat pipe with a check valve (CLOHP/CV): a thermodynamic behaviour study. Heat and Mass Transfer, 2015. 51(9): p. 1219-1228.
4. Bhuwakietkumjohn, N. and T. Parametthanuwat, Thermal performance of a top heat mode closed-loop oscillating heat pipe with a check valve (THMCLOHP/CV). Journal of Applied Mechanics and Technical Physics, 2015. 56(3): p. 479-485.
5. Bhuwakietkumjohn, N.; Parametthanuwat, T. The top heat mode of closed loop oscillating heat pipe with check valves at the top heat mode (THMCLOHP/CV): a thermodynamic study. Int J Mech Mater Eng. 2014 2014/08/07;9(1):1-10.
6. Parametthanuwat, T. and S. Rittidech, Silver Nanofluid Containing Oleic Acid Surfactant As Working Fluid In The Two-Phase Closed Thermosyphon (TPCT): A Thermodynamic Study. Nanoscale and Microscale Thermophysical Engineering, 2013. 17(3): p. 216-235.
7. Thanya Parametthanuwat, Sampan Rittidech*, Adisak Pattiya, Yulong Ding and Sanjeeva Witharanaม Application of silver nanofluid containing oleic acid surfactant in a thermosyphon economizer. Nanoscale Research Letters, 2011. 6(1): p. 315.
8. T. Parametthnuwat, S. Boothaisong, S. Rittidech*, K. Booddachan, " Heat Transfer Characteristics of a Two-Phase Closed Thermosyphon Using De-Ionized Water Mixed with Silver Nano", Heat and Mass Transfer, 46(2010):281-285,
9. T. Parametthanuwat, K. Booddachan and S.Rittidech* "Thermosyphon Installation for Energy Thrift in a Smoked Fish Sausage Oven (TISO)" Energy(2010), 35 2836- 2842
10. T. Parametthanuwat, S. Rittidech*, A. Pattiya. "A correlation to predict heat-transfer rates of a two-phase closed thermosyphon (TPCT) using silver nanofluid at normal

operating conditions". International Journal of Heat and Mass Transfer (2010). 53(21–22), pp4960–4965

BOOK CHAPTER

1. T. Parametthanuwat and N. Bhuwakietkumjohn, "Application of Nanofluid in Thermosyphon (TPCT) A–Review": NANOTECHNOLOGY SERIES, VOL. 1: Fundamentals and Applications, Publisher: Studium Press LLC, 2013

CONFERENCES

1. T.Parametthanuwat and N. Bhuwakietkumjohn, "Heat-transfer characteristics of thermosyphon rectangular tube" Heat and Mass transfer 15th, 30 -31 March, 2016 in Al's Resort Hotel, Koh Samui, Suratthani, Thailand
2. T.Parametthanuwat, N. Bhuwakietkumjohn and M. Saengprapaitip, "Design of Chicken Baking Drum with Charcoal Fuel for Household" Heat and Mass transfer 15th, 30 -31 March, 2016 in Al's Resort Hotel, Koh Samui, Suratthani, Thailand
3. T.Parametthanuwat and S. Rittidech, "A TWO PHASE CLOSED THERMOSYPHON USING SILVER NANOFLUIDS ; A THERMAL RESISTANCE BEHAVIOUR STUDY", Heat and Mass transfer 13th, 13 -14 March, 2014 in Chanthaburi : Thailand
4. T.Parametthanuwat and N. Bhuwakietkumjohn, "A THERMAL BEHAVIOUR OF I-SHAPE A TWO PHASE CLOSED THERMOSYPHON ;ANGLE OF INCLINATION STUDY" , Heat and Mass transfer 13th, 13 -14 March, 2014 in Chanthaburi : Thailand
5. N. Bhuwakietkumjohn and T.Parametthanuwat, "ENERGY SAVING FOR HERB CHICKEN OVEN" , Heat and Mass transfer 13th, 13 -14 March, 2014 in Chanthaburi : Thailand
6. N. Bhuwakietkumjohn and T.Parametthanuwat, "Silver nano-ethanol mixture effect on heat transfer performance in n closed-loop oscillating heat-pipe with check valve (CLOHP/CV)", Fifth International Conference on Science, Technology and Innovation for Sustainable Well-Being (STISWB V), 4-6 September, 2013, in Luang Prabang, LAOS.

7. T.Parametthanuwat and N. Bhuwakietkumjohn, “I-shape-two phase closed thermosyphon ; A thermal behaviour study”, Fifth International Conference on Science, Technology and Innovation for Sustainable Well-Being (STISWB V), 4-6 September, 2013, in Luang Prabang, LAOS.
8. K. Booddachan and T. Parametthanuwat, “The Investigation of Gas Generation Effect for Inverse Metal Fuel Cell”, 4th International Conference on Science, Technology and Innovation for Sustainable Well-Being (STISWB IV), 10-12 August 2012, Pattaya Thailand
9. T. Parametthanuwat, S. Thonglat, P. Tadtiang, K. Booddachan and S. Rittidech*, “Thermosyphon application for energy thrift on oven Smoked fish sausage” The 10th Annual Conference of Thai Society of Agricultural Engineering “International Conference on Innovations in Agricultural, Food and Renewable Energy Productions for Mankind”, School of Agricultural Engineering, Suranaree University of Technology, Nakhon Ratchasima, Thailand; 1-3 April 2009.
10. T. Parametthanuwat, S. Rittidech*, K. Booddachan, “Effect of Inclination Angles and Aspect ratios on Heat Transfer Characteristics of a Two-Phase Closed Thermosyphon Using De Ionize Water Mix Silver Nano” The 9th International Heat Pipe Symposium (Heat Pipe Science and Technology), 17- 20 November 2008, Monash University Sunway Campus, Malaysia
11. T. Parametthanuwat, K. Booddachan* “Energy Saving Analysis of Double Cool Technique Air – Conditioning System” School of Agricultural Engineering, Suranaree University of Technology, Nakhon Ratchasima, 2007